In presenting this dissertation in partial fulfillment of the requirements for an advanced degree at Idaho State University, I agree that the Library shall make it freely available for inspection. I further state that permission for extensive copying of my dissertation for scholarly purposes may be granted by the Dean of the Graduate School, Dean of my academic division, or by the University Librarian. It is understood that any copying or publication of this dissertation for financial gain shall not be allowed without my written permission.

Signature _____

Date _____

Investigating HSP90 Inhibition and Functional Precision Medicine Treatment in Cancer and Tumor Organoid Cell Cultures of Synovial Sarcoma

by

Matthew Kirkham

A dissertation

submitted in partial fulfillment

of the requirements for the degree of

Doctor of Philosophy in the Department of Pharmaceutical Sciences Idaho State University

Spring 2023

Committee Approval

To the Graduate Faculty:

The members of the committee appointed to examine the dissertation of Matthew Kirkham find it satisfactory and recommend that it be accepted.

_____

Major Advisor

_____

Committee Member

_____

Committee Member

_____

Committee Member

_____

Graduate Faculty Representative

Animal Welfare Research

Mice experiments were conducted with the approval of the Idaho State University institutional animal care and use committee and protocols 757/775 in accordance with legal and ethical standards.

Idaho State
UNIVERSITY

Office for Research - Research Outreach & Compliance
921 S. 8th Avenue, Stop 8046 • Pocatello, Idaho 83209-8046

September 25, 2017

Jared Barrott, PhD
921 S. 8th Ave
MS 8333
Pocatello, ID 83209

RE: Your application dated 8/24/2017 regarding study number 757: Preclinical testing of sarcoma

Dear Dr. Barrott:

Thank you for your response to requests from a prior review of your application for the new study listed above. Your study is eligible for Designated Member Review (DMR).

This is to confirm that your application is now fully approved. The protocol is approved through 9/25/2020.

You are granted permission to conduct your study as most recently described effective immediately. The study is subject to annual review on or before 9/25/2018, unless closed before that date.

Please note that any changes to the study as approved must be promptly reported and approved. Contact me (208-282-2179; fax 208-282-4723; email: anmlcare@isu.edu) if you have any questions or require further information.

Sincerely,

Tom Bailey
IACUC Coordinator

Acknowledgments Page

I would like to acknowledge my wonderful family and my wife, Morgan, who has continually supported me as I have worked through the long journey of earning my PhD. Without the support of my family, this task would have been even more daunting and I appreciate all the sacrifices they have made for me.

I would also like to acknowledge Dr. Jared Barrott and the faith and support he has shown me throughout my research. I appreciate the risk he took by bringing me on as a researcher in his lab and allowing me to head an ambitious and experimental project with no guarantee of success.

I would also like to acknowledge Dr. Jeffrey Rosentreter who helped me get started on my academic journey while earning my undergraduate degree. His oversight and encouragement of independent research techniques helped me to form my work ethic and research capabilities that have carried through to this day.

Thank you to the Idaho INBRE foundation for their support and funding of our research into 3D modeled cell culture and organoids.

Finally, I want to thank the Biomedical and Pharmaceutical Sciences department for accepting and funding me as a graduate student and all of the support I have received from all of the professors within the department over the years.

Table of Contents

List of Figures

List of Tables

List of Abbreviations and Symbols

Aha1 – ATPase homolog 1

ALI – air-liquid interface

BAF – barrier-to-autointegration factor

CTD – carboxy-terminal domain

FPKM – Fragments per kilo base of transcript per million mapped fragments

GEMM – genetically engineered mouse model

HDAC – histone deacetylase

HSP – Heat Shock Protein

HSR – Heat Shock Response

LLI – liquid-liquid interface

MMP2 – matrix metallopeptidase 2

NTD – amino-terminal domain

OPG – Osteoprotegerin

PRC2 – Polycomb Repressive Complex 2

SS – Synovial Sarcoma

SWI/SNF – switching/sucrose nonfermenting

TMB – Tumor Mutational Burden

Abstract

Investigating HSP90 Inhibition and

Functional Precision Medicine Treatment

in Cancer and Tumor Organoid

Cell Cultures of Synovial Sarcoma

Dissertation Abstract—Idaho State University (2023)

Synovial Sarcoma is a rare, malignant muscle cancer that commonly effects adolescents. Lack of testing opportunities and viable treatment options and innovation in the last thirty years highlights the need for novel, groundbreaking therapies. HSP90, a chaperone protein responsible for stabilizing proteins under stress, can be hijacked by cancer to induce oncogenic signaling. Inhibition of HSP90 may allow deregulation of the cancer machinery and force apoptotic vulnerability. Of interest to this inhibition study is the capability to overcome limitations of traditional two-dimensional and current three-dimensional cell culture models deemed incapable of fully replicating the biological setting. Three-dimensional cell cultures utilizing advanced structural matrices and scaffolds aim to bridge the gap between the biological and laboratory setting, mimicking the tumor environment to a high degree. Drug screening in this environment will help to ease the translational burden from *in vitro* studies to clinical trials. Three-dimensional culture in combination with sampling of patient cancer tissue to develop patient-derived organoids looks to deliver a tailored therapy to each patient based on their

unique cancer, an approach deemed Functional Precision Medicine. Utilizing these advanced culture techniques, along with a novel inhibition therapy, this research looks to provide a new standard of treatment in the continuing fight against synovial sarcoma and other soft tissue cancers.

Key Words: Synovial Sarcoma, HSP90, cancer, cell culture, patient-derived organoids, Functional Precision Medicine, SS18-SSX, Metastatic

1. Introduction and Background

With new therapeutic breakthroughs and the advancement of the scientific community's understanding of cancer, it is easy to feel as though certain subsets of the cancer-afflicted population have been left on the sideline. This is especially true of synovial sarcoma, a rare cancer with a limited subset of genetic mutations that would allow for drug-targeted therapies to come to prominence. My research looks to explore patient prognosis with an emphasis in the event of heterotopic ossification, expand treatment options available to those diagnosed with synovial sarcoma, and establish more efficient models for the future direction of drug screening for all types of cancer.

1.1. History and Origin of Synovial Sarcoma

Synovial sarcoma (SS), a misnomer for what might be more accurately described as soft tissue muscle cancer, has a complicated history, stretching back to the first attributed recorded case in 1865(1), although the first consistent morphological description was not recorded until nearly 50 years in 1910(2). After various opinions over correct terminology, the term *synovial sarcoma* was finally decided on in 1934 in French and 1936 in English. SS was first characterized by its biphasic morphology consisting of spindle-shaped and epithelial cell appearance. Though initially thought to be synovial in origin due to its common proximity to synovial membranes, it was decided to originate instead from an "undifferentiated" mesenchymal stem cell.

SS has shown a predilection for developing near or adjacent to bone tissue, with the hypothesis that bone provides an anti-apoptotic niche allowing transformed cells to grow by

secreting the decoy receptor osteoprotegerin (OPG)(3,4). It has been shown that, in fact, SS originates more closely from the periosteum than from muscle cells; the periosteum forms the highly vascularized connective tissue surrounding bone. SS has even been found to ossify in some patients, potentially altering patient prognosis, though the impact of ossification has not been thoroughly confirmed(5–9).

1.2. Genetic Profile and Effects of Synovial Sarcoma

The primary drivers of SS are fusion proteins that are generated from either fusion oncogene SS18-SSX1/SSX2/SSX4. These oncogenes arise from a chromosomal translocation event of t(X;18)(p11.2;q11.2) occurring on chromosomes X and 18 (figure 1). The resultant fusion oncoproteins, or proteins that aid in cancer development, drive synovial sarcoma pathogenesis through the disruption of both the SWI/SNF

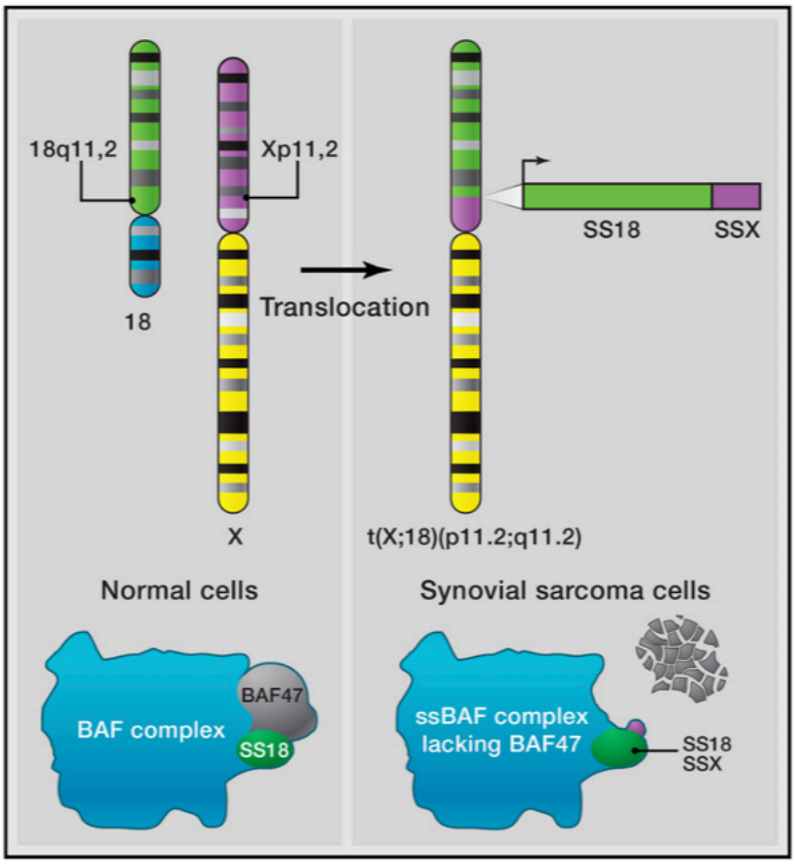

Figure 1. Chromosomal translocation event responsible for the generation of the SS18-SSX fusion gene. Oncoproteins generated from this gene proceed to produce downstream effects, such as the disruption of the BAF complex seen here (8).

(switch/sucrose fermenting) and Polycomb Repressive complexes(10–15). A retrospective study of 3,228 patients found that being male, as well as being over 35 years of age at the time of diagnosis, are typically associated with a poorer prognosis (16). Rate of diagnosis between males and females is approximately 1:1, with a slightly higher rate of 52.9% in males (16–18)

The SWI/SNF complex was initially discovered in yeast over 20 years ago, and is responsible for many functions of chromatin remodeling(19). As such, it is considered integral in controlling transcription and any mutations with regards to the complex hold the potential to be amplified through altered gene expression throughout the genome. It has been suggested that the SS18-SSX gene and resultant proteins compete with non-altered SS18 proteins for occupancy of the BAF complex, specifically BAF47, a subunit of the SWI/SNF complex known for its tumor suppressant activity(20); other researchers have countered this claim, stating BAF47 is not displaced by SS18-SSX(21). However, most research agrees that the SS18-SSX fusion protein, once bound to the BAF complex, acts to retarget the SWI/SNF complex to Polycomb Repressive Complex 2 (PRC2) repressed domains within the genome and activates them(22).

Research from McBride et al. worked to further elucidate the mechanism, showing how the altered BAF complex causes epigenetic changes, while also seeking to uncouple the effects of BAF47 loss from the effects of SS18-SSX inclusion within the complex (figure 2). They determined loss of BAF47 to be a loss of function mutation, causing BAF complex targeted genes to no longer be activated, while inclusion of SS18-SSX yields a gain of function mutation, activating genes through retargeting that were not previously active. SS has been determined to be unique in this regard in that it yields both a loss of and gain of function mutation.

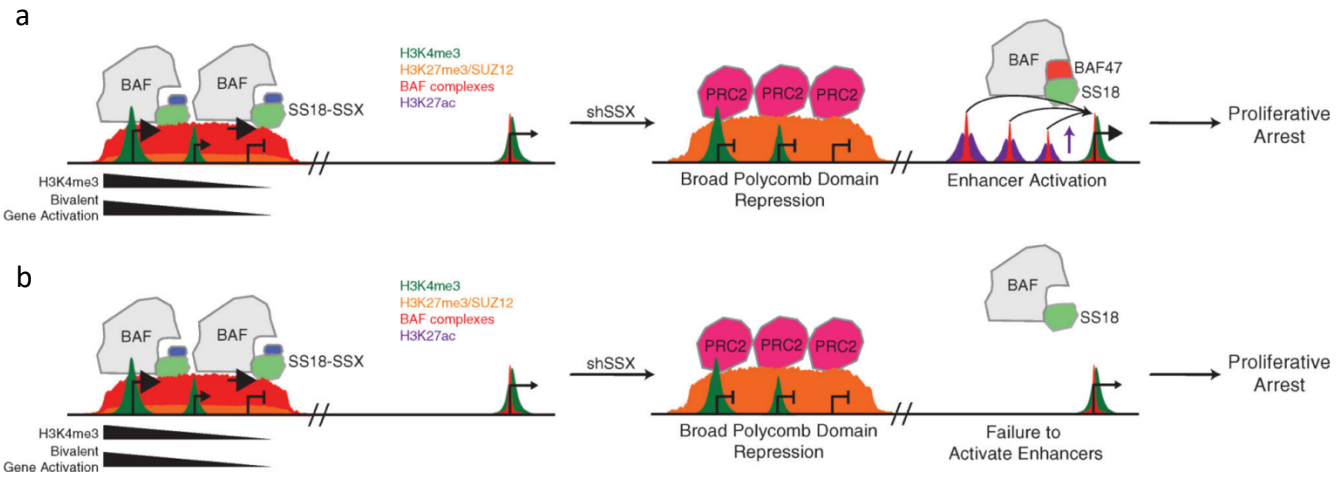

Figure 2. a. The SS18-SSX fusion directs BAF complexes to broad polycomb domains, opposing polycomb-mediated repression to activate bivalent genes. Upon suppression, BAF complexes return to distal sites, mediating enhancer reactivation. **b.** In the absence of BAF47, SS18-SSX suppression results in similar restoration of gene silencing at broad polycomb domains, as well as proliferative arrest, but without restoration of enhancer accessibility and activation(12).

1.2.1. Treatment and Drug Targeting of Synovial Sarcoma

SS is typically considered an adolescent cancer, affecting primarily teenagers and young adults, but can occur in any age group. There are approximately 800 new documented cases each year, or 1-2 cases per 1 million people. Because of this low occurrence rate, there are a limited number of approved treatment methods available. The primary intervention for SS is surgical resection with negative margins, but this is often complicated due to involvement of surrounding anatomy that make complete tumor resection nearly impossible without limiting damage to the patient (23,24). Radiation therapy is commonly employed either in conjunction with or post-surgery in an effort to increase the negative margin after resection, especially when complete resection is impossible. The greatest likelihood for positive patient outcome is associated with early diagnosis and resection; a retrospective analysis of 63 patients with surgical resection at 10

years showed 82% local recurrence-free survival and 95% distant recurrence-free survival (25). This same study suggested that radiation and chemotherapy treatment post-operation did not show a significant increase in patient outcomes.

Regarding chemotherapy, only seven drugs have been approved for clinical use by the FDA (26). Of those, doxorubicin hydrochloride is the primary chemotherapeutic option when used in combination with surgical resection and radiation therapy (27). However, doxorubicin yields its own issues concerning cardiotoxicity and long-term treatment; patients are limited to a cumulative dose of 550mg/m^2 of body surface area, typically achieved across 4-6 treatments within 6 months (28,29).

Even with this approved course of treatment, patient survivability rates range from only 36-75% across five years, with survivability plummeting in the event of metastasis (17). 50% of patients diagnosed with SS develop metastasis within five years of diagnosis, and of those who develop metastasis, 90% end up succumbing to their disease(30). Recurrence or metastasis has a low recourse for treatment outside of further resection and radiation therapy, as doxorubicin lifetime limits have likely been achieved during the first round of treatments. From these figures, it is apparent that there is a definite need to broaden the current understanding of SS and perform more research in an effort to provide more therapeutic options to those diagnosed.

One of the factors complicating the available research into the treatment of SS is the fact that it has a known low mutational burden (TMB), on average less than five mutations per million base pairs(31), thus SS pathogenesis is being driven primarily by epigenetic modifications(32,33). As such, this makes SS difficult to target with current approved treatments and medications, as

there is no apparent gene or protein mutation that volunteers as a potential target. Still, multiple pre-clinical studies are being investigated to target the SS18-SSX fusion oncoprotein downstream effects which aide in proliferation and metastasis of SS(34–36).

Though the chromosomal translocation is not considered a targetable mutation, other options for SS treatment remain to be explored. While investigating HDAC (histone deacetylase) inhibitors within various cancers with the hopes of overcoming and targeting epigenetic modifications, the Nielson group found that multiple SS cell lines showed a reduction in cell viability in response to treatment with HSP90 inhibitors, as seen in figure 3. On average, a greater than 75% reduction in cell viability was observed, suggesting that there must be some relation between HSP90 and SS that would be worthy of further investigation(37).

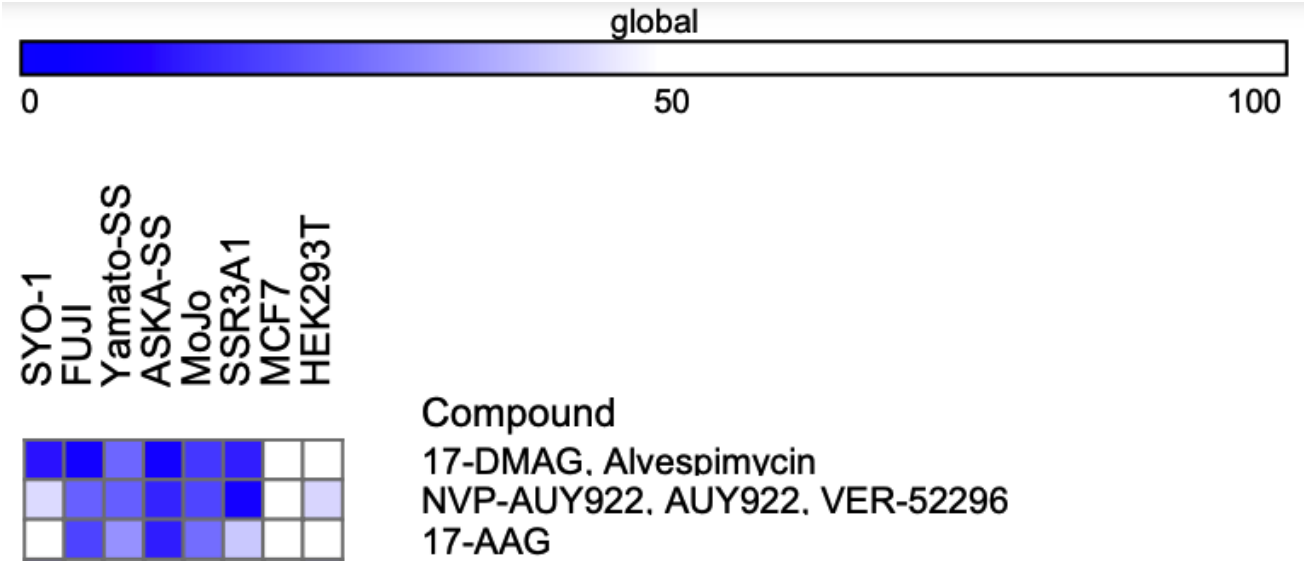

Figure 3. Anticancer drug screening revealing HSP90 inhibitors as candidates for synovial sarcoma treatment. Cell viability reduction is observable across all SS cell lines, with little to no reduction in cell viability observed for breast cancer MCF7 or normal tissue Human Embryonic Kidney Cells HEK293T

1.2.2. Ossification Profile and Genetic Contributions

Ectopic ossification, the painful development of spontaneous bone tissue in otherwise soft tissue, is an extremely rare occurrence that has been found to coincide with some instances of SS. However, this is an extremely rare event of less than 10% in an already rare cancer with a low diagnosis of approximately 2 cases in every million people(3,7,38,39). A full and thorough analysis of genetic contributions, as well as change to patient prognosis in the presence of ossification, has thus been difficult to determine due to a low pool of examinable instances.

Genetically engineered mouse modeling in order to recapitulate the human biology of a metastatic SS model using an SS18-SSX1/2 expression and *Pten* deletion can be used to provide an increased study basis in order to correlate ossification presence to patient prognosis. This model can also help to provide a genetic profile that may indicate the likelihood of ossification development within a patient beforehand. This mouse model has been extensively profiled for pathophysiology, histology, and molecular expression(4,14,39–43).

1.3. HSP90 and Biological Function

The discovery of HSP90, along with the entirety of the larger HSP (heat shock protein) family, was initially observed accidentally when fruit flies Drosophila melanogaster were left at higher-than-normal temperatures. Upon observation, it was noted that chromosomes of the flies were “puffy,” reasoned to be the activation and increased expression of specific proteins in response to heat stress, otherwise known as the heat shock response (HSR)(44,45). However, HSP90 and other HSPs are upregulated not just during high-temperature events, but also during

hypoxic and nutrient deprivation events, functioning as a protein-stabilizing chaperone for many clients under a variety of high-stress conditions (46).

HSPs are designated and classified by molecular mass, which is to say HSP90 has a mass of about 90,000 Daltons, with an estimated weight of 84.5 kDa for the alpha form, and 83.2 kDa for the beta form. These two isoforms can be distinguished through the appending of a letter when there are multiple HSPs of similar mass, i.e. HSP90aa1 and HSP90ab1(47). Two additional isoforms are also known, though they are not as well characterized. These are HSP90B1, found in the endoplasmic reticulum, and TRAP1, localized to mitochondria (48,49). HSP90aa1 and HSP90ab1, the main focus of this discussion, differ in number of amino acids and unique sequences at a few key points. HSP90aa1 consists of 732 amino acids, while HSP90ab1 consists of 744, with the amino acids ESEDK removed between phosphorylation sites in HSP90ab1, as well as the substitution of the amino acids TQTQDQPM for VHHG at the N-terminal end of HSP90ab1 (50).

HSP90aa1, or HSP90α, is considered to be an inducible isoform, becoming upregulated during heat shock and other cellular stress events (51). Polymorphisms of HSP90α have shown a link to poorer patient prognosis as well as being frequently associated with tumorigenesis through increased affinity of ATP and ATPase activity (52,53).

HSP90ab1, or HSP90β, is regarded as more constitutively expressed, helping to fold and stabilize proteins within the cytoplasm at all times (54). It has also been observed to become upregulated in certain cancers, such as non-squamous small cell lung cancer, also being linked to a poor patient prognosis (52). Upregulation of HSP90β has been reported to promote

angiogenesis and metastasis (55,56). HSP90β contributes to metastasis through the AKT and Wnt/β-catenin signaling pathways, stabilizing and promoting increased levels of LRP5. LRP5 enhances Wnt signaling leading to stabilization and nuclear import of β-catenin, and thus increased transcription of TCF, Snail, and Slug, proteins that activate the endothelial-mesenchymal transition (EMT) (53). The de-differentiation of endothelial cells to mesenchymal cells promotes migration and metastasis of cancer cells, further reducing patient prognosis.

Though HSP90β is considered to be the constitutive protein of the two, there has been evidence to show that HSP90α can become upregulated to such a point within cancer that it also becomes considered constitutive as the cancer relies heavily on it for oncoprotein stabilization (57).

Heat shock proteins have been found to be biologically and evolutionarily conserved among many species across all three of the organized kingdoms, with the gene *htpG* isolated from *E. coli* homologous to Hsp83 within *Drosophila* and Hsp82 in yeast(58,59). HSP90 has been observed to be involved in nearly all physiological events, including signal transduction, cell cycle progression, and transcriptional regulation. The method of action of the HSP90 complex works to enable correct protein folding, activation, transport, and degradation(60–64). HSP90 is known to associate with a number of co-chaperones, from CTD-interaction promoters such as Hop to enzymatic and activity enhancers, like isomerases and activator of HSP90 ATPase homolog 1 (Aha1) that acts to stimulate and increase ATPase activity(65–68).

Tumor cells are considered to be in a “stressed’ state as they constantly compete for resources in an effort to proliferate, and often have many oncogenic mutations present. Cancer

can thus hijack HSP90 in order to not only stabilize oncoproteins, but remain bound to or destabilize critical tumor suppressor proteins such as p53 when in an activated state(69–72). This dependence on HSP90 has been observed through increased levels of HSP90 in many types of cancer and tumors, leading to a poorer prognosis in fibrosarcoma, glioblastoma, breast cancer, pancreatic carcinoma, and synovial sarcoma patients with elevated HSP90 expression(73–81). However, beyond having higher expression of HSP90, there are other factors that must affect cancer malignancy and patient outcomes, as there are many normal tissues such as brain, bladder, and spleen, that also exhibit elevated HSP90 expression(82,83).

Activation is the next factor to be considered in HSP90 effect on tumor promotion. The Picard laboratory has documented over 400 client proteins that are modified or stabilized by HSP90(84), with many mediating signal transduction pathways involved in cellular growth, apoptotic evasion, differentiation, and metastasis(83,85,86). Some studies have suggested that HSP90 in tumors exists only in multi-chaperone complexes, driving ATPase activity and thus increasing inhibitor affinity by 100-fold(87). This assumes that all HSP90 has the opportunity to bind ATP equally, while actually only about 20-30% are free to bind ATP as seen in figure 4(88). The supporting hypothesis holds that ligand-binding HSP90 is present in complex with several co-chaperones, but an “inactive” pool of HSP90 does not exist with co-chaperones. Thus, it is difficult to quantify “activated” HSP90 and the role it plays between cancer tissue and normal tissue, and more must be considered beyond merely the abundance and active state of HSP90.

Turning to look at localization of HSP90 within cancer cells, it becomes apparent that this factor is of key importance. For the majority of the time that HSP90 has been known and

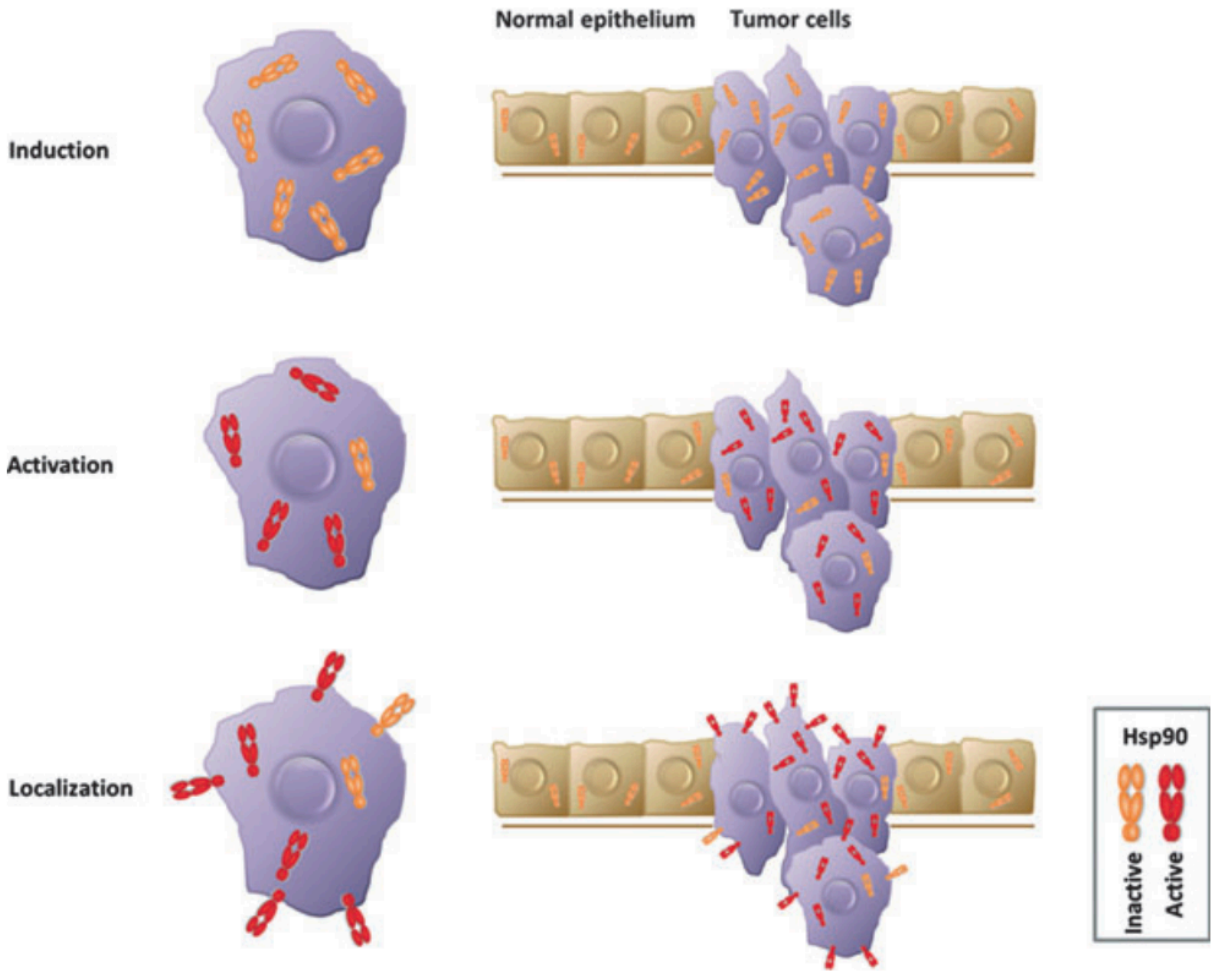

Figure 4. Differences in HSP90 in tumor and normal cells. A greater amount of HSP90 is induced in tumor cells. Activation of HSP90 (red) via co-chaperone complexes instigates surface localization in cancer cells, while normal cell HSP90 remains within the cytosol. (55)

investigated, it was believed that it resided solely within the cytoplasm of the cell; more recent work has placed HSP90 both anchored to the surface membrane of the cell and also secreted into the extracellular space, particularly in tumor cells such as fibrosarcoma, glioblastoma, breast cancer, pancreatic carcinoma, and most important to this discussion, synovial sarcoma (74,77–81). The secretion of HSP90 into the extracellular space has been implicated in promoting metastasis through the stabilization of migratory factors like matrix metallopeptidase-2 (MMP2)

(81). The presence of surface-bound HSP90 makes an attractive target for cancer-specific inhibition. HSP90 is expressed on the cellular surface at less than 10% of the total cellular content of HSP90 (89), and may be implicated in signaling to surrounding cells and the immune system that the cell is endangered. This signaling can potentially reroute supplemental materials towards the cancer cell and promote further growth and metastasis (90). In some forms of cancer, such as lung carcinoma, HSP90 has also been shown to stabilize cachexia and muscle catabolism by activating TLR4 on surrounding tissue after being released from tumor cells through extracellular vesicles (91).

As previously mentioned, HSP90 has been documented to chaperone over 400 client proteins; among this list are several *bona fide* oncoproteins that contribute to Hanahan and Weinberg's canonical "Hallmarks of Cancer" (92), with a selection of these oncoproteins detailed in Table 1 below (46,93–95). With the three factors of induction, activation, and localization considered, it is evident that HSP90 can be considered to play a significant role in the induction, maintenance, and proliferation of cancer. Such an important part of the cancer machinery, therefore, should be considered in the possible treatment of cancer, especially with regards to SS.

Table 1. Multiple Hallmarks of Cancer and their associated HSP90 Clientele(46,93–95)

Hallmark	Client Protein
Evasion of Apoptosis	Akt(46), Rip, P53(46), Survivin(93), Apaf-1(94), Bcl2(46), IGF-IR
Sustained Angiogenesis	VEGFR(94), HIF1(46), Akt, FAK, Src(46)
Limitless replicative potential	Telomerase(46,94), n-TERT(93)
Tissue invasion and metastasis	MMP-2(46), c-MET(93)
Self-sufficiency in growth signals	EGFR(94), Raf(94), Bcr-Abl(95), ErbB-2(95), Src, Akt, MEK(94)
Insensitivity to anti-growth signals	Plk-1, Cdk4(93), Cdk6(93), Myt-1, cyclin-D(93)

1.3.1. Structure and Method of Action of HSP90

HSP90 forms a homodimer complex in order to stabilize and interact with client proteins; each monomer consists of an amino-terminal domain (NTD) that binds with ATP, a middle domain that mediates ATP hydrolysis and client-HSP90 binding, and a carboxy-terminal domain (CTD) responsible for dimerization and co-chaperone interaction (96,97). The N-terminal domain, as stated, is primarily responsible for ATP interaction and binding, and provides the basis of function for HSP90 inhibition(98). The middle domain functions in the role of ATPase activity, interacting with various co-chaperones to define HSP90 function and client binding (99,100). The C-terminal domain terminates with the MEEVD functional motif, characteristically associated

with cytosolic HSP90 and functioning to direct and anchor co-chaperone interaction with the middle domain (101,102).

The binding profile of ATP with HSP90 is considered unusual, in that the interaction with ATP does not occur at the phosphates, but instead with the base and sugar bound in the N-terminal domain, with the γ-phosphate becoming available for hydrolysis after the middle domain associates with the NTD(103). This unique binding motif with ATP affords the advantage of making HSP90 highly and specifically targetable, providing the opportunity for inhibitory research across many diseases, but especially within the realm of cancer research.

1.3.2. Current HSP90 Inhibitors

With the discovery of the larger role of HSP90 as a potential stabilizer for oncogene expression, many groups have sought to find new and effective means of inhibiting HSP90 in a cancer setting. The first molecule discovered to effectively inhibit HSP90 was geldanamycin (GA), a natural product derived from the bacteria *Streptomyces hygroscopicus* in 1970 by DeBoer et al. while searching for new antibiotics(104). However, the HSP90-inhibitive effects of geldanamycin were not profiled until a molecular study of tyrosine kinase inhibitors using benzoquinone ansamycins by Whitesell et al. in 1994, when they found that geldanamycin bound HSP90 both stably and specifically, and eliminated formation of an *src*-HSP90 heteroprotein complex(105). Another natural product, isolated in 1979 from *Penicillium lueo-aurantium* by Nozawa, radicicol was found initially as an antibiotic, but has not seen as much development clinically(106). Both

natural products showed promise pre-clinically, but fell short during clinical trials due to their poor aqueous solubility, limited stability *in vivo*, and severe hepatotoxicity(107).

However, derivatives of these natural products have shown clinical value. 17-AAG, an allyl amino GA derivative, showed less toxicity and potent *in vivo* activity through client protein depletion and Heat Shock Factor 1 (HSF1)-dependent HSP induction, but had limited solubility which created formulation problems(108–110). 17-DMAG, another GA derivative, improved upon 17-AAG's water solubility problems, making it administrable both orally and intravenously, while also showing lower toxicity and greater potency(111,112).17-DMAG was also found to be more bio-available through its independence from the need for reductive metabolism of the benzoquinone group by NQO1/DT-diophorase(112). A further list of GA derivatives, all of which have entered clinical trials, include IPI-504, 17-AAG, and IPI-493, but further development has been halted for all but IP-504, citing poor pharmaceutical properties or formulation difficulties(113–117).

1.3.3. Novel HSP90 Inhibitors

The Haystead group out of Duke University has investigated the need for successful HSP90 inhibition that can also be more specifically targeted to cancer in order to avoid wide-scale biologic effects, such as the concern of ocular toxicity and temporary HSP90 inhibition-induced blindness, brought about by degradation of the photoreceptor cell layer and outer nuclear layer of the retina(118–120). HS-10, HS-131, and HS-198 all act to inhibit HSP90 at the ATP-specific pocket on the NTD, but display various properties in order to help determine method of action

and target specificity. HS-10, the parent compound of all derivative inhibitors, is a small, relatively non-polar molecule capable of freely traversing the lipid bilayer and freely inhibiting cytosolic HSP90. This uninhibited traversal has the potential to yield greater inhibitory effect, but may also lead to accumulation in unintended tissues and yield off-target effects.

From HS-10, the Haystead group performed many derivative modifications, adding various functional groups and linking compounds. Of particular interest in my studies is HS-131, characterized by a six-unit PEG linker chain binding the HS-10 parent compound to a fluorescent moiety(121). The PEG chain separates the fluorescent aspect of the compound from the ATP-binding motif, allowing for effective HSP90 inhibition. The fluorescent moiety serves two functions: first, it adds a large, polarized structure to the compound which eliminates the possibility of free traversal across the cell membrane, requiring HS-131 to be endocytosed; second, it allows for the possibility of imaging, providing visualization in the event of accumulation of HS-131 within target cells and tissues. This double-sided aspect of HS-131 lends

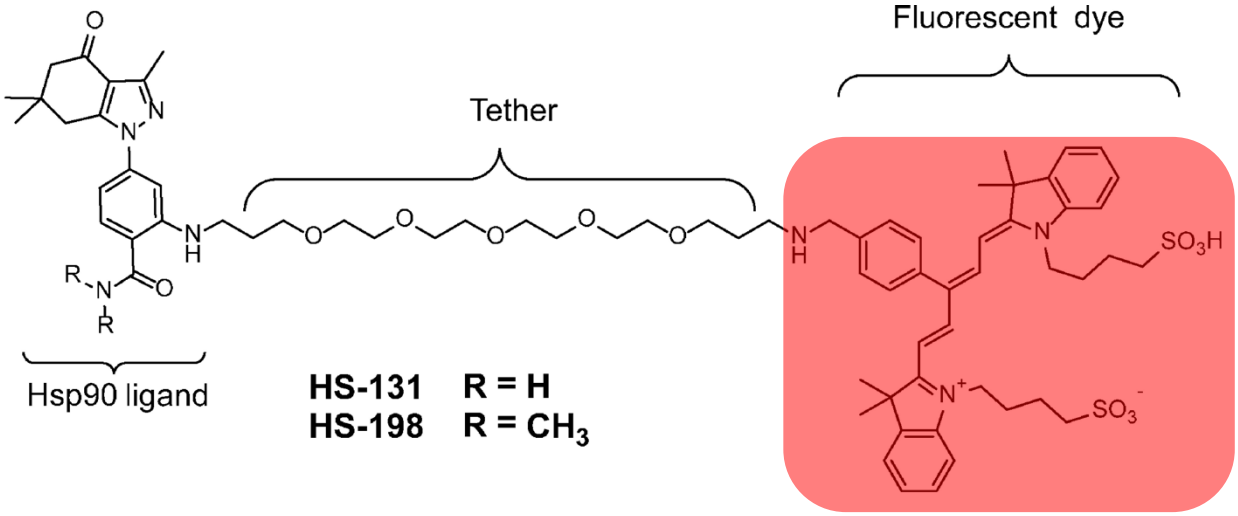

Figure 5. Chemical structure of uninhibited HSP90 inhibitor HS-10, the HSP90-binding ligand, and its derivative compounds HS-131 and HS-198. The addition of a fluorescent moiety lends the therapeutic agent diagnostic properties (83).

itself to the term theranostics, or the ability of a compound to be both therapeutic and diagnostic simultaneously, a property which I will utilize throughout my studies, as will be discussed later.

Finally, HS-198 is a nearly identical derivative compound to HS-131, with the key difference being the substitution of two hydrogen atoms bound to the amine functional group of the HSP90-binding ligand for two methyl groups, as seen in figure 5. This substitution hinders the ability of the ligand to inhibit HSP90 by increasing the steric hindrance of the ligand in such a way that no binding can occur. This removal of functionality allows HS-198 to perform as a negative control; with no HSP90 binding, active endocytosis should not occur, and there should be no distinguishable accumulation within SS cells and tissues. The repeated inclusion of the

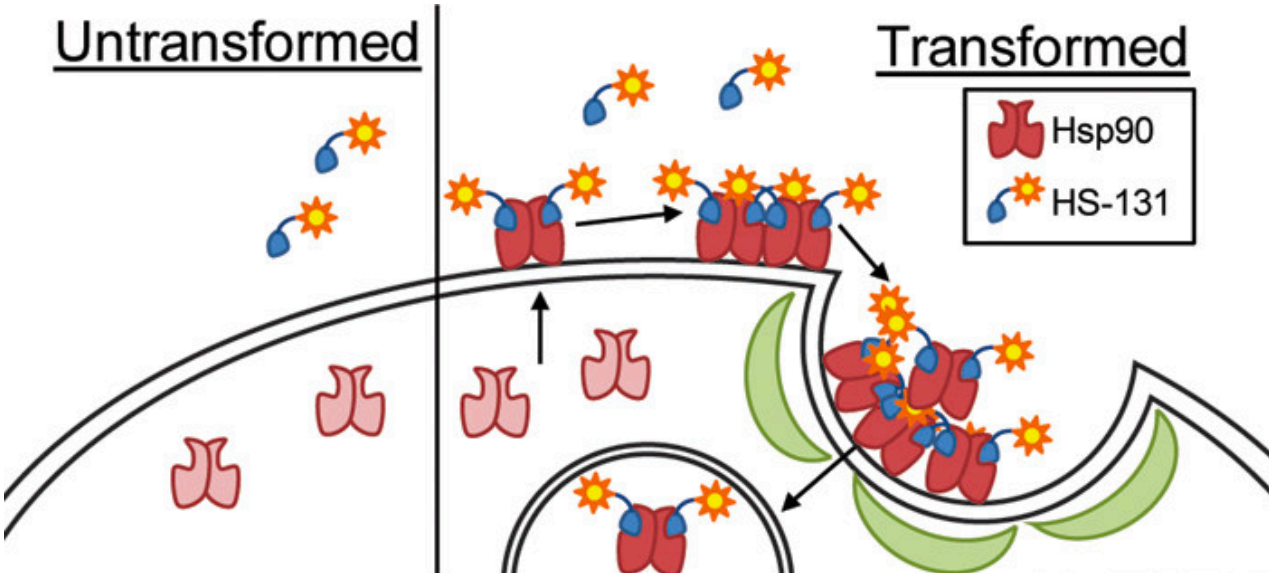

Figure 6. Low stress, untransformed expression of HSP90 on the left, and high stress transformed expression of HSP90, including expression and internalization of HSP90 and subsequent internalization of HS-131 after N-terminal binding. Reprinted with permission from *Crowe LB, Hughes PF, Alcorta DA, Osada T, Smith AP, Totzke J, et al. A Fluorescent Hsp90 Probe Demonstrates the Unique Association between Extracellular Hsp90 and Malignancy in Vivo. ACS Chem Biol. 2017 Apr 21;12(4):1047–55.* Copyright 2017 American Chemical Society.

fluorescent moiety will allow confirmation that accumulation does not occur, as no fluorescence should be measurable.

1.4. 3D Cell Culture and Benefits

While it is known that cells must be in a high-stress or activated state in order to initiate upregulation of HSP90, there remains the question if typical *in vitro* culture conditions are capable of driving HSP90 upregulation. We believe, based on observations discussed within this paper, that traditional two-dimensional cell culture may not be sufficient in order to consistently produce HSP90 upregulation within the cell membrane among synovial sarcoma cultures. Thus, a more robust model capable of replicating *in vivo*, physiological stresses on cancer cells is required to fully capture the most reliable and reproducible *in vitro* modeling.

Three-dimensional cell culture appears to hold the promise of allowing high-throughput screening techniques while still yielding physiologically relevant outcomes. Though not a new technique, 3D culture has gained significant popularity within the last decade as many groups look to overcome the translational disparity between drug screening and clinical trials. The benefits of 3D culture and differences as compared to 2D culture will be reviewed in the following section.

1.4.1. Traditional Culture Techniques and Shortcomings

Traditional cell culture techniques have been established for over a century, and involve taking an existing population of cells from a biological environment, placing them into a sterile

culture flask with supplemented culture media, and allowing the cells to grow in an incubator held at 37ºC and 5% CO_2(122). This technique, with some variations, has allowed for *in vitro* culture and studies of many different primary cancers, which are particularly robust and can adapt to such non-biological conditions. Many cell lines adhere to the bottom of the flask and flatten out before beginning to reproduce across the flask surface. After a number of days, when the cells have reached confluency, the cell culture media is removed and the cells are detached from the flask bottom enzymatically using trypsin or mechanically removed from the flask with a plastic scraper. At this point, cells can be counted and replated to continue proliferation, as well as being partitioned out into smaller well plates to allow for drug interaction studies or other assays(123).

In vitro cell culture has allowed for the elucidation of cell biology, tissue morphology, disease mechanism of action, drug action, and protein production, and have had a critical impact on many preclinical and cancer research studies, as well as studies on gene function(124,125). The adaptability of cancer cells to allow such culture and studies has led to many breakthroughs in chemotherapeutic discoveries and treatment options. And yet, while many new potential treatments have been discovered and started down the path of clinical trials, over 95% of these trials are deemed as failed ventures(126). It is apparent the two-dimensional environment cannot fully replicate the *in vivo* setting in which cancer originates and thrives, and, besides being unable to match the morphological and communication needs of the cells, can in fact lead to aberrations in protein expression observable over long periods of time. One measurable change over time is transcriptional drift. This is a phenomenon where genetic expression of a population

of cells actually alters over time, changing coordination among groups of genes that work together and favoring those cells that may be better suited to survive in a slightly more hypoxic or otherwise less-than-normal environment. The effect of transcriptional drift has been profiled by many groups(127,128), including those in synovial sarcoma(42). Furthermore, two-dimensional cell culture and testing does not allow for free cellular interaction and treatment. As the cells flatten out, there is only a single facet of interaction available, changing cellular functions such as cell adhesion, immune cell interactions, cellular communication, and drug uptake(129,130). The cellular division cycle has been documented to be altered, as well as a loss of phenotypic diversity and cell polarity(131–133). Cultured cells also have uniform access to media, oxygen, and nutrients at the single interface layer, not representative of a true biological system in which gradients of all of these components occur(134).

In spite of these shortcomings, 2D cell culture has continued as the mainstay for *in vitro* studies for a number of reasons; it is a commonly applied and understood practice, and is particularly amenable to high-throughput protocols. Commercially, many supplemented medias and culture dish setups are available that allow the simple addition of cells and media for establishment and outgrowth to occur. This large selection of pre-made components also means a lower operating cost associated with bulk production methods(123,135).

1.4.2. 3D Culture Techniques and Benefits

In contrast, 3D cell culture has only begun to become more widely known, with new techniques and materials becoming available for various cancer types every year. 3D culture is

based on many of the same principles as 2D culture. The primary difference between 2D and 3D culture is the addition of some form of 3D matrix or scaffold, as in figure 7. The most common 3D matrix is currently basement membrane extract (BME), commercially known as Matrigel, a hydrogel that acts to support cells and replicate the *in vivo* environment. Other types of 3D matrix include laminin, collagen, poly-D-lysine (PDL), vitronectin, and alginate. Each of these different matrices provide various stiffness and support profiles dependent on the needs of the cells of

interest. In order to be cultured, cells are suspended in the extracellular matrix (ECM) of choice, Matrigel for this example, which remains liquid when held around 4ºC, and then polymerizes at 37ºC before being submerged in culture media. Different groups have looked into the most efficient method for Matrigel shape and size, ranging from the Clevers group recommending small, 10µL droplets cultured adjacent to each other(136), to the Soragni group's recommendation of "micro" rings plated around the perimeter of each well of a 96-well

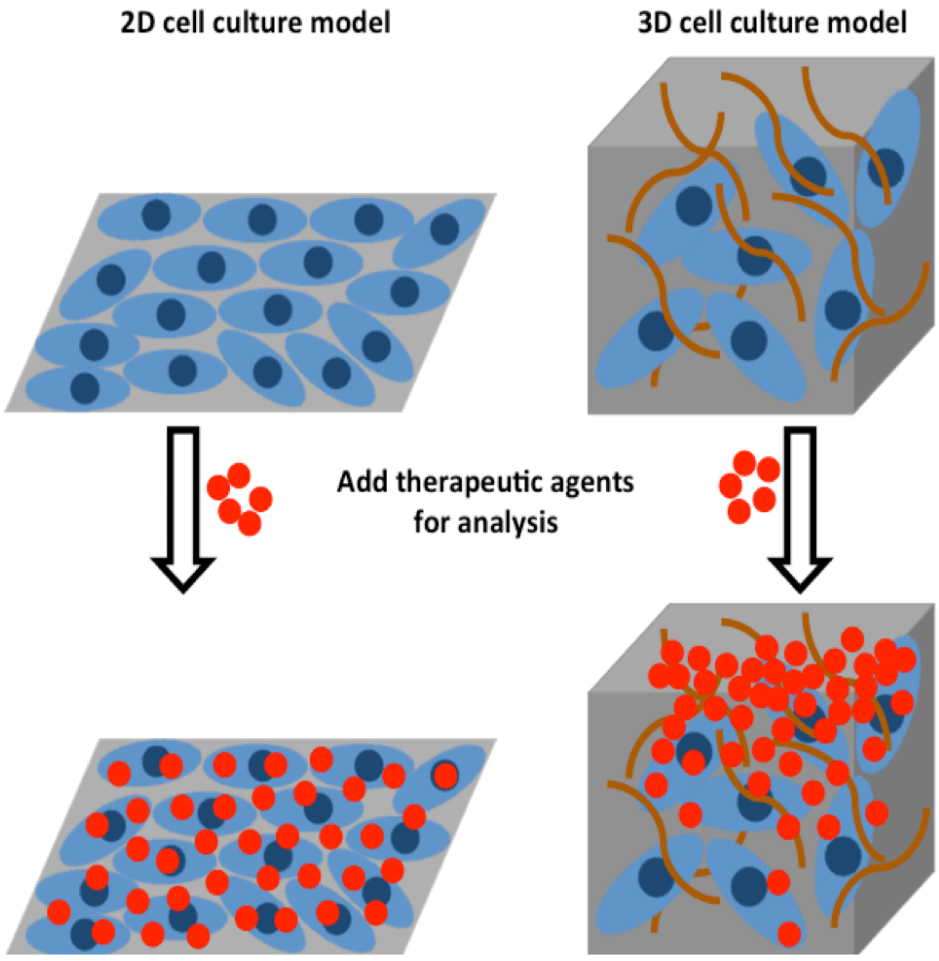

Figure 7. Comparative schematic of two-dimensional and three-dimensional cell culture techniques, demonstrating cellular accessibility (99).

plate(137). Dependent on the type of tissue culture, different chemokines and supplements may also be added to the culture media to encourage growth and cell differentiation and proliferation(138,139). Cultures are then allowed to proliferate in 3D, with media changes every 2-3 days. As cells are now suspended, they are able to retain the morphological shape associated with *in vivo* growth, and can freely send and receive cell-signaling chemicals from every facet. Access to oxygen and growth media is also initially unrestricted, allowing for rapid colonization during culture establishment.

As organoids, or small, tumor-like clusters of cells, begin to develop, a greater concentration of cells in a denser body form than in traditional 2D culture. Centralized, layered points of growth also lead to the development of an organoid core, where access to oxygen and nutrients becomes highly competitive and growth is reduced. The inside of the organoid thus begins to become necrotic, especially with reduced access to oxygen, as seen in the normal tumor environment. This is further exacerbated by only apical delivery of oxygen to the cells, limited by the slow diffusion rate of oxygen into the media(140). In an effort to overcome this obstacle, many groups have developed novel culture protocols designed to continue to provide growth

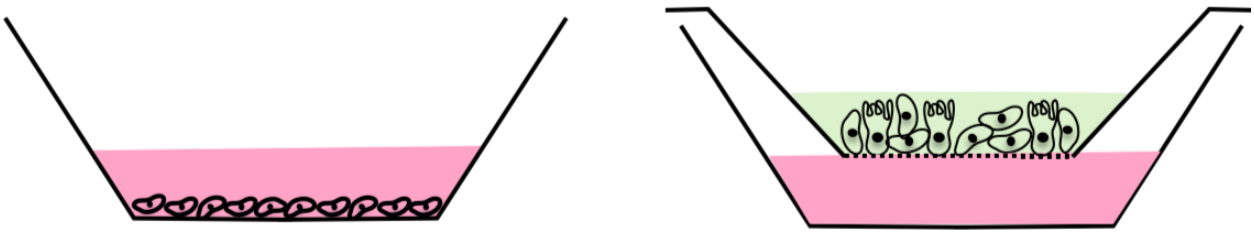

Figure 8. Comparative schematic of two-dimensional, submerged cell culture, left, and the technically demanding air-liquid interface, right (104).

supplements while increasing gas exchange capabilities. Of note is the air-liquid interface (ALI) developed by the Kuo lab, seen in figure 8, in which cell cultures are placed on a liquid-permeable support to culture and suspended just touching the culture media, while left entirely open to air from above(141). The cell culture relies on capillary forces in order to supply nutrients and remain wetted; as such, the culture is very sensitive to changes in liquid level and must be monitored almost constantly.

In order to simplify the rigorous technical demands of the ALI setup, a liquid-liquid interface has also been explored. In this protocol, the 3D matrix remains submerged in culture media, but floats on top of a much denser blood substitute liquid; this liquid has a high diffusion profile for respiratory gases, allowing gas exchange between the interface of the substitute and culture media, as seen in figure 9. Perfusion of the blood substitute moves media through the cell culture, promoting diffusion of oxygen and lower adaptive stress to cell cultures. The liquid-

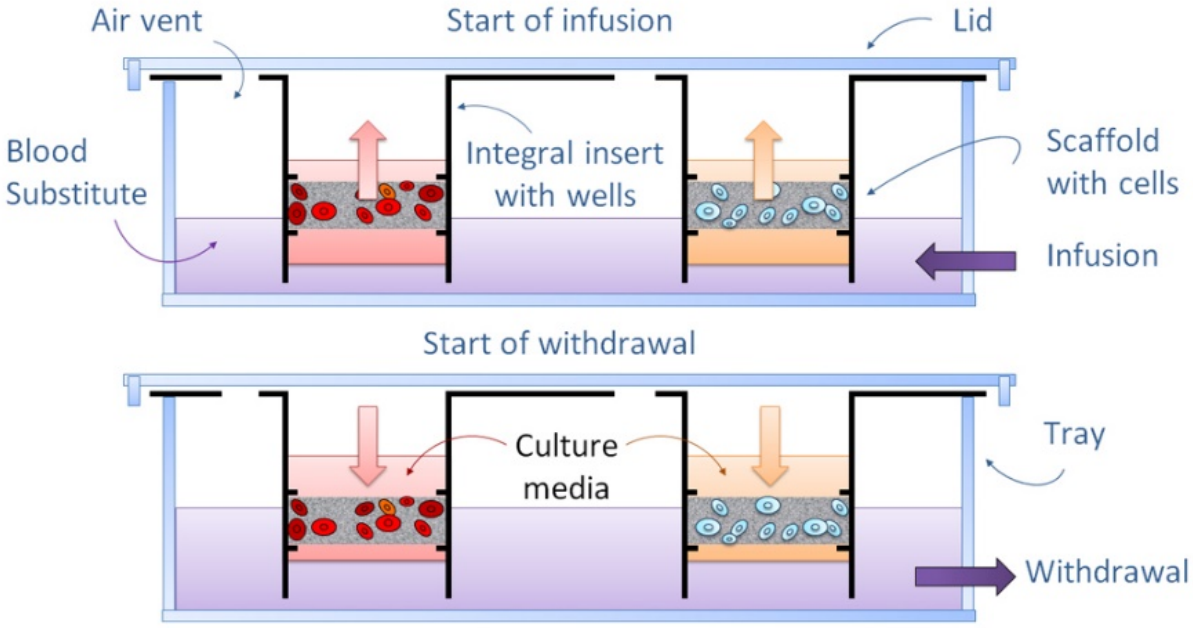

Figure 9. Schematic of Lena Bioscience Perfusion Pal® liquid-liquid interface, which utilizes a high-gas-exchange-rate blood substitute to overcome apical oxygen delivery.

liquid interface (LLI) can be seeded onto directly, or pre-loaded with a BME such as Matrigel on a fiberglass scaffold to encourage 3D organoid formation. Use of the scaffold also allows placement of the culture either on the LLI, at the ALI, or in between, as individual cultures may require(142).

This increased oxygen diffusion has been shown to better maintain dissolved oxygen levels within culture media and to also increase CYP450 enzymatic activity as compared to traditional 2D cell culture methods, yielding more accurate drug screening interactions comparable to an *in vivo* setting(142).

1.4.3. Patient Derived Organoids and Functional Precision Medicine

Primary cell lines, in conjunction with traditional cell culture, have been the standard of drug discovery research for nearly a century, leading to many cancer treatment options being developed without the need for in-human testing. However, it is becoming apparent that primary cell lines derived from donor patients in the past are not a “one size fits all” method for determining the best course of treatment for every patient. As cell culture technology advances and the scientific research infrastructure becomes more robust, many groups are looking to developing direct patient models, or “patient derived organoids” (PDOs).

PDOs are established from a patient biopsy or tumor resection. A portion of the tumor can be digested into smaller fractions and cultured in a 3D matrix intended to mimic the ECM, encouraging formation of tumor organoids. These organoids can then be screened against compounds of interest or new formulations to determine direct patient response. Typical testing

consists of a broad panel of active compounds at a sub-cytotoxic concentration applied to determine if any inhibition occurs. Any compounds which induce a certain threshold of inhibition, i.e., 50% cytotoxic activity, are then singled out and a titration curve assay can be performed to determine optimal treatment concentration, or the IC50. These results can then be communicated back to the patient's healthcare team as alternative or supplemental treatment options for the patient's specific cancer.

The approach of using patient derived material and screening against a broad panel of treatment options to find the most effective response has also been deemed "Functional Precision Medicine" (FPM). In the traditional and frequently current treatment regimens for cancer treatment using chemotherapy, a patient is diagnosed with a certain type of cancer and then assigned a treatment based on said diagnosis; i.e., if you are diagnosed with colon cancer, you are typically treated with 1 of 15 approved treatments, or possibly a combination from those 15. These approved treatments are based on past success in treatment of that type of cancer and then back-applied through genomic profiling. While the completion of the Human Genome Project and the expansion of genomic understanding has advanced treatment for many cancers, the majority of cancers still remain without effective treatment or unexplained relapses(143,144). Coupled with the fact that not every patient responds positively or effectively to their prescribed chemotherapy regimen, it is apparent that there is a considerable amount of information and potential treatment options that are left unexplored.

1.4.4. Epigenetic Contribution to Cell Culture and Screening

There are two prominent contributing factors to the variation of patient response among single treatments: pharmacokinetics and epigenetics(145,146). Pharmacokinetics, or the uptake and movement of drugs through the body, is considered primarily with the aspects of absorption, distribution, metabolism, and excretion (ADME); patient variability in these four branches will clearly have an impact on the efficacy of any therapeutic treatment. However, I will specifically explore the aspect of epigenetics, especially considering the predisposition of SS to alter the epigenetic makeup of the patient's affected cells.

Epigenetics, meaning "in addition to changes in genetic sequence," describe the process and effect of the alteration of genetic expression without actual change in the genetic sequence. These changes determine which genes are considered active and which proteins are transcribed as a result. Considered "silencing," gene deactivation is a common, necessary process in order to avoid overexpression of certain proteins and genes; i.e., gene silencing in female mammals to eliminate a double-expression of X-chromosome gene products. However, gene silencing can also act against the host to repress tumor suppressor genes, induce anemia, or encourage organ overgrowth. Gene silencing can be achieved through three primary pathways: DNA methylation, histone modification, and RNA-associated silencing.

DNA methylation acts to add a methyl group in a highly specific manner, occurring exclusively between cytosine and guanine nucleotides that are phosphate-linked, known as CpG sites. These CpG sites are methylated by DNA methyl transferases (DNMTs), altering the

appearance and structure of the DNA. This modification changes the gene's interaction with histone proteins and transcriptional machinery within the nucleus(147–149).

Histones, or bundles of protein that provide a scaffold to which DNA is wound to create nucleosomes, can also undergo modifications that alter the arrangement of chromatin within the nucleus. These modifications are acetylation, or the addition of an acetyl group to lysine within the histone, and methylation, the addition of a methyl group to the same. Acetylation is typically associated with active chromatin, where the acetyl groups provide repellent forces that prevent chromatin from compacting, thus remaining available for DNA transcription. Deacetylation allows chromatin to compact, complexing to heterochromatin and becoming inactive. Methylation, on the other hand, is associated with both active and inactive domains of chromatin, acting instead as a marker where methylation of a heterochromatin region may mark silent DNA, such as inactivated X chromosomes as discussed above, or on the same histone, may mark active genes on a different lysine. Finally, RNA-associated gene silencing through antisense transcripts, noncoding RNAs, or interfering RNA, all of which can alter gene expression through heterochromatin formation, histone modification, and DNA methylation (148).

1.5. Summary of Introduction and Testable Hypotheses

Thus, we will investigate the impact of HSP90 inhibitors in synovial sarcoma. The presence of extracellular HSP90 will provide a selective target so as to minimize off-target toxicity. HS-131 is an HSP90 inhibitor that depends on the ectopic expression of HSP90 for efficacy. I hypothesize

that metastatic synovial sarcoma will have an upregulated expression of HSP90, revealing ectopic expression at the cell membrane and observable circulation.

With regards to *in vitro* and *in vivo* treatment using HS-131, I hypothesize that there will be selective reduction using HS-131 as compared to HS-10, confirmed by lack of cellular uptake of HS-198. *In vivo* treatments using theranostic HS-131 will act to confirm cellular specificity and proof of inhibitor uptake. I also hypothesize that the effects of HS-131 will be exacerbated in 3D organoid models as compared to 2D cell cultures, as the 3D organoid models recapitulate the tumor microenvironment seen in patients and genetically engineered mice with synovial sarcoma. By studying the impact of HS-131 in 3D organoid models, effects such as transcriptional drift and epigenetics can be adequately addressed to overcome potential mechanisms of resistance and translate success clinically. I also hypothesize that the presence of heterotopic ossification will lead to a worse prognosis and decreased likelihood of survival in correlation with synovial sarcoma diagnosis.

2. Methods and Materials

2.1. Mice Ossification

Mouse ossification experiments were conducted with the approval of the Institutional Animal Care Committee in accordance with legal and ethical standards established by the National Research Council and published in the Guide for the Care and Use of Laboratory Animals. The previously described Rosa26-LSL-SS18-SSX2 mice were maintained on a mixed strain background, C57BL/6 and SvJ(43). Mice were genotyped with the following primers: Rosa26-LSL-

SS18-SSX2 (F flox - AAACCGCGAAGAGTTTGTCCTC, F wt – GTTATCAGTAAGGGAGCTGCAGTGG, R - GGCGGATCACAAGCAATAATAACC). TATCre was dosed by 10 µL intramuscular injections at 50 µM at 1 month of age.

2.2. Histology

Mouse tissues were fixed in 4% paraformaldehyde overnight, and embedded in paraffin. Paraffin-embedded tissues were stained by immunohistochemistry by rehydrating slides through a citrosolv and ethanol dilution wash. Hematoxylin and eosin staining was performed as previously described(41).

2.3. Transcriptome Analyses

Total RNA was isolated with the RNeasy mini kit (QIAGEN). For transcriptome sequencing of TATCre tumors, RNA was prepared using the Illumina TruSeq RNA kit (Illumina), checked with the Bioanalyzer RNA 6000 chip (Agilent Technologies), captured using the RiboZero method (Illumina), and 50-cycle end-read sequenced on an Illumina HiSeq 2000. Reference fasta files were generated by combining the chromosome sequences from mm10 with splice junction sequences generated by USeq (v8.8.8) MakeTranscriptome using Ensembl transcript models (build 74). Reads were aligned with Novoalign (v2.08.01), allowing up to 50 alignments per read. USeq's SamTranscriptomeParser selected the best alignment for each and converted the coordinates of reads aligning to splices back to genomic space. Differential gene expression was

measured using USeq DefinedRegionDifferentialSeq, which counts the number of reads aligned to each gene and then call DESeq2 (v1.4.5) using default settings.

For NanoString gene expression analysis, RNA was isolated from three different tumor cell populations: GFP+, CD11b+/Ly6C+/Ly6G+, and CD11b+/Ly6Cmid/F4-80+/MHC IIhigh. 10 ng of RNA was combined with the mouse immunology panel of 545 gene probes and analyzed on the nCounter (NanoString).

2.4. Statistics and Analysis

Genes of interest were selected from a list of bone development genes that were then verified to have bone expression using https://www.genecards.org/. After confirming the gene, the expression was checked under the TISSUES section. Any genes that had expression in bone or bone marrow were selected as genes of interest.

The Pten loss-induced tumor group (n=5) and muscle tissue group (n=3) were sampled and tissues processed to determine gene expression. FPKM, Log2, and Adjusted P values were obtained from analysis, and results were ordered by highest to lowest Adjusted P value. Using these FPKM values, a heatmap was generated for all genes of interest.

Shared genes of interest between metastatic vs muscle and metastatic vs nonmetastatic tissues were found by sorting columns alphabetically and finding the overlap, then plotted using Adobe Illustrator in an area-proportional Venn diagram showing the overlap of genes shared between both groups.

Human tumor sample data sets were accessed using NCBI GEO, Series GSE54187, from Stanford University Department of Pathology. Gene expression data was extracted and analyzed using an unpaired t-test to determine if statistical significance between metastatic and nonmetastatic tumor samples existed for each gene of interest.

NanoString data was analyzed for significance by averaging fluorescence signal from tumor cells (n=4) and MDSC cells (neutrophils, macrophages, monocytes, n=8) for ossifying genes and performing a one-way ANOVA to determine statistical significance, verified with a post-hoc unpaired t test.

2.5. *In vitro* Culture and Testing

Human Yamato and HSSY-II synovial sarcoma cell lines as well as SJSA-1 and U2-OS osteosarcoma cell lines were maintained in RPMI with 10% FBS and 1% penicillin/streptomycin. For *in vitro* analysis, cells were plated at 1.00 x 10^4 cells/well and were treated via serial drug dilution with drug concentrations of 10µM, 5µM, 2.5µM, 1µM, 0.5µM, 0.25µM, 0.1µM, 0.05µM, 0.025µM, and 0.01µM HSP90 inhibitors and 100nM, 50nM, 25nM, 10nM, 5nM, 2.5nM, 1nM, 0.5nM, 0.25nM, and 0.1nM doxorubicin hydrochloride (MedChem Express HY-15142), delivered via a Dispendix iDOT liquid handler.

2.6. Resazurin Toxicology Assay

For cell viability assays, 10µL of Resazurin Toxicology solution (Sigma-Aldrich TOX8-1KT) (0.05 mg/mL) per 100uL of culture media was incubated at 37ºC with treated cells for 2 hours.

Analysis was performed using a multimodal Varioskan Lux in fluorescence mode at wavelengths of 560 nm excitation, 590 nm emission. Each inhibitor was tested in triplicate against doxorubicin.

2.7. Western Blot Analysis

Cells were collected after passaging, spun down to a pellet, and media decanted. Pellet was then resuspended in mild cell lysis buffer, 300uL for every 1 million cells, and centrifuged at 4ºC, 12,000 rpm for 10 minutes. Supernatant was collected and stored separately, and pellet was resuspended in 200uL of RIPA buffer with proteinase inhibitors, then centrifuged again for another 10 minutes. RIPA supernatant was also collected in another separate microcentrifuge tube. Protein concentrations were measured using a Qubit analyzer and Qubit Protein BR Assay Kit (Thermofisher A50668). Samples were diluted as needed to 50 ug total protein concentration (1ug/uL) with 10uL of 5x SDS and enough ultra-purified water to make a total volume of 50uL. Samples were then placed in a Thermocycler at 95ºC for 10 minutes.

Samples were loaded in a submerged 4-12% tris-glycine gel plate that had been loaded in a western blot electrophoresis chamber, with 6uL protein ladder in the second well and samples loaded sequentially after that. After loading, 100V potential was applied until samples migrated out of loading wells, and then increased to 160V and monitored until protein ladder had reached ~85% to bottom of the gel. Proteins were transferred to PVDF membrane by applying 100V potential for 1 hour. Primary antibody solution was prepared in 5% milk/PBT, 1:1000 PBT/milk to antibody. After transfer, membrane washed with PBT solution with shaking for 10 minutes, then

replaced with PBT/milk and washed with shaking for 1 hour. After 1 hour, PBT/milk was replaced with 1:1000 primary antibody solution, shaken for 1 hour, then placed in the fridge overnight.

The next day, primary antibody solution was collected and replaced with PBT, then shaken for 5 minutes, dumped, and repeated twice more. A 1:10,000 secondary antibody/HRP solution was prepared in PBT/milk and applied to membrane, then shaken for 1 hour. After 1 hour, membrane was washed with shaking using PBT for 5 minutes each three times. Chemiluminescent Radiance Q kit was applied according to packaged instructions and incubated for 2 minutes. Membrane was then imaged on an Azure Biosystems c600.

2.8. ELISA Kit Analysis

HSP90 detection in serum was performed using a Proteintech Colorimetric Sandwich ELISA Kit (KE00054) using serum samples from genetically engineered mice with and without TATCre induced tumors. The standard curve was prepared by reconstituting lyophilized standard with 2mL of included sample diluent, followed by six 1:1 serial dilutions to obtain seven standard points along the curve. Blood was collected from freshly euthanized mice by drawing from the vena cava. Blood was placed in EDTA-coated tubes and centrifuged at 1200 rpm for 15 minutes. The clear supernatant was transferred to a new tube. After reaction with HSP90 detection antibody and HRP-conjugated antibody, standards and samples were washed and exposed to TMB substrate. Standards and samples were read using a Varioskan Lux in absorbance mode at 450 nm. Statistical analysis of each data set was performed using one way ANOVA, followed by a post-hoc analysis using an unpaired t test.

2.9. Dose-Response and Cell Viability Analysis

After fluorescent readout was measured via Resazurin assay, baseline measurements were subtracted by averaging the negative control values and subtracting from all wells. Positive control values were then averaged and divided into each sample and converted to percentage to determine cell viability within each sample. After averaging values from each triplicate sample, Graphpad Prism was employed to generate heatmap representations for cell viability readouts.

2.10. *In vivo* Testing and Animal Models

All procedures were approved by the Idaho State University Institutional Animal Care and Use Committee protocol 757 and 775. The mouse models used in these experiments were the Rosa26-LSL-SSM2/SSM2 (Previously described Halder et al.(40)) which contains the SS18-SSX2 fusion oncogene and is termed non-metastatic, and the Rosa26-LSL-SS18-SSX2/SS18-SSX2;*Pten*lox5/lox5 (Previously described Barrott et al. (41)) which contains the SS18-SSX2 fusion oncogene as well as a TATcre mediated *Pten* removal mechanism and is termed the metastatic model. Mice were bred and weaned at 21 days of age. At one month, mice received a subcutaneous 10uL injection of 50uM TATcre protein (Excellgen Cat. # EG-1001) into the left hind limb to initiate sarcoma pathogenesis. The site of injection was sterilized topically with 70% ethanol prior to injection to reduce the risk of infection. Mice were monitored for tumor development and typically developed tumors between 2-4 months. Mice were monitored for signs of distress, ulceration or difficulty ambulating secondary to tumor growth and euthanasia

was employed in these cases. All 38 mice were euthanized at the end of the study after achieving morbidity. Both male and female mice were used in all studies.

Accumulation studies were performed after tumors achieved a volume of 200 mm^3, after which mice were injected intraperitoneally with 50 mg/kg of HS-131 inhibitor

Tumors were allowed to develop until reaching a volume of 200 mm^3, which occurred approximately at 4-6 months of age. Average starting tumor volume of all mice treated was 397.0 ± 260.6 mm^3. Cohorts were established to be treated with doxorubicin hydrochloride, HS10, HS131, HS198, HS10 with dox, HS131 with dox, HS198 with dox, dox only, and saline-injected vehicle control, that were treated 3 times a week with their respective HSP90 inhibitor and once a week with doxorubicin for 28 days. Mice were treated with 5 mg/kg doxorubicin hydrochloride in PBS, 5 mg/kg HSP90 inhibitor HS-10, HS-131, or HS-198 in PBS, or a combination of doxorubicin and one HSP90 inhibitor via tail vein injection for doxorubicin or IP injection for the HSP90 inhibitors, per current field established protocols. Sterile PBS was utilized for all control groups. For HSP90 inhibitors, doses were given intraperitoneally three times a week for 28 days or until the tumor ulcerated or reached a volume exceeding 1500 mm^3. For doxorubicin hydrochloride, doses were initially delivered via tail vein injection, but changed to intraperitoneally once a week for 28 days or until the tumor ulcerated or reached a volume exceeding 1500 mm^3 hydrochloride. Reasoning for the change in delivery was the development of large areas of scabbing around the tail vein injection site, causing discomfort for the mice.

Motility becomes hindered after tumor volume exceeds 1500 mm^3, which is deemed inhumane according to established mouse protocols and mice are considered to have reached

morbidity. After 28 days, treatment was discontinued and tumor sized continued to be monitored with digital calipers. Tumor volumes were calculated using the formula: tumor volume = length $\times$ width^2/2.

2.11. Organoid Culture Media Preparation

Gibco AdDMEM/F12 growth media (Gibco™ 12634028) must be supplemented with 1% penicillin-streptomycin (Atlanta Biologicals, B21110), 10mM HEPES buffer, and 1X GlutaMAX(100X) supplement (Gibco™ 35050061) in order to encourage organoid growth and expansion. 5mL pen-strep, 500uL 1M HEPES buffer, and 5mL GlutaMAX were added to 500mL of AdDMEM/F12 growth media to prepare the AdDMEM/F12+++ formulation.

2.12. Mouse and Patient Tumor Digestion and Proliferation

For mouse models, after mice were euthanized, tumors were excised, weighed, and then diced into 1-3mm^3 portions before being placed into a 15mL conical tube with 200uL of trypsin EDTA 0.125%, 3uL ROCK inhibitor, and 3mL AdDMEM+++ growth media. The conical tube was then incubated at 37ºC for 45-60 minutes, with agitation every 15 minutes by pipetting up and down with a P1000 pipet tip, with 5mm cut off from the end to avoid clogging, to aid in tissue breakdown. After 45 minutes, a 10uL aliquot was taken from the digestion tube and observed under magnification to determine if cell clumps of roughly 3-10 cells are observable. If cell clumps appear too large, the sample digestion was continued for another 15 minutes and aliquoted for observation once more.

Once digestion has finished, the sample was topped to a volume of 10mL with ice-cold AdDMEM+++, then centrifuged for 5 minutes at 4ºC and 225xg. Supernatant was aspirated, and the pellet was resuspended in another 10mL of ice-cold AdDMEM+++. Using a 100um cell strainer, the suspension was filtered, collecting the filtrate into a new 15mL conical tube and centrifuging as before, aspirating the supernatant. The resultant pellet was resuspended in 1mL of AdDMEM and cell count was performed using trypan blue exclusion. Cells were then suspended in Corning Matrigel (Corning 356231) or another equivalent BME at a concentration of 250,000 cells/mL, making sure Matrigel concentration did not fall below 8mg/mL.

Using a 24-well culture plate pre-warmed a minimum of 1 hour at 37ºC, 10uL droplets were dispensed in the plate, 3 per well with ample distance so the droplets didn't merge, using a 10uL pipettor. After plating the droplets, the plate was quickly inverted to avoid cells settling to the plate bottom, and placed in the cell incubator at 37ºC for 30-60 minutes to allow Matrigel to polymerize. Once droplets were set, the plate was removed and up-righted, and the droplets were covered with 500uL of AdDMEM+++ supplemented with 10uM ROCK inhibitor and 100ug/mL primocin pre-warmed to 37ºC to minimize Matrigel breakdown. The plate was then placed in the incubator cabinet. Organoid establishment was determined over the next three days, observing for cellular outgrowth, and media changes performed every 3-4 days.

When 85-90% confluency was attained within the majority of Matrigel droplets, or multiple large organoid clusters were observable, organoid splitting was performed. Droplets were displaced from the well bottoms using a P1000 pipettor, and the entire solution was pipetted up and down ~10 times to encourage Matrigel breakdown. Media and cells were

collected into a 15mL conical tube, no more than 3mL per tube, and topped to 10mL with fresh, ice-cold AdDMEM+++ and centrifuged as before. Supernatant was aspirated and pellets resuspended in 1mL of TrypLE Express Enzyme(1X) (Gibco™ 12605010) then incubated at 37ºC for 5 minutes, followed by agitation with a P1000 tip topped with a P10 tip to help organoid dissociation. Organoids are then washed and centrifuged once more with 10mL AdDMEM+++ and suspended in Matrigel for further proliferation or drug screening.

2.13. Tumor Organoid Drug Screening

After splitting and resuspension into Matrigel, organoids were plated in 96-well plates, one droplet per well, and topped with 100uL AdDMEM+++/Primocin. Organoids were cultured for 2-3 days to allow recovery and establishment, then treated as described above using HSP90 inhibitors and doxorubicin hydrochloride or a custom 131 FDA-approved drug panel consisting of various methods of therapeutic potential.

After treatment has been applied for 72 hours, media was replaced with a solution of 1:1 CellTiter-Glo 3D:media (Promega G9681) and incubated for 30 minutes at room temperature or 10uL of 0.05 mg/mL Resazurin were added, and measurements were performed using a Varioskan Lux.

2.14. Perfusion Pal Scaffold and Organoid Establishment

The LLI system was provided by Lena Biosciences. The Perfusion Pal® system consists of a syringe pump which can be programmed to oscillate between two set volumes (Lena Biosciences,

LBS1002), a 48-well insert and holding tray (Lena Biosciences, LBS1004), the blood substitute (Lena Biosciences, LBS1009), and the SeedEZ scaffolds (Lena Biosciences, LBS1014). 93mL of blood substitute was added to the tray and drawn into a 50mL syringe through a length of silicone tubing. The syringe was held upright and slowly depressed until all air bubbles were removed and pushed through the tubing until a volume of 5mL is obtained within the syringe. The scaffold insert was then placed into the tray.

Scaffolds were prepared by placing scaffolds onto an empty 96-well plate to reduce surface contact. 40uL of Matrigel were placed onto each scaffold and allowed to absorb into the scaffold. The plate was then loosely covered to avoid contamination and transferred to the cell incubator cabinet to allow Matrigel to polymerize at 37ºC for 30 minutes. After polymerization, scaffolds were then placed into the 48-well insert at a slight angle before lying flat just on the surface of the blood substitute, in order to minimize air being trapped below the scaffold. Empty wells were filled with 240uL sterile PBS to provide equal pressure across the plate and minimize the effects of Pascal's law.

200uL of freshly passaged cells or organoids were then added at a concentration of 30,000 cells/mL AdDMEM+++ media. The entire well plate was then placed in the incubator cabinet, with tubing leading outside the cabinet to the syringe. The syringe was attached to the syringe pump, and the oscillating program was initiated to withdraw and infuse 17mL indefinitely, with a flow rate of 0.047mL/min, or 16 volume changes per day.

Imaging was performed by addition of NucBlue nuclear stain and Calcein AM live-cell dye on the Molecular Devices ImageXpress Pico to determine cellular outgrowth. Results were compared to Matrigel-embedded organoids to determine relative outgrowth efficiency.

3. Results

Overall analysis of synovial sarcoma proved the potential for viable targeting strategies to be considered. *In vitro* and *in vivo* analysis of HSP90 inhibitors and their effects synergistically have yielded great response. Establishment and expansion of 3D tissue cultures has also been deemed as successful, with 3D cultures able to be generated from both single cell suspensions and fresh resected tissues. I will cover these results in more detail below.

I propose the following hypotheses:

1. Ossification within SS tumors will yield poorer patient prognosis and decreased likelihood of survival.
2. RNA expression of HSP90 will be significantly upregulated within SS tissue, both metastatic and non-metastatic, as compared to normal muscle tissue.
3. HSP90 protein will be expressed ectopically within the cellular membrane of metastatic SS tissue as compared to non-metastatic SS tissue.
4. Circulating HSP90 will be observable within blood samples obtained from metastatically-induced mice compared against non-metastatic and non-diseased mice blood samples.

5. Synergistic treatment effects will be observable in treatment with novel inhibitor HS-131 and doxorubicin hydrochloride as compared to treatment with doxorubicin hydrochloride.
6. Specific cellular targeting will be achievable through the proposed mechanism of HS-131 cellular uptake in metastatic samples compared to non-metastatic samples.
7. Combinatorial treatment with inhibitor HS-131 and doxorubicin hydrochloride will slow and reduce tumor growth within an *in vivo* setting in diseased mice as compared to mice treated with vehicle only.
8. 3D culture and therapy will yield more physiologically relevant, translatable results as compared to 2D cultures of equivalent cells.

3.1. Ossification and Prognosis Analysis

This portion of the study included 463 mice with some variant of synovial sarcoma. The four subcategories consisted of homozygous expression of SS18-SSX1 (hss1) (n-88), heterozygous expression of hss1 (n=94), homozygous expression of SS18-SSX2 (hss2) (n=124), and heterozygous expression of hss2 (n=157). All mice concomitantly expressed *Pten*, with deletion occurring spatial via TATCre injection into hindlimbs to drive sarcomagenesis. Mice were observed for tumor growth and spontaneous ossification observed via palpitation and tissue sectioning with staining.

3.1.1. Gross and Histological Analysis of Mouse Synovial Sarcoma

First observations were made upon tumor resection during necropsy on whether tumors exhibited unusual hardness or bone-like structures. Tumors were then observed after histological staining with hematoxylin and eosin (H&E) staining for presence of ossification.

As observed in figure 10, Ossification was identified by the presence of eosinophilic (pink) uncalcified boney matrix (i.e., osteoid) with some regions exhibiting basophilic (purple) calcium

salt deposits. Out of the 463 mice observed, only 33 (7.1 %) demonstrated these ossification characteristics.

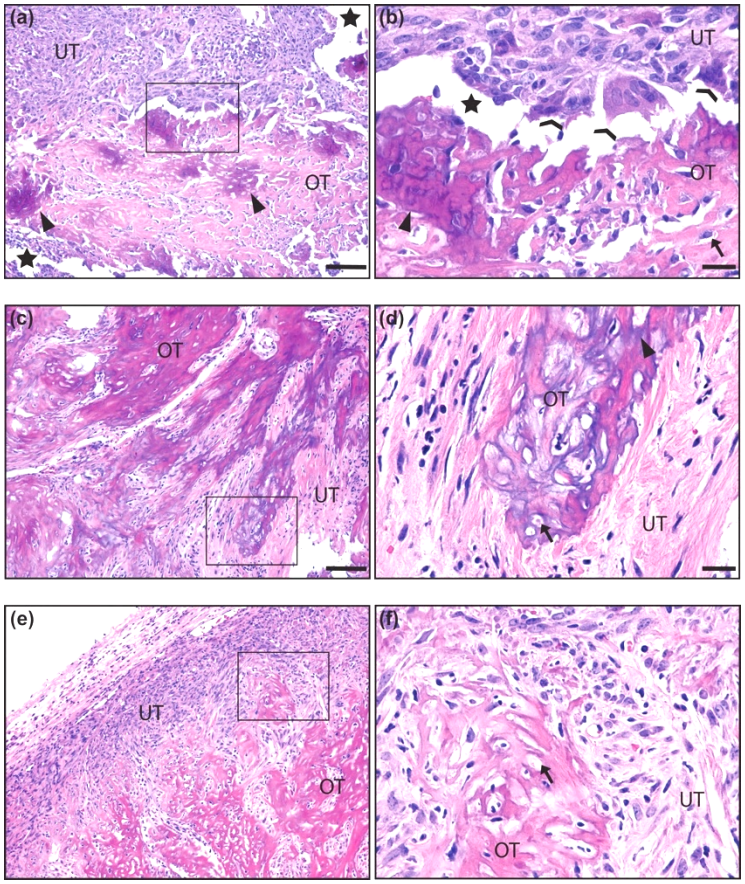

Figure 10. Histological representation of ossification in mouse synovial sarcoma. (**a-b**) 10 X and 40 X insert of synovial sarcoma with ossified tumor matrix (OT) exhibiting calcium salt crystals (purple) embedded in osteoid (pink). The unossified tumor matrix (UT) contains sarcoma cells that are more epithelioid in appearance, and two osteoclast-like multinucleated giant cells are seen at the interface of the ossified matrix (**c-d**) 10 X and 40 X insert of synovial sarcoma with a more extensively calcified matrix interfaced with spindle-shaped tumor cells that are loosely packed in a fibrous stroma. (**e-f**) 10 X and 40 X insert of synovial sarcoma with uncalcified osteoid matrix interfaced with a dense population of spindle-shaped tumor cells embedded in a fibrous stroma. Scale bars in the 10 X images = 100 µm and scale bars in the 40 X images = 20 µm. OT = Ossified Tumor, UT = Unossified Tumor, Arrow = lacunae, Arrowhead = calcium salt deposits of ossified tumor matrix, Chevron = osteoclast-like multinucleated giant cells, Star = artificial space at the interface of ossified and unossified tumor matrix.

3.1.2. Differences in Ossification Phenotype Between Heterozygous and Homozygous Fusion Gene Expression

Heterozygous expression of either hSS1 or hSS2 had a higher prevalence of ossification compared to the homozygous group, 13.8% and 10.2%, respectively (figure 11a). Mice homozygous for either gene became moribund at 8.3 weeks after TATCre injection, before ossification could occur (figure 11b-c) ($z = 6.54$, $p < 0.001$).

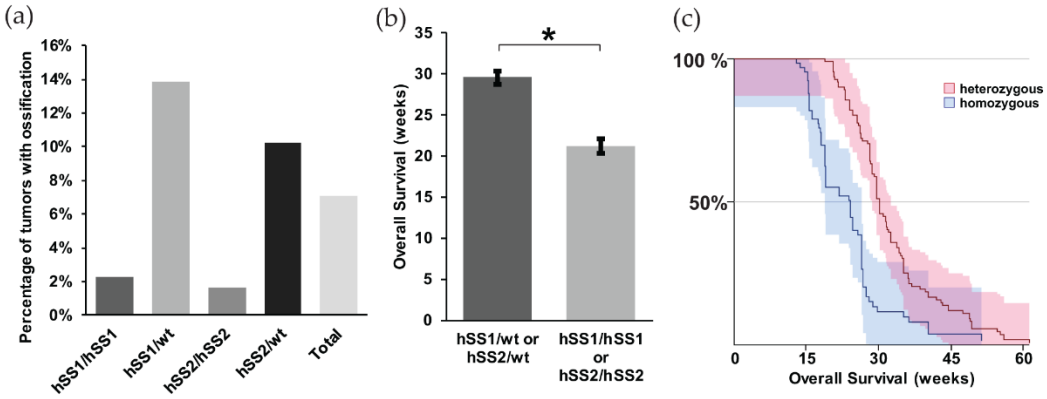

Figure 11. Prevalence of ossification within mouse synovial sarcomas. Representative bar graphs of: (**a**) percentage of mice showing evidence of ossification among heterozygous (n = 251) and homozygous (n = 212) phenotypes of *hSS1* and *hSS2*. Only 7.1% of total mice exhibited ossification through palpitation; (**b**) overall survival of heterozygous and homozygous genotypes in weeks, demonstrating heterozygous phenotypes to have a higher survival rate than homozygous genotypes; (**c**) and Kaplan Meier Survival curve of heterozygous and homozygous genotypes. Shaded area represents 90% CI.

3.1.3. Bone Reactivity Detected by Radiography at a Higher Incidence than Histological Ossification

Fifty random synovial sarcomas on 31 mice were radiographically imaged to assess gross interactions between the bone and the tumor. Some of the mice had bilateral tumors in the hindlimbs. It was observed that 72% of the metastatic sarcomas that express heterozygous hSS1 or hSS2 exemplified abnormal bone inflammation or direct growth and interaction at the surface of the bone. (figure 12, Table 2).

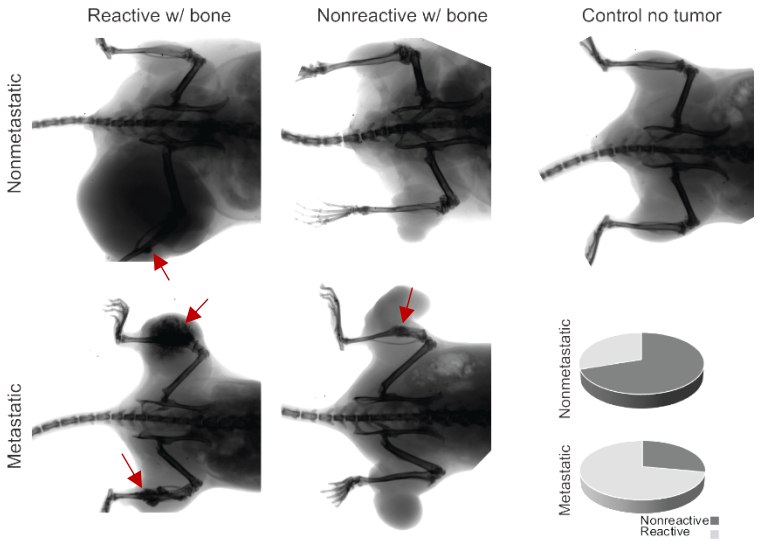

Figure 12. Radiographic imaging of metastatic and nonmetastatic mice with development of ossifying tumors, showing bone inflammation (red arrows) and interaction or lack of interaction for both groups. Control demonstrates lack of ossification in healthy mouse model, and pie charts indicate proportionality of reactivity in nonmetastatic mice (30%) and metastatic mice (72%).

The hSS1/hSS2 heterozygous metastatic categories exhibited a mean 11.6% penetrance of the ossification phenotype upon gross and histological examination (figures 10 and 12). Within the 10 nonmetastatic synovial sarcomas imaged, only three displayed bone interaction; this

interaction was also neither as extensive nor invasive as seen in the metastatic model (figure 12). Using a Fisher's Exact Test, we determined that this was significantly lower than the 72% seen in the metastatic model (p-value = 0.024) (Table 2).

Table 2. Fisher's Exact Test comparing number of tumors with bone interaction between nonmetastatic and metastatic synovial sarcomas.

	Non-reactive with bone	**Reactive with bone**
Nonmetastatic synovial sarcoma	7	3
Metastatic synovial sarcoma	14	36

3.1.4. Underlying Gene Expression of Bone Development Genes in Metastatic Model of Synovial Sarcoma

RNA expression was analyzed for 65 genes involved in osteoblast differentiation. Enrichment of osteogenic genes of interest were observable for nearly all bone development genes in all sarcoma tissues, with no upregulation of these genes detected in any of the muscle tissue (figure 13a).

Using a p-value cut off of <0.05 that was corrected for multiple hypothesis testing, 46 genes were identified that were significantly upregulated between the normal muscle tissue and the primary synovial sarcomas from the metastatic model. A similar comparison of gene enrichment was conducted between primary tumors from non-metastatic and metastatic mice, and 26 bone development genes were detected that were upregulated in the tumors from the metastatic model.

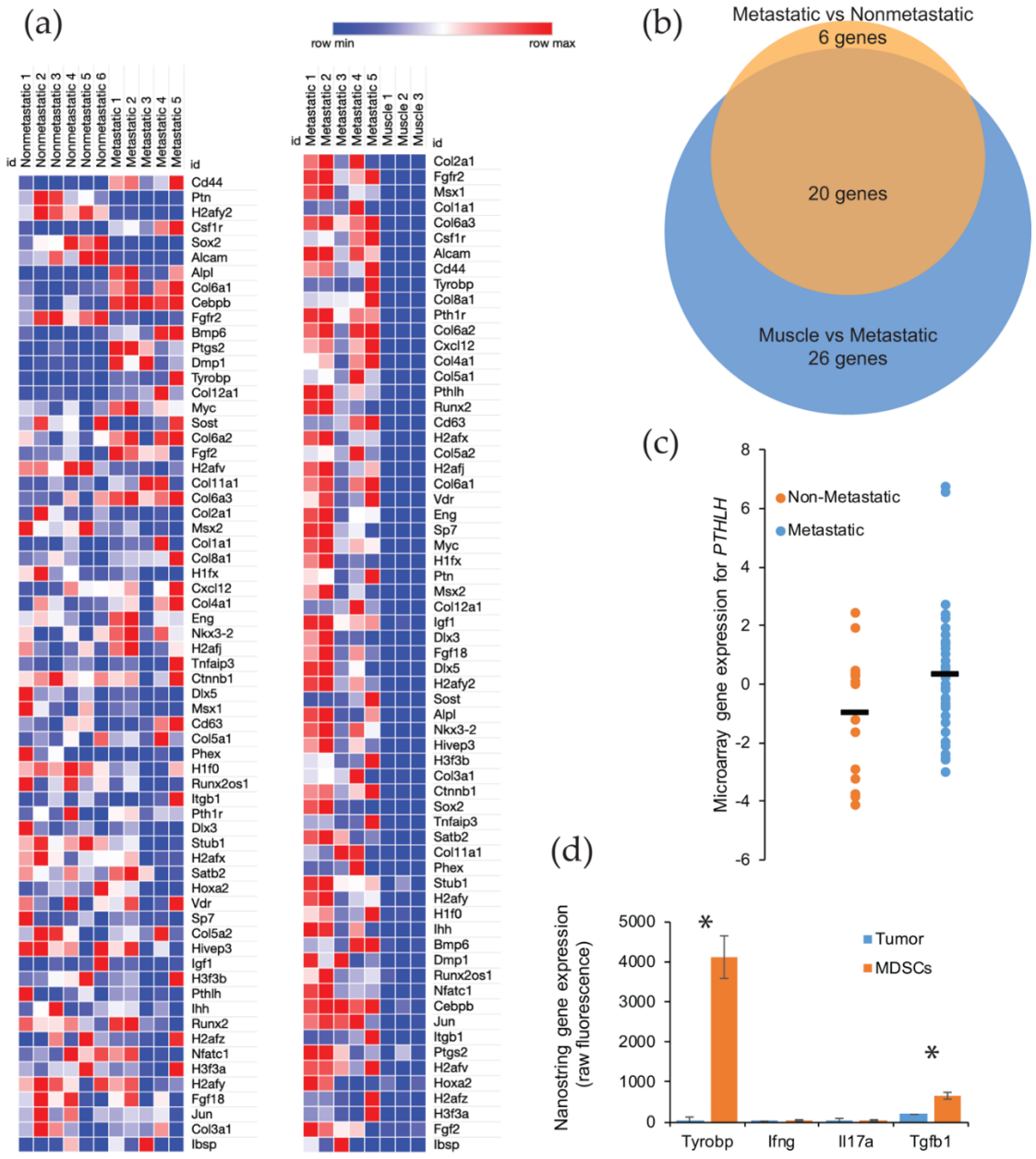

Figure 13. Gene expression of ossification genes found upregulated in mouse and human metastatic synovial sarcoma. (**a**) Heatmap showing RNA expression and upregulation (red) or downregulation (blue) of bone development genes in *Pten* loss-induced tumors comparing nonmetastatic to metastatic (left) and metastatic to muscle tissue (right); (**b**) 46 genes were analyzed and determined statistically different between metastatic and normal muscle tissue by an adjusted p-value threshold of < 0.05. Venn diagram representing statistically significant bone development genes from nonmetastatic vs. metastatic samples (orange, 26 genes) and muscle vs. metastatic samples (blue, 46 genes) showing overlap of 20 genes of interest between groups; (**c**) Comparison of nonmetastatic to metastatic human synovial sarcoma sample expression of

PTHLH, showing spread and mean (bar) of each group. Statistical significance was found with regards to upregulation of *PTHLH* in metastatic tumors in these patients. p-value = 0.039; (**d**) After fluorescence activated cell sorting, NanoString sequencing was performed to identify gene expression for secreted proteins involved in ossification that were unique to myeloid derived suppressor cells (MDSCs).

Using the NCBI GEO Dataset GSE54187, human synovial sarcomas were bifurcated into nonmetastatic (n = 15) and metastatic (n = 42). The 47 genes identified in the mouse comparison were analyzed across the human tumors, and only one gene was found to be significantly different: parathyroid hormone-like hormone (*PTHLH*) (p=0.0391, 95% CI=−2.56 to −0.068) (figure 13c). We also measured signals from the sorted populations by NanoString sequencing and found several genes that were uniquely expressed in the MDSCs and have a functional history in ossification (figure 13d). The gene that represented the largest enrichment in MDSCs (130-fold) was *Tyrobp* (p=0.0006). Other genes that were identified as potential sources of ossification were *Ifng*, *Il17*, and *Tgfb1*(150). All of these exhibited a 4-fold enrichment over the tumor cells, but only *Tgfb1* was statistically significant (p=0.0076).

3.1.5. Gross Metastasis is Loosely Correlated with the Presence of Ossification, But Survival is More Favorable in Mice with Ossification

When compared, the fraction of metastatic mice between sarcomas with and without ossification indicated that gross metastasis increased from 42% to 65% in synovial sarcomas with ossification. However, the statistical analysis by a Fisher's Exact Test only demonstrated a p-value of 0.086 (Table 3).

Table 3. Fisher's Exact Test comparing metastasis between non-ossifying and ossifying synovial sarcomas

	Nonmetastatic	Metastatic
Non-ossifying synovial sarcoma	60	44
Ossifying synovial sarcoma	7	13

Using heterozygous mice expressing *hSS1* or *hSS2*, a Kaplan Meier Survival analysis was performed between mice with and without ossification. The mice with ossification exhibited, on average, a six-week longer survival (figures 11a, b) (z=2.81, p=0.0005).

To investigate if ossified cells or cells with the potential to ossify were more likely to metastasize and colonize the lungs, we evaluated pulmonary synovial sarcoma metastases for the presence of ossification (figure 14). Only one mouse that exhibited rampant metastatic disease with large pulmonary metastases displayed hard tumors. All the other mice with lung metastases demonstrated normal synovial sarcoma morphology by H&E with no obvious presence of ossification (figure 14).

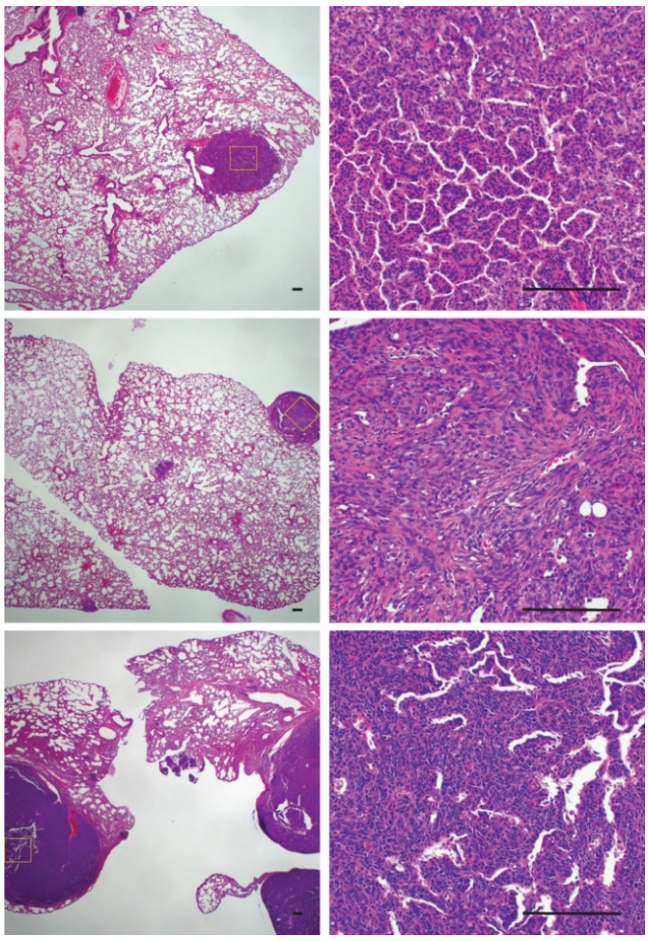

Figure 14. Histological sections of pulmonary metastases demonstrating a lack of ossification within tumors. Scale bars = 100 µm

3.2. RNA Sequencing and Analysis of HSP90 expression in Synovial Sarcoma

After analysis of heterotopic ossification and correlation to synovial sarcoma outcomes, it was established that there is still a need to better define the tumor microenvironment and prognostic biomarkers. As it had been established that HSP90 must hold some significance through the screening observed in figure 3, our attention turned towards quantifying and locating HSP90 expression within SS. I looked to answer if higher inflammation is associated with an upregulation of HSP90 and if these results can be compared between *in vitro* and *in vivo* culture environments. Inflammation and ossification are not observable within traditional cell culture, so the establishment of a diagnostic biomarker that can be measured *in vitro* would act to confirm a comparable model.

Performance of RNA sequencing analysis revealed a significantly increased expression of both major forms of HSP90, HSP90aa1 and HSP90ab1, as compared to noncancerous muscle tissue also taken from the left hindlimb. Significance was determined via one-way ANOVA for both metastatic and non-metastatic reads as compared to normal tissue, and verified post-hoc using Dunnett's multiple comparisons test. In figure 15a, Metastatic expression of HSP90aa1 showed an average expression of 17.72 ± 5.097 FPKM ($p=0.0007$), non-metastatic an average expression of 15.98 ± 2.785 FPKM ($p=0.0050$), and normal tissue an average expression of 2.498 ± 1.433 FPKM. For HSP90ab1 (figure 15b), Metastatic expression showed an average expression

of 386.3 ± 40.54 FPKM (p=0.0010), non-metastatic an average expression of 418.1 ± 47.29 FPKM (p=0.0011), and normal tissue an average expression of 231.9 ± 56.64 FPKM.

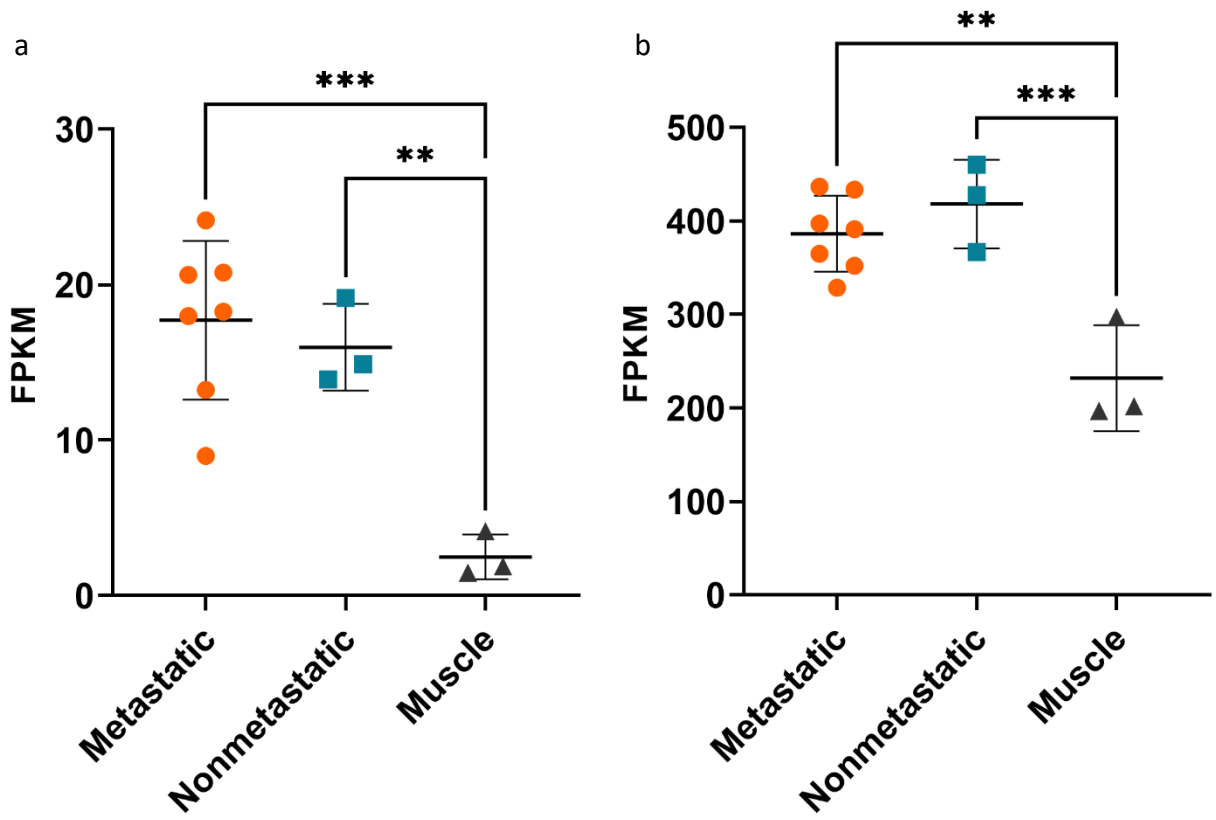

Figure 15. RNA-sequencing reads of metastatic synovial sarcoma (n=7, circles), non-metastatic synovial sarcoma (n=3, squares), and non-diseased muscle tissue(n=3, triangles). All tissue samples were excised from genetically engineered mouse models with various degrees of gene activation. Significant upregulation of HSP90 was observed in both metastatic and nonmetastatic tissue for both isoforms a) HSP90aa1: ***p=0.0007, **p=0.0050, b) HSP90ab1: ***p=0.0010, **p=0.0011

3.3. HSP90 Protein Localization Determination

Two samples were derived from primary mouse SS cells and developed as described above. Following Western Blot analysis, densitometry measurements of bands arising from SS GEM models, alongside qualitative visual measurements, indicated a higher amount of HSP90

present within the cytoplasm of mouse tumor cells, but also clearly present HSP90 bound within the cellular membrane as well (figure 16). Samples were averaged and plotted for both cytoplasm and membrane fractions. An unpaired t test showed a significant difference between amount of HSP90 present in the cytoplasm and membrane (p=0.0429). Cytoplasm: 125,184 ± 13,588 DU,

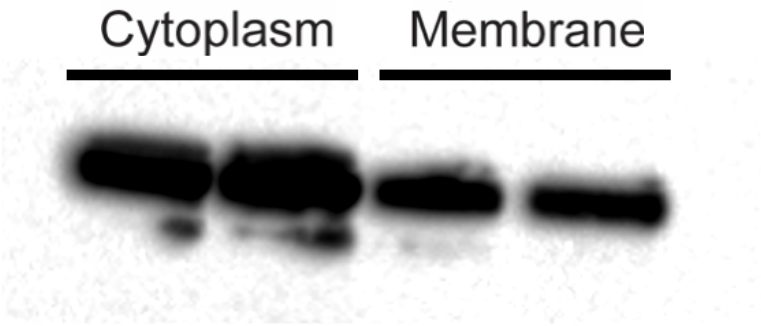

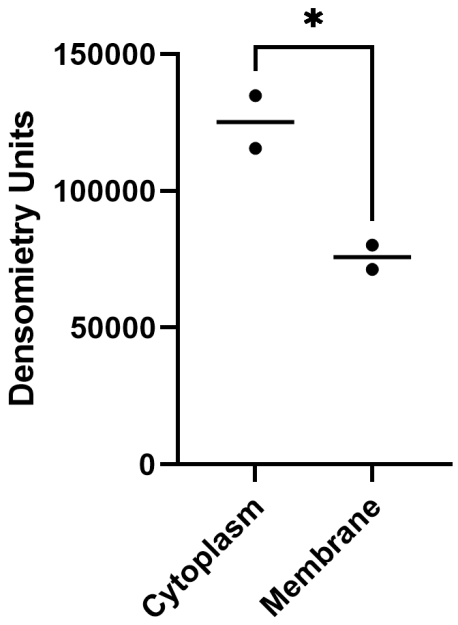

Figure 16. Western blot analysis of expression and localization of HSP90 within mouse SS tissue. Expression within the cytoplasm, as anticipated, is abundant. Membrane localization is also evident at more than half the abundance of cytoplasm-bound HSP90. A significant amount of HSP90 was observed as compared to

Membrane: 75,773 ± 6,271 DU. (Densitometry units)

3.4. HSP90 Protein Quantification within Circulation

Plasma analysis via ELISA showed significant upregulation of circulating HSP90 in metastatic mice models as compared to non-metastatic and non-diseased mice models (figure 17). Circulating HSP90 in metastatic mice was determined to have an average of 195.3 ± 55.35 pg/mL, compared to an average of 7.227 ± 7.326 pg/mL and 0.00 ± 0.00 pg/mL in non-metastatic and normal mice, respectively. Significance was determined through one-way ANOVA

(p<0.0001), with post-hoc comparisons via Tukey's multiple comparisons test detailing significant differences between metastatic/non-metastatic mice (p=0.0003) and metastatic/normal mice (p=0.0002).

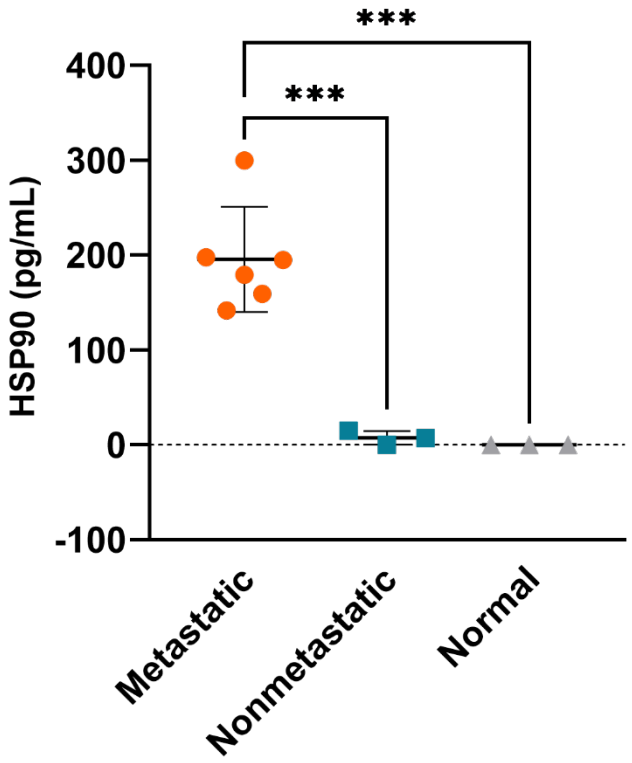

Figure 17. HSP90 present in picograms *per mL* circulating in serum of metastatic (n=6, circles), non-metastatic, (n=3, squares) and normal mice (n=3, triangles), as determined by an HSP90 ELISA immunoassay kit. Significant circulation of HSP90 was observed within the metastatic samples when compared to both non-metastatic and normal mice samples. ***p<0.0005

3.5. *In Vitro* Treatment with HSP90 Inhibitors to Establish Baseline Response

Yamato and HSSY-II, SS cell lines, and SJSA-1 and U2OS, v osteosarcoma cell line, were treated with each HSP90 inhibitor separately along a concentration curve in an effort to determine an IC50 and baseline response curve to each inhibitor before combining the inhibitors with doxorubicin hydrochloride to determine any combinatorial effects. As seen in figure 18, HS-10 was the only inhibitor to yield a decrease in cell viability across all four cell lines, while HS-131 decreased cell viability in three cell lines and HS-198 had no effect on cell viability across all four cell lines, as would be anticipated.

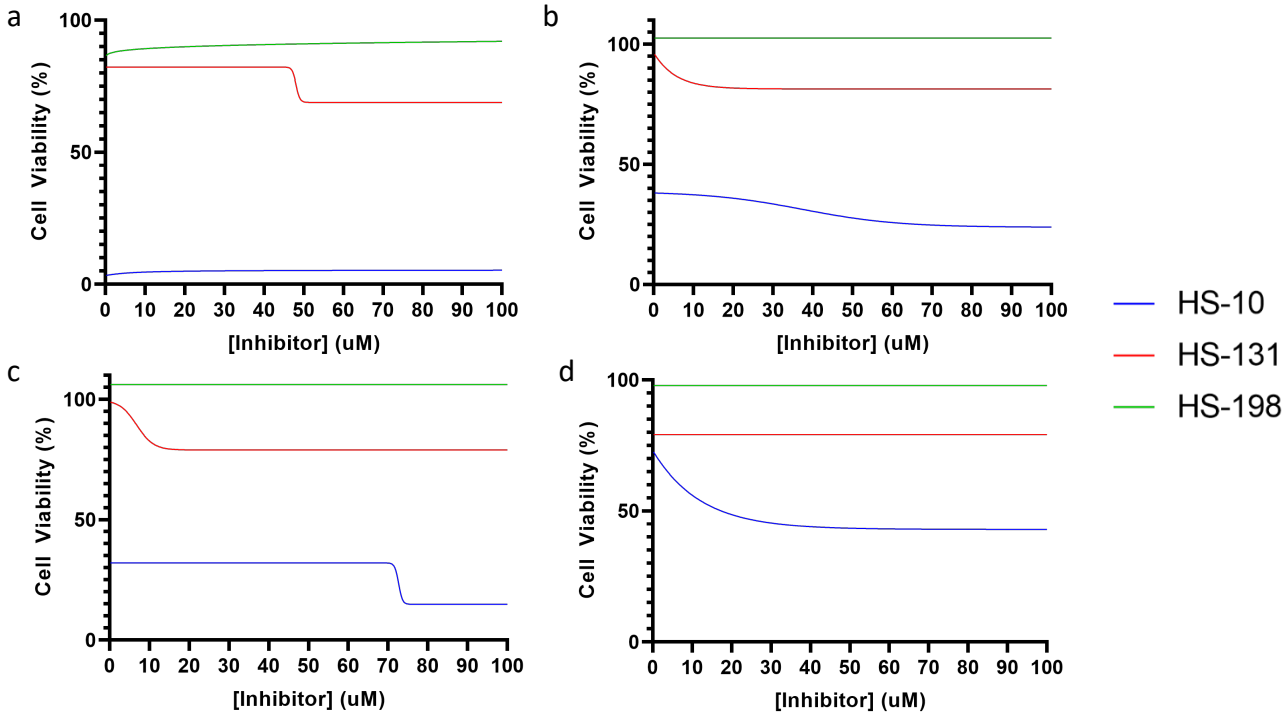

Figure 18. Dose response curves of inhibitors HS-10, HS-131, and HS-198 as tested against a) Yamato and b) HSSY-II, synovial sarcoma cell lines, and c) SJ-SA1 and d) U2-OS, osteosarcoma cell lines.

3.6. *In Vitro* Combinatorial Treatment with HSP90 Inhibitors and Doxorubicin Hydrochloride

After initial determination of the presence of elevated HSP90 and membrane-bound localization, two-dimensional cell cultures of SS were decided to be the next relevant step for investigating our novel HSP90 inhibitors. Initial investigation on inhibitor effects was performed utilizing the novel Duke inhibitors alone against each drug was delivered using serial dilution along separate axes, with the second to last column reserved for untreated cells and the last

column reserved for media alone, to act as positive and negative controls, respectively; HSP90 inhibitor dilutions increased along the columns, and doxorubicin dilutions increased along the rows, as seen in figure 13.

3.6.1. HS-10 and Doxorubicin Hydrochloride

Exposure of HS-10 and doxorubicin showed increasing cytotoxicity greater than 50% with increase in either HS-10 or doxorubicin, with additional increases in cytotoxicity and the greatest inhibitory effect can be observed at the highest concentration of each treatment, as seen in figure 19.

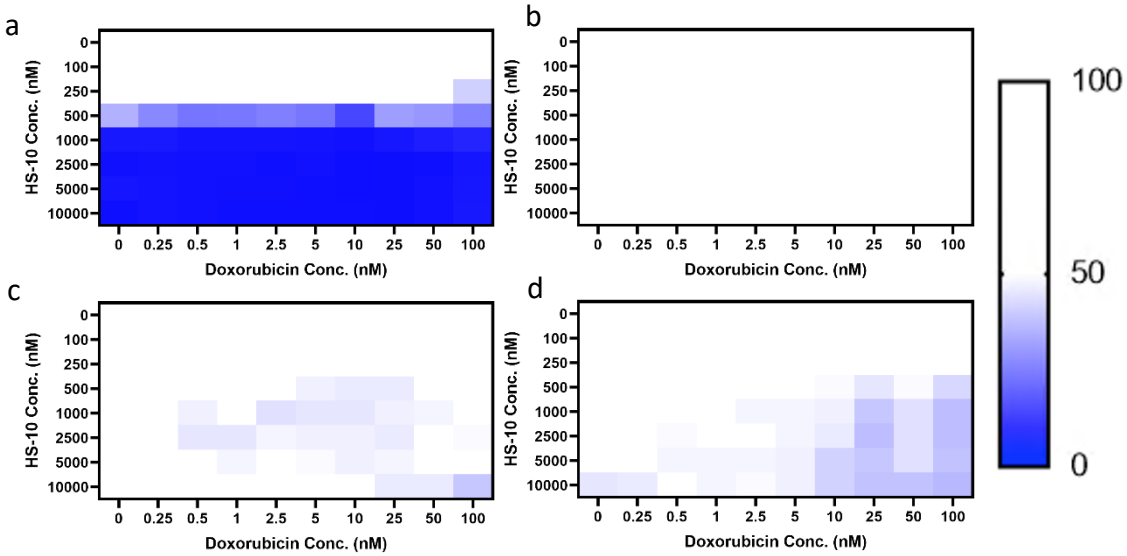

Figure 19. Combinatorial treatment of HS-10 inhibitor and doxorubicin at varying concentrations, increasing from left to right for doxorubicin and bottom to top for HS-10. Strong inhibitory effects can be observed for Yamato, with varying result among other cell lines. a) Yamato SS cell, b) HSSY-II SS cells, c) SJSA-1 osteosarcoma cells, d) U2-OS osteosarcoma cells

3.6.2. HS-131 and Doxorubicin Hydrochloride

When HS-10 is replaced with HS-131 *in vitro*, there is a marked difference. In figure 20, there appears to be very little, if any, inhibitory or cytotoxic effects across any of the cell lines below 50%.

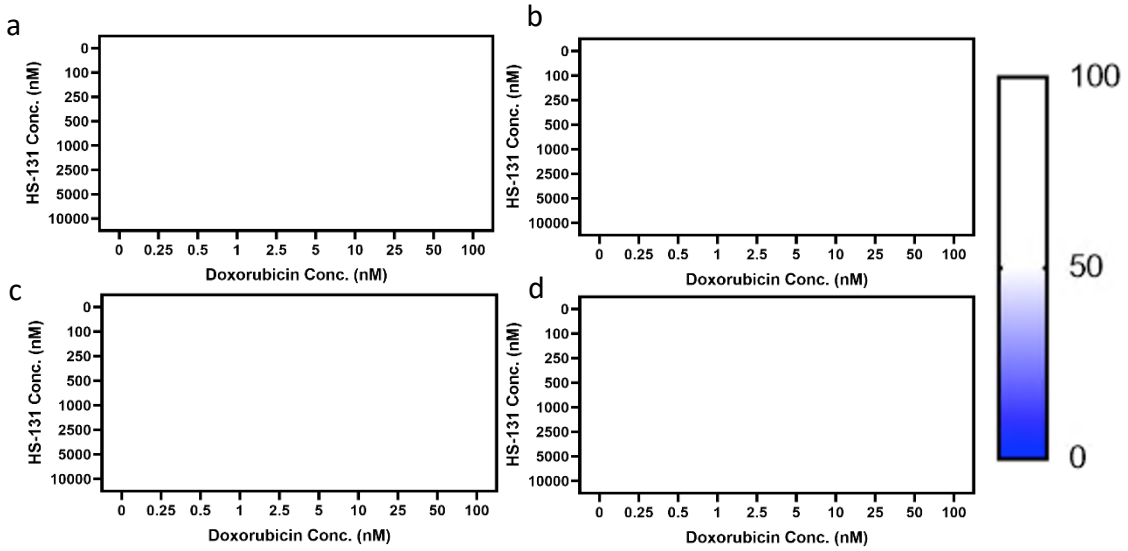

Figure 20. Combinatorial treatment of HS-131 inhibitor and doxorubicin at varying concentrations, increasing from left to right for doxorubicin and bottom to top for HS-131. No inhibitory effects can be observed from any cell line. a) Yamato SS cell, b) HSSY-II SS cells, c) SJSA-1 osteosarcoma cells, d) U2-OS osteosarcoma cells

3.6.3. HS-198 and Doxorubicin Hydrochloride

Similarly, looking at HS-198, the negative control of our HSP90 inhibitor, there was almost no decrease in cell viability below 50%, except for the maximum combination dose at 100 nM doxorubicin and 10 µM HS-198 in the HSSY-II cell line, as seen in figure 21b.

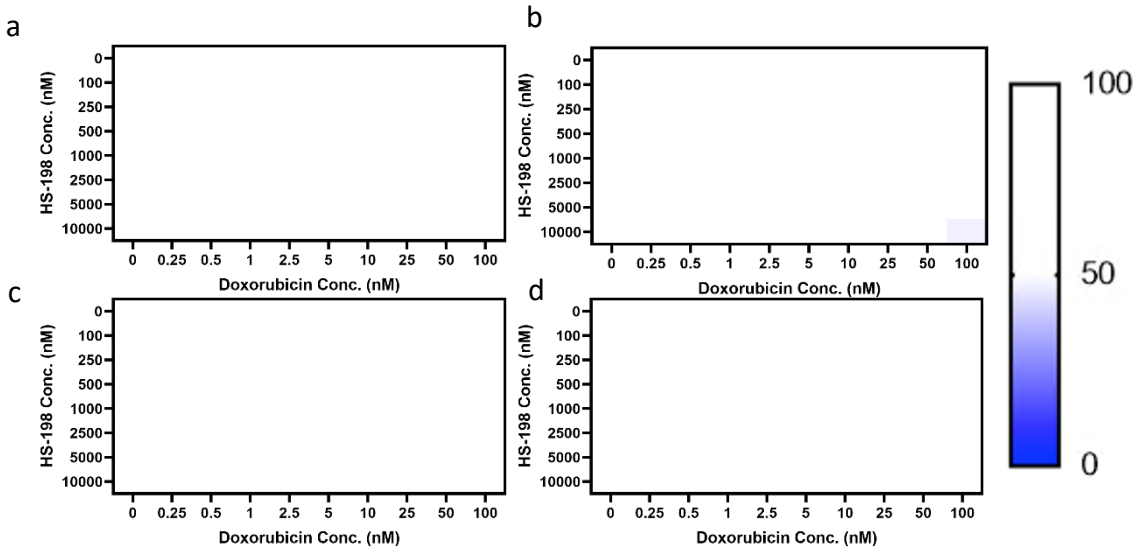

Figure 21. Combinatorial treatment of HS-198 inhibitor and doxorubicin at varying concentrations, increasing from left to right for doxorubicin and bottom to top for HS-198. Very slight inhibitory effects can be observed within HSSY-II, with no inhibitory effects among other cell lines. a) Yamato SS cell, b) HSSY-II SS cells, c) SJSA-1 osteosarcoma cells, d) U2-OS osteosarcoma cells

3.7. *In Vitro* Accumulation of HSP90 Inhibitor HS-131

Using a Molecular Devices ImageXpress Pico cell imaging system, a 24-hour accumulation study was performed to determine if internalization occurs as proposed and could be visualized with the uptake of HS-131 (figure 23). Yamato SS cells were treated with 100uM HS-131 and imaging was taken every hour at 37ºC, 5% CO2, 85% humidity and using a 20x objective at 695nm absorbance.

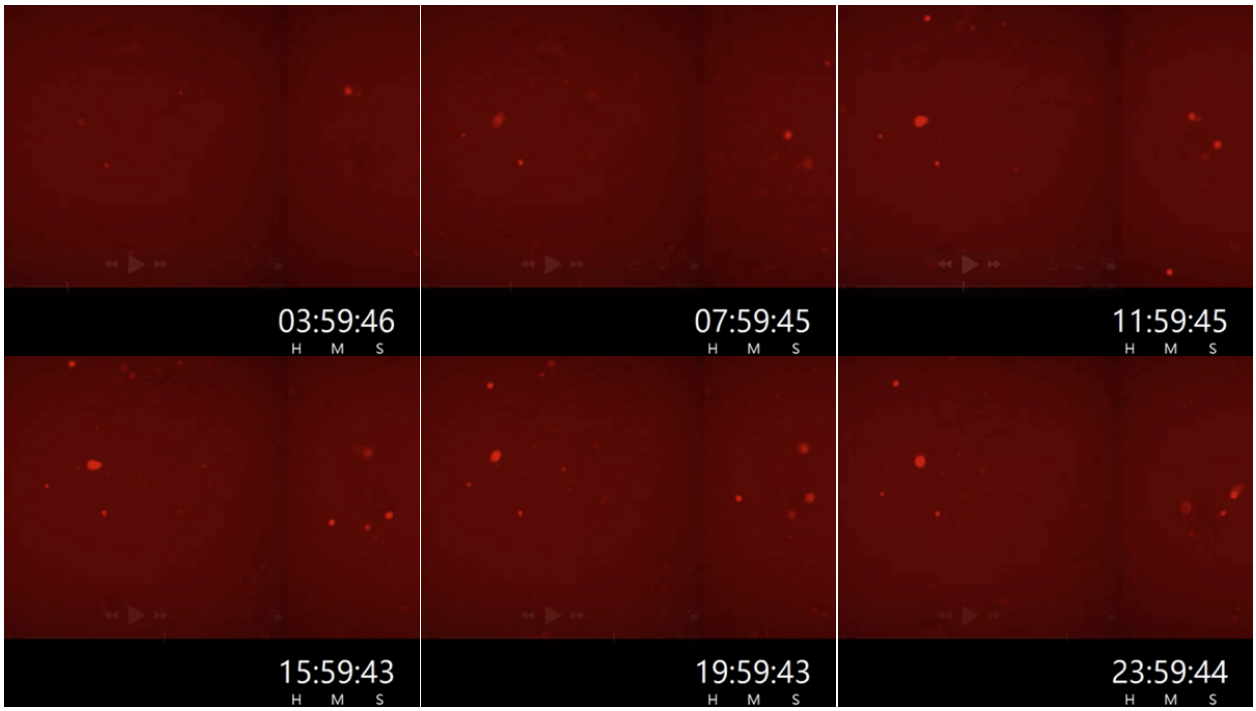

Figure 22. Timelapse over 24 hours of HS-131 uptake into Yamato synovial sarcoma cells. Aggregation is visible as bright red spots. Potential exocytosis can also be seen as smaller red spots around brighter spots.

3.8. *In Vivo* Distribution and Accumulation of HSP90 Inhibitor

24-hour accumulation after intraperitoneal injection of HS-131 within a metastatic SS GEMM mouse model revealed local accumulation of inhibitor primarily in tumor tissue. Some

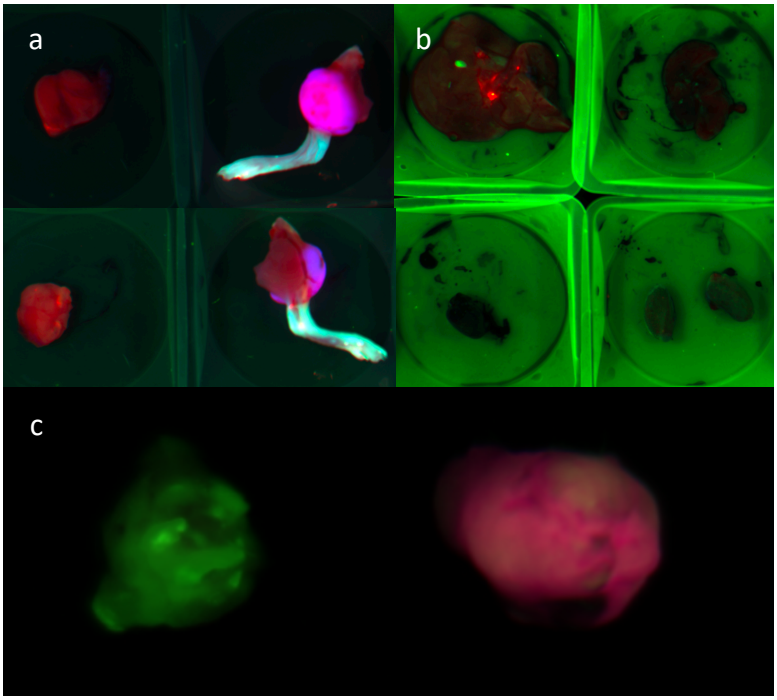

Figure 23. a) 24 hours after intraperitoneal injection, accumulation of HS-131 is present within the tumor (right), as well as within the lungs (left). Accumulation of HS-131 within the lungs can be contributed to metastasis of synovial sarcoma. b) Accumulation is visible within the liver (top left), but not the thyroid (top right), kidneys (bottom right), and heart (bottom left). c) Accumulation within non-metastatic (left) and *Pten*-deletion induced metastatic (right) SS tumors from mice models. Lack of ectopic HSP90 in non-metastatic SS does not allow accumulation within

accumulation was also observed within lung tissue and the liver, as seen in figures 23a and b. Within a non-metastatic SS model, after inhibitor exposure, there is no visible accumulation within the tumor, while direct comparison to a metastatic tumor shows evident accumulation

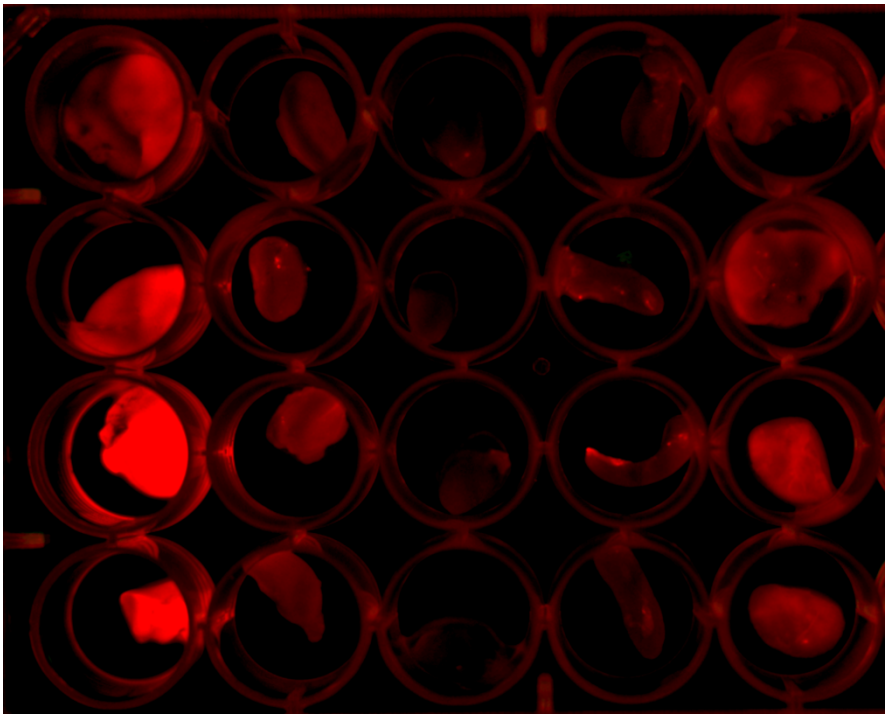

Figure 24. Repeated HS-131 accumulation on four separate mouse models of SS. Presence of HS-131 can be observed within tumor tissue (left), lung tissue (second from left), spleen (second from right), and liver tissue (right). HS-131 is not readily observable within heart tissue (center).

(figure 23c). Repeated accumulation studies corroborated original findings, detailing HS-131 within the tumor, lungs, liver, and slight accumulation within the spleen (figure 24).

3.9. SS GEMM *In Vivo* Dosing and Survival Analysis of HSP90 Inhibitor

In establishing cohorts for in vivo inhibitor trials, we wanted to verify that each cohort was comparable in both starting mass and tumor volume. We established 7 cohorts of mice with various treatment parameters; saline control (n=9), doxorubicin hydrochloride (n=3), HS-10 (n=5), HS-131 (n=3), HS-198 (n=3), HS-131/doxorubicin, (n=5), and HS-198/doxorubicin (n=4).

After tumor presentation was observed at a minimum of 200 mm^3, each mouse was injected with their designated treatment, three times a week intraperitoneally for the novel inhibitors, once a week through tail vein injection for doxorubicin. Doxorubicin delivery was switched to IP injection once a week after two weeks as significant scabbing and irritation was present at the tail base of the treated mice.

Each cohort was measured for mass and tumor volume, then values were averaged and plotted. The average starting mass of each cohort was: control; 28.13 ± 3.31 g, doxorubicin; 36.87 ± 9.45 g, HS-10; 20.56 ± 1.43 g, HS-131; 27.91 ± 4.13 g, HS-131/Dox; 24.02 ± 1.80 g, HS-198; 40.80 ± 9.49 g, HS-198/Dox; 26.35 ± 3.67 g. The average starting tumor volume of each cohort was: control; 368.8 ± 139 cm^3, doxorubicin; 825.9 ± 574 cm^3, HS-10; 243.9 ± 37.1 cm^3, HS-131; 411.0 ± 301 cm^3, HS-131/dox; 211.6 ± 98.9 cm^3, HS-198; 460.6 ± 150 cm^3, HS-198/dox; 535.2 ± 167 cm^3 (figures 25a and b).

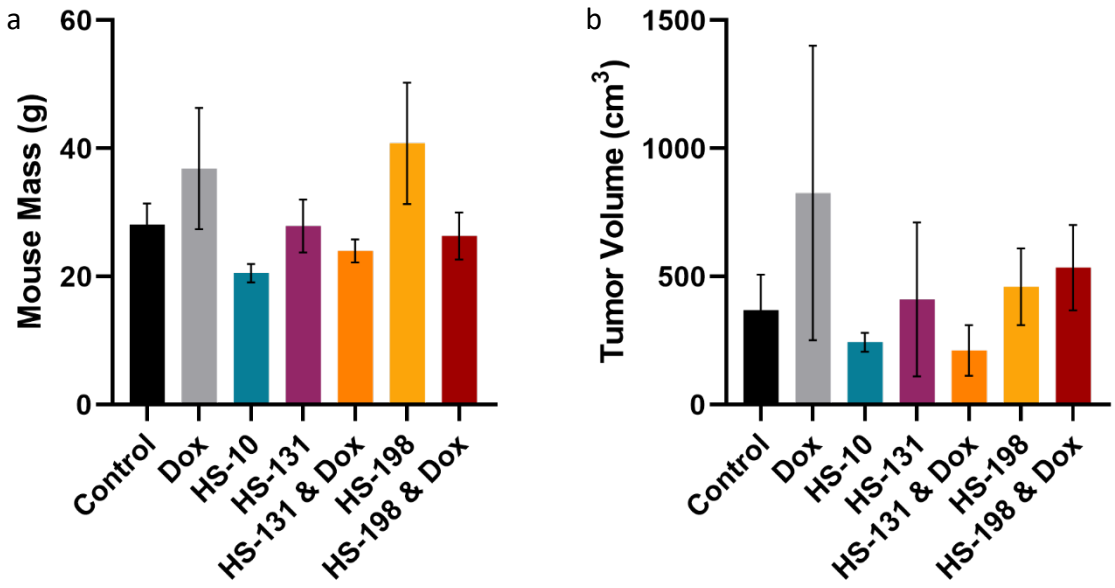

Figure 25. a) Average body mass of each cohort and b) average tumor volume of each cohort at the initial dosing with respective treatments. All cohorts were determined to be within comparable range.

After morbidity was achieved among all cohorts, mass (figure 26) and tumor volume (figure 27) were plotted among each cohort. An average comparison of each cohort was also established (figures 28a and b). A Kaplan Meyer survival analysis was performed to determine change in prognosis with each treatment (figure 30). A significant increase in likelihood of survival was observed for the HS-131/doxorubicin cohort (Mantel-Cox: $p<0.0001$; Gehan-Breslow-Wilcoxon: $p<0.0005$)

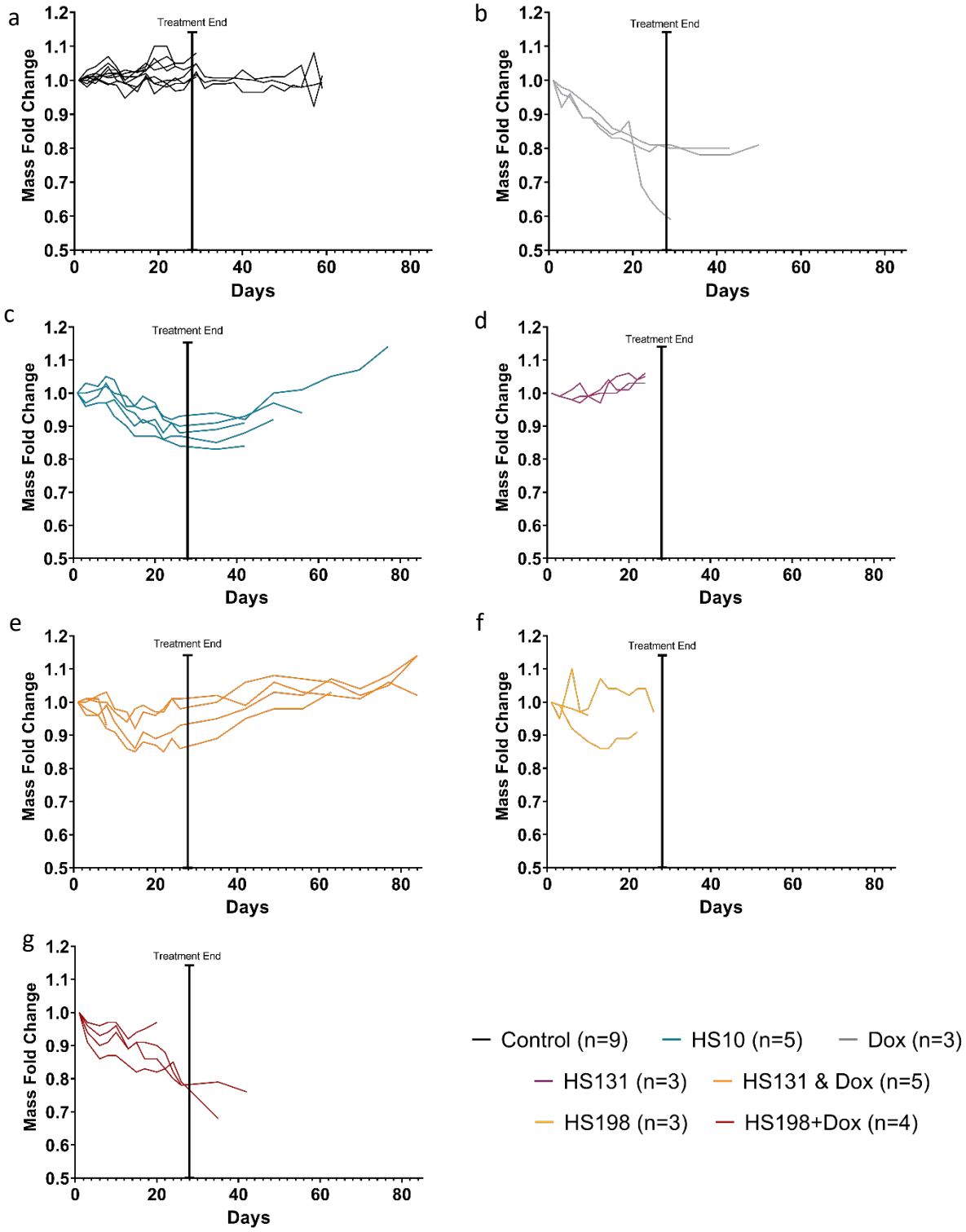

Figure 26. Body mass change for in vivo trials of HSP90 inhibitors with and without doxorubicin in combinatorial therapy for synovial sarcoma genetically engineered mice. *a) Control, b) Doxorubicin Hydrochloride, c) HS-10, d) HS-131, e) HS-131+Dox, f) HS-198, g) HS-198+Dox*

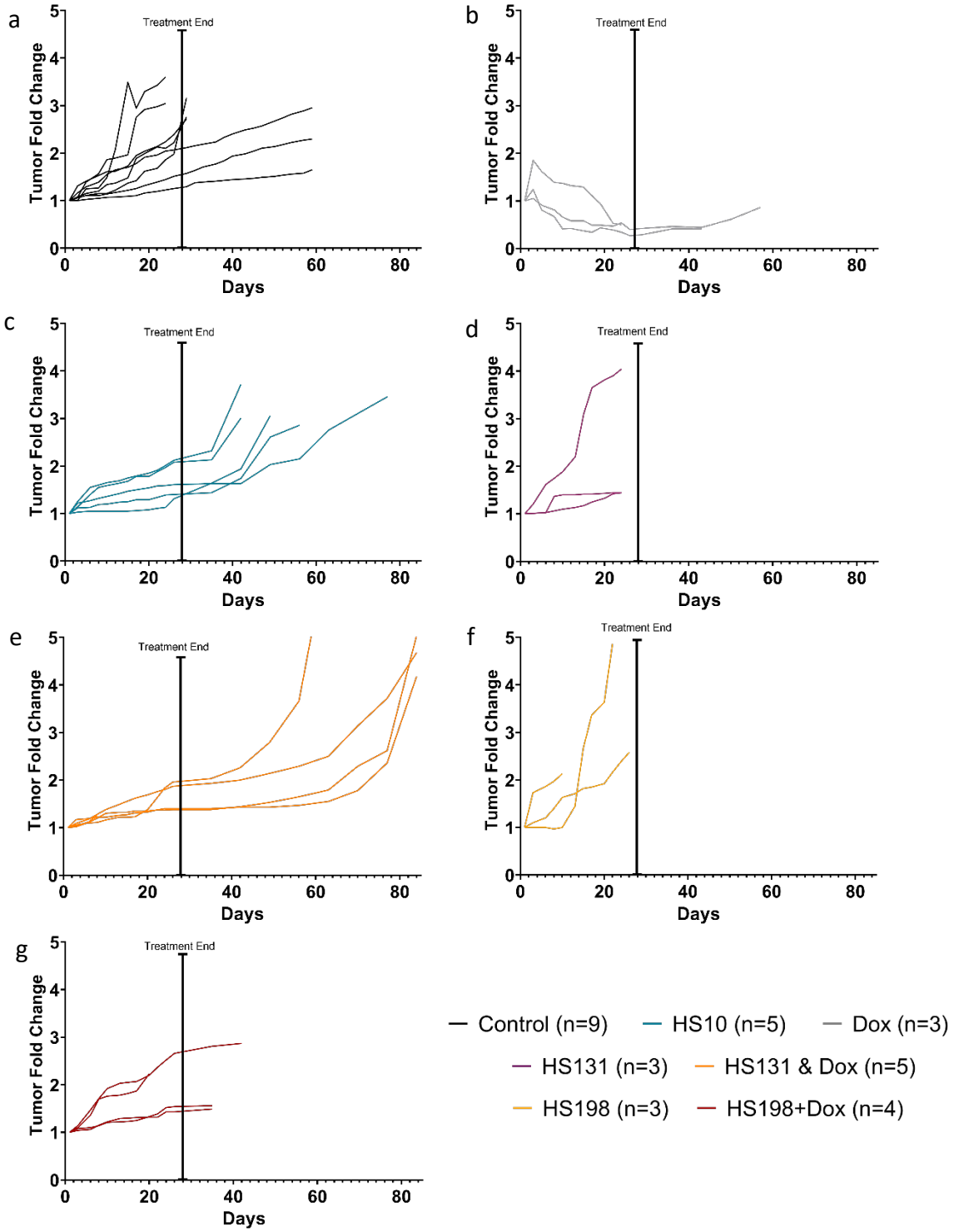

Figure 27. Tumor volume fold change for in vivo trials of HSP90 inhibitors with and without doxorubicin in combinatorial therapy for synovial sarcoma genetically engineered mice. Growth suppression is observable particularly in the HS-131/doxorubicin combination treatment**.** *A) Control, B) Doxorubicin Hydrochloride, C) HS-10, D) HS-131, E) HS-131+Dox, F) HS-198, G) HS-198+Dox*

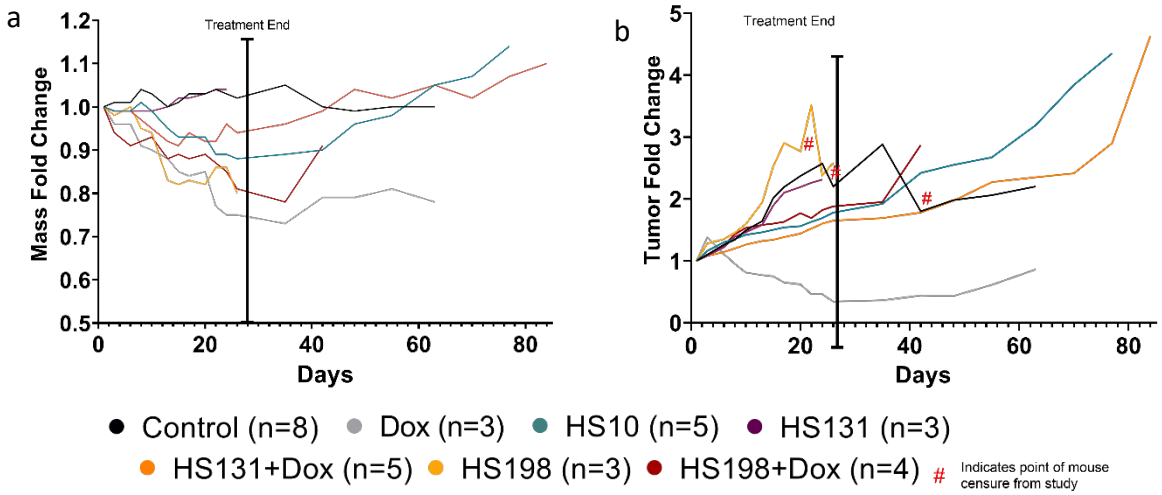

Figure 28. Taking the average of each cohort, the a) mass fold change and b) tumor volume fold change were plotted against treatment days. Mass changes in the doxorubicin and HS-198/doxorubicin cohort show evidence of systemic toxicity. Tumor volume measurements indicate doxorubicin alone showed the most effective initial reduction in tumor size, but ending of treatment allows for tumors to quickly re-proliferate.

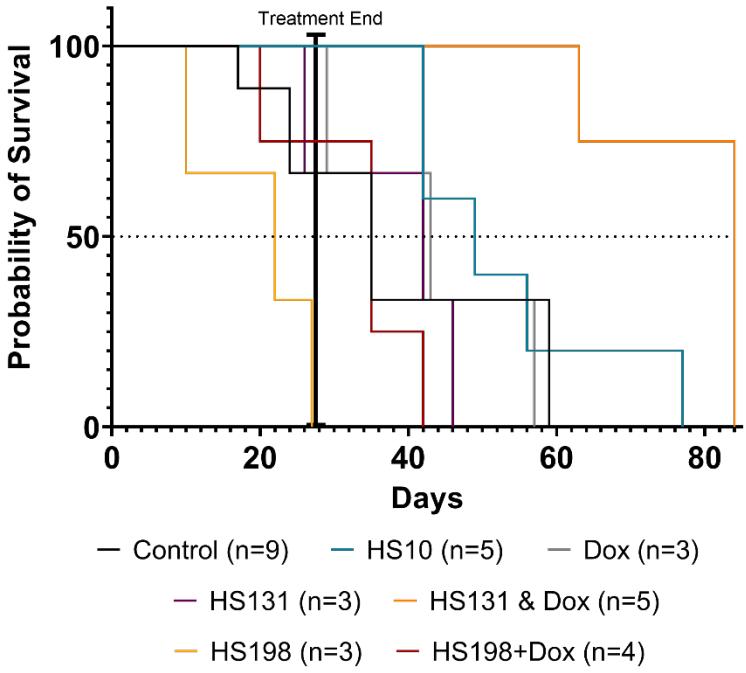

Figure 29. Kaplan-Meier survival analysis of seven cohorts of mice. Probability of survival was significantly increased within the HS-131/doxorubicin combinatorial treatment group as compared to all other cohorts($p<0.0001$).

3.10. 3D Culture Development and Organoid Establishment

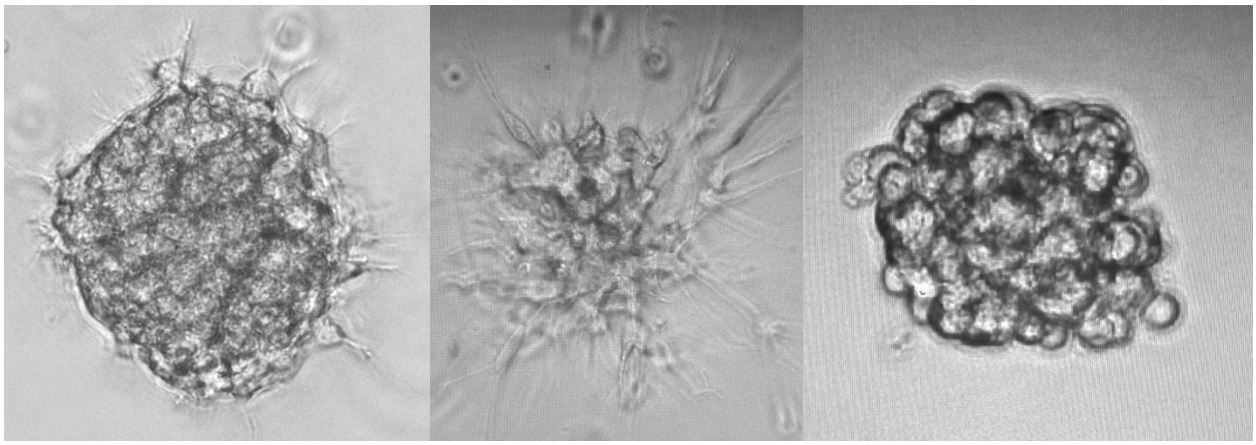

Figure 30. a) Mouse-derived SS tumor organoid, b) Yamato cell line tumor organoid, and c) patient-derived neuroendocrine tumor organoid, cultured in Matrigel. Establishment of organoids is evident through clustering of cells in tight spheres, with outgrowth beyond

In order to more accurately compare samples and methods, we sought to develop a more robust *in vitro* analysis model more capable of accurately predicting *in vivo* outcomes. Successful organoid culture establishment of three primary tumor types was achieved: GEMM-derived tumor digest, Yamato single cell suspension, and neuroendocrine patient-derived tumor digest, as seen in figure 30.

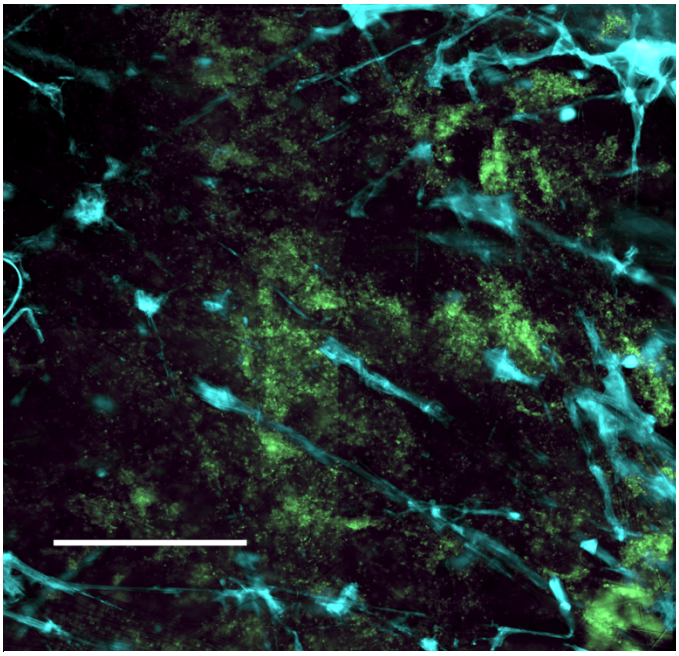

Figure 31. Z-stack image of Yamato cells on the PerfusionPal® seedEZ scaffold, stained with NucBlue and Calcein AM. Large clusters of cells can be observed, indicating successful 3D culture establishment.

Outgrowth of Yamato cells in the 3D scaffold format was observed to show considerable proliferation. Fluorescent staining revealed multiple layers of growth throughout the scaffold. Nuclear

structures were observable in the forefront, while large clusters of cell bodies are visible at a deeper layer of the scaffold as seen in figure 31.

4. Discussion

4.1. Ossification and Prognosis Analysis

I will here elaborate on the effect that ossification within SS has on change in prognosis compared to SS without ossification present, as well as the prevalence of developing ossification in the case of SS diagnosis. I hypothesize that the genetic profile required to induce ossification alongside SS will have deleterious effects on survival outcome.

4.1.1. Gross and Histological Analysis of Mouse Synovial Sarcoma

As observed in figure 10, Ossification was identified by the presence of eosinophilic (pink) uncalcified boney matrix (i.e., osteoid) with some regions exhibiting basophilic (purple) calcium salt deposits. Both calcified and uncalcified regions contained cells embedded in small lacunae, typical of an ossified or ossifying matrix. Many lacunae were empty, likely an artifact caused by histological processing. Coalescing trabeculae of ossified matrix were integrated into the non-ossifying tumor stroma, which consisted of numerous spindle shaped cells with a mix of small, hyperchromatic nuclei and large euchromatic nuclei with prominent nucleoli; mitotic bodies; and giant multinucleated cells that resembled osteoclasts. Out of the 463 mice observed, only 33 (7.1 %) demonstrated these ossification characteristics.

4.1.2. Differences in Ossification Phenotype Between Heterozygous and Homozygous Fusion Gene Expression

Upon further inspection at the different variants of synovial sarcoma within our model, it was noted that the heterozygous expression of either *hSS1* or *hSS2* had a higher prevalence of ossification compared to the homozygous group, 13.8% and 10.2%, respectively (figure 11a). This is likely due to the slow development of ossification and a faster disease progression in mice homozygous for either *hSS1* or *hSS2*. As such, mice homozygous for either gene became moribund at 8.3 weeks after TATCre injection, before ossification could occur (figure 11b-c).

4.1.3. Bone Reactivity Detected by Radiography at a Higher Incidence than Histological Ossification

The prevalence of bone inflammation in synovial sarcomas in these mice was significantly higher than expected. All mice exhibiting ossification belonged to the *hSS1/wt* or *hSS2/wt* subcategory with *Pten* loss, which is also referred to as our metastatic model of synovial sarcoma. The *hSS1/hSS2* heterozygous metastatic categories exhibited a mean 11.6% penetrance of the ossification phenotype upon gross and histological examination (figures 10 and 12). We further investigated the *hSS1/wt* or *f* subcategory with wildtype *Pten*, also referred to as our nonmetastatic model of synovial sarcoma. It was noted that in the 10 nonmetastatic synovial sarcomas imaged, only three displayed bone interaction; this interaction was also not as extensive and invasive as seen in the metastatic model (figure 12).

4.1.4. Underlying Gene Expression of Bone Development Genes in Metastatic Model of Synovial Sarcoma

To further investigate the relative role of osteogenic signaling in metastatic versus nonmetastatic synovial sarcomas, RNA expression was analyzed for 65 genes involved in osteoblast differentiation. Only one of the tumors used for these analyses was identified with an ossifying center, though all tumors demonstrated significant upregulation of genes involved in bone development. This is especially observable when comparing gene expression in metastatic synovial sarcomas versus control muscle tissue. Enrichment of osteogenic genes of interest were observable for nearly all bone development genes in all sarcoma tissues, with no upregulation of these genes detected in any of the muscle tissue (figure 13a).

After comparing primary tumors from our metastatic model to muscle, it was next evaluated if there was a significant enrichment between the non-metastatic model and the metastatic model. 46 genes were identified that were significantly upregulated between the normal muscle tissue and the primary synovial sarcomas from the metastatic model. A similar comparison of gene enrichment was conducted between primary tumors from non-metastatic and metastatic mice, and 26 bone development genes were detected that were upregulated in the tumors from the metastatic model. Not surprising of these upregulated genes, 20 genes were shared between the two comparisons (figure 13b). The 6 unshared genes (*CEBPB, BMP6, PTGS2, DMP1, FGF2,* and *H2AFV*) are likely the important contributors to the ossifying phenotype seen in the metastatic synovial sarcomas.

To further explore the relationship in upregulated genes in the metastatic mouse model, we turned our attention to a human database. Using the NCBI GEO Dataset GSE54187, human synovial sarcomas were bifurcated into nonmetastatic (n=15) and metastatic (n=42). The 47 genes identified in the mouse comparison were analyzed across the human tumors and only one gene was found to be significantly different, parathyroid hormone-like hormone (*PTHLH*) (figure 13c). This gene is intriguing in that it is downstream of *RUNX2*, a master regulator of bone development and ossification and high expression has been correlated to faster disease progression in a number of cancers due to the overexpression of *PTHLH*(151). Among its putative functions for cancer progression is the activation of myeloid-derived suppressor cells (MDSCs) in the bone marrow(152). These immune cells have the ability to promote growth and angiogenesis, while interfering with T-cell immune responses(153). We posited that these recruited MDSCs could also be triggering an ossification phenotype in our metastatic model of synovial sarcoma. We have already seen an overwhelming presence of macrophages, monocytes, and neutrophils within the tumor microenvironment of metastatic synovial sarcomas in mice(41). We measured signals from the sorted populations by NanoString sequencing and found several genes that were uniquely expressed in the MDSCs and have a functional history in ossification (figure 13d). The gene that represented the largest enrichment in MDSCs was *Tyrobp*. This gene is involved in bone cyst formation in Nasu-Hakola disease(154).

4.1.5. Gross Metastasis is Loosely Correlated with the Presence of Ossification, But Survival is More Favorable in Mice with Ossification

We noticed a trend among mice with synovial sarcomas and intratumoral ossification: they exhibited an increased prevalence of gross metastasis. Within the heterozygous mice for either *hSS1* or *hSS2*, we already noted a higher prevalence of ossification and an associated longer survival in heterozygous mice.

It is unclear if ossification portends a worse prognosis in synovial sarcoma. In particular, considering the evidence that metastasis is more obviously present when synovial sarcomas exhibit ossification, we wanted to investigate this correlation more thoroughly. The null hypotheses, however, cannot be rejected as no significance was established between worse prognosis and presence of ossification; ossification does not contribute to metastasis, nor a faster time to morbidity.

The increased rate of metastasis in ossifying synovial sarcomas raised questions about the cellular phenotype of the metastatic lesions. As only one mouse exhibiting rampant metastatic disease with large pulmonary metastases displayed tumors that are solid upon palpitation, and all other mice with lung metastases demonstrated normal synovial sarcoma morphology by H&E with no obvious presence of ossification, this led us to conclude that metastasis and ossification are independent events, but both are dependent on time.

4.2. RNA Sequencing and Analysis of HSP90 expression in Synovial Sarcoma

Before any attempt of treating SS with an HSP90 inhibitor was made, validation of HSP90 as target and the hypothesis that HSP90 expression is increased within SS was first performed. Our hypothesis states that both increased RNA expression and increased protein content of HSP90 within SS cells should be observed, and are paramount to successful targeting for our proposed treatment. We determined that RNA-sequencing and protein expression analysis would be appropriate assays to help elucidate these details.

RNA-sequencing analysis was performed on hindlimb tissue from three different status of mice: *Pten*-deletion induced metastatic tumor, non-metastatic tumor, and normal muscle tissue (figure 15). Each mouse was verified to possess the same genotypic profile through PCR analysis. Total normalized read counts of both HSP90aa1 and HSP90ab1 show similar expression between metastatic and non-metastatic samples, and considerably greater expression when compared to normal muscle tissue. Statistical analysis through both one-factor ANOVA and unpaired t-tests revealed a significant difference of both metastatic (aa; p=0.0007, ab; p=0.0011) and non-metastatic (aa; p=0.0050, ab; p=0.0010) tissue when compared to normal muscle tissue for both isoforms, as well. Although the *ab* isoform shows more than a ten-fold increased expression compared to the *aa* isoform, there is a greater difference comparatively between cancerous tissue and normal tissue in the *aa* isoform. Also, as previously discussed, the *ab* isoform, being considered constitutive, would be expected to be at an already higher level than the inducible *aa* isoform even before overexpression through upregulation (54). As for normal tissue expression of HSP90, as discussed during the introduction, HSP90 is found ubiquitously throughout all cells

within the body(60–64). Thus, the non-zero read counts in muscle tissue are not out of the ordinary, and are reasonably anticipated. The null hypothesis can then be rejected, as there is a significantly increased expression of HSP90 RNA when compared to normal muscle tissue.

4.3. HSP90 Protein Localization within Synovial Sarcoma

With the knowledge that there is in fact an increased expression of HSP90 relative to normal tissue, we sought to prove the hypothesis that SS should show expression of ectopic, membrane-bound HSP90. Western blot analysis was employed to verify and compare HSP90 presence not only within the cytoplasm, but bound to the membrane as well.

From figure 16, HSP90 is evident both within the cytoplasm and expressed on the cell membrane. Cell lysis releases cytoplasmic HSP90 for collection before the cell membrane is broken down using RIPA buffer. Western Blot analysis using HSP90 antibody revealed an elevated amount of HSP90 bound to the membrane, but at seemingly lower levels than cytoplasmic concentrations. This provides evidence for the hypothesis and potential mechanism of uptake of the polar HS-131 inhibitor through binding to membrane-bound HSP90(155).

This conclusion led us into the next investigation; does ectopic expression of HSP90 aid in the metastatic process, and can mesenchymal cells as well as extracellular HSP90 be quantified within circulation?

4.4. HSP90 Protein Quantification within Circulation

After confirmation of increased RNA expression of HSP90 within the cancerous cells and localization within the cell membrane, it was pertinent to determine if this increased transcriptional expression also translates into increased protein expression of HSP90 and consequently greater metastasis. Our hypothesis holds that membrane-bound HSP90 stabilizes the extracellular environment, including MMPs, and thus facilitates increased invasive characteristics. ELISA protein analysis was determined to be the most accurate and reliable method for metastatic determination. Plasma samples were also decided to be the most effective means of determining the amount of HSP90 within circulation, if any.

After ELISA analysis, it can be shown that without upregulation of HSP90 leading to ectopic expression, HSP90 is not found in circulation within non-induced, normal mouse models (figure 17). When SS is induced through lox-Cre recombination and RNA expression is increased, but *Pten* deletion does not occur, ectopic expression is less likely, and little, if any, circulating HSP90 is observed. When *Pten* deletion occurs concurrently with SS initiation, a metastatic profile is achieved, increasing ectopic and extracellular expression of HSP90. This results in a significant difference of circulating HSP90 in metastatic mice when compared to both non-metastatic and normal muscle tissue (p=0.0091). This significant increase of circulating HSP90 is likely to coincide with cells transitioning from an endothelial state to a mesenchymal state and entering circulation.

The null hypothesis was once again rejected, as the metastatic profile was significantly linked to circulating HSP90 and the non-metastatic and non-diseased profiles did not reveal a significant amount of HSP90 within circulation.

4.5. *In Vitro* Treatment with HSP90 Inhibitors to Establish Baseline Response

In order to assess the effectiveness of HSP90 inhibition on synovial sarcoma cells and tumors, both *in vitro* and *in vivo* models of different varieties of SS were utilized. Osteosarcoma cell lines were also utilized for comparative reference. These results were utilized to establish the effectiveness of treatment beyond a simple two-dimensional culture analysis and into a biological setting, forming the first preliminary stages of translational research for HS-131.

Two-dimensional *in vitro* cell models were initially employed to determine a baseline response to each of the three HSP90 inhibitors; HS-10, HS-131, and HS-198. Our hypotheses were expectant to see a decrease in cell viability with treatment of HS-10 and HS-131, which should both be able to traverse the cell membrane, while there will be little if any decrease in cell viability utilizing HS-198, as steric hindrance should not allow binding to HSP90 and thus negate active transport through the membrane.

HS-10, being uninhibited in uptake due to lack of the fluorescent moiety, seems to be freely able to pass through the cell membrane, and was observed to decrease the amount of cell viability after 72 hours of exposure across all four cell lines (figure 18). Thus, the null hypothesis can be rejected with regards to HS-10.

HS-131, with the exception of Yamato SS cell lines, did not decrease cell viability, and in fact appeared to have a positive effect. This was an unexpected outcome, particularly with the disparity between the two SS lines. Had Yamato and HSSY-II both had viability decreases and SJSA-1 and U2-OS had no decrease or a viability increase, it could be explained that osteosarcomas must not tend to express HSP90 on the cellular membrane. Regardless, we failed to reject the null hypothesis with regards to treatment with HS-131.

Finally, HS-198 followed the trend of not contributing to cellular viability decrease, but in fact seemed to promote cellular growth at higher concentrations as well. As no significance was established within treatment utilizing HS198, we once again failed to reject the null hypothesis.

The increases in cell viability for both HS-131 and HS-198 are difficult to explain, and more research would need to be performed to fully explore this phenomenon.

4.6. *In Vitro* Combinatorial Treatment with HSP90 Inhibitors and Doxorubicin Hydrochloride

My results indicate treatment with uninhibited HS-10 (figure 19) showed efficacy particularly against Yamato synovial sarcoma cells, but with less efficacy among osteosarcoma cells, and with no response above 50% inhibition in HSSY-II. Other groups have purportedly had success in reducing osteosarcoma cell viability using other HSP90 inhibitors(156–158). Notably, these groups used different human osteosarcoma cell lines and different inhibitors. These inhibitors may have a different method of action or uptake profile with regards to osteosarcoma as compared to the Duke novel inhibitors.

With combinatorial treatment using HS-131 (figure 20), there were no decreases in cell viability below 50% among any of the investigated cell lines. This result is surprising, especially among the SS cell lines, where we expected to see effective uptake as doxorubicin begins to effect cellular division. A possible explanation for what would seem to be lack of cellular uptake could be that when *in vitro*, the SS and osteosarcoma cell lines are not undergoing any type of stress, and therefore not upregulating HSP90 and promoting expression to the cellular membrane.

As anticipated, the sterically hindered HS-198 molecule proved ineffective at providing an antagonistic effect across any of the studied cell lines (figure 21). The one well of HSSY-II that does show viability below 50% is almost assuredly a result of the increased doxorubicin concentration.

4.7. *In Vitro* Accumulation of HSP90 Inhibitor HS-131

Regarding the potential capabilities of HS-131 to be utilized theranostically, we wanted to determine if accumulation of HS-131 could be visualized using fluorescent imaging techniques. The most effective way to determine if there is efficient uptake of HS-131 was a time-lapse method, so initial accumulation and increasing concentration within cells would be observable.

Around the 12-hour mark, maximum uptake appears to occur within the cells. Beyond this timepoint, smaller packets of HS-131 appear to become expelled from within the main cell bodies. We propose that this occurs through exocytosis, as the cell enters a state of disruption and begins to export HSP90 to stabilize the surrounding environment and begin signaling for resource prioritization.

4.8. *In Vivo* Distribution and Accumulation

After establishing the ability of HS-131 to become internalized within SS cells, and before beginning *in vivo* assays of combinatorial therapy, it was pertinent to confirm that internalization was achievable within a biological setting. Beyond establishing internalization, we also wanted to confirm targeting within cancerous tissue and avoidance of accumulation within normal tissue.

In order to verify HS-131 uptake within our SS mouse model, we injected a mouse presenting with a hindleg tumor with 50 mg/kg HS-131 interperitoneally, and allowed 24 hours for distribution and accumulation of the inhibitor. After 24 hours, the mouse was euthanized and dissected, followed by fluorescent imaging on an Azure Biosystems c600. As seen in figure 23, accumulation was clearly evident within the tumor, visible as bright pink fluorescence, and no accumulation was visible in the surrounding tissue. Relevant elimination and functional organs were also imaged, with accumulation visible within the lungs and liver of the mouse. We propose that accumulation within the lungs corresponds to metastasis of mesenchymal SS cells, and accumulation within the liver occurred as part of natural metabolic clearance.

4.9. SS GEMM *In Vivo* Dosing and Survival Analysis of HSP90 Inhibitor

With proof of effective accumulation and uptake of HS-131 within SS cells, our studies then moved to investigate the effectiveness of the novel inhibitors on tumor growth and inhibition.

During treatment, mouse mass change was recorded to monitor for systemic toxicity (figure 26), and tumor volume change was recorded to monitor treatment efficacy (figure 27).

Some toxicity was observed, presenting as a mass change of 10% or greater between measurements, but only with use of doxorubicin. One mouse in the doxorubicin cohort and one mouse in the HS-198/doxorubicin cohort showed evidence of systemic toxicity, but all other mice from all cohorts did not appear to show any evidence of toxicity.

With regards to treatment efficacy, tumor growth suppression in the saline control group (black) was verified to be non-existent. HS-198 inhibitor (yellow) showed a similar pattern of no growth suppression, also anticipated, as we did not predict HS-198 would be able to internalize within SS cells. Doxorubicin (grey), HS-10 (blue), HS-131 (plum), and HS-198/doxorubicin (red) showed moderate tumor growth suppression until the end of the 28-day treatment regimen, and then tumor growth is seen to quickly resume at uncontrolled rates. However, the cohort treated combinatorially with HS-131/doxorubicin (orange) showed tumor growth suppression both within the 28-day treatment period and beyond into an extended period after the end of treatment. Significant tumor growth resumed beyond twice the length of the treatment period in most incidents.

Analysis of each cohort via a Kaplan-Meier survival curve (figure 29) also serves to illustrate the positive change in survival outcome with regards to the effects of the HS-131/doxorubicin treatment regimen, as the combinatorial cohort showed a significant increase ($p<0.0001$) in survival probability, on average at least double of all other cohorts. This significant increase in survival is very encouraging in terms of the clinical potential for novel HSP90 inhibitor HS-131. I believe these results merit expanded investigation in the future.

4.10. 3D Culture Establishment of Soft Tissue Sarcomas

The Clevers group model was utilized as a starting point for tumor digestion and culture protocols(136). After multiple initial failures, it was discovered that while synovial sarcoma tumors can be digested using only trypsin and collagenase in culture media, other types of soft tissue sarcomas, such as breast cancer and rhabdoid tumors, have far more connective stroma and need additional reagents like hyaluronidase(159).

We were able to establish successful organoid cultures of three primary tumor types: GEMM-derived tumor digest, Yamato single cell suspension, and neuroendocrine tumor digest, as seen in figure 30. Hepatocarcinoma, breast cancer, and rhabdomyosarcoma tumors were unable to be cultured; however, we believe this to be more at fault of the collection or storage protocol rather than a shortcoming in our established procedure, as we received the samples after a commercial lab had already attempted to establish organoids from these samples as well.

Significant efforts were also made to establish the Perfusion Pal® model of 3D culture. This model comes with a unique learning curve, but ultimately should help lead to more robust cell culture capable of retaining the original tumor phenotype over time. It was observed that improved oxygen delivery within the culture was present; the media of cell cultures without perfusion began to shift to yellow from pink within 1-2 days, indicating culture conditions are becoming more acidic and unsustainable. After the addition of perfusion to the system, the culture media returned to the initial pink hue, indicating return to physiological pH by increasing gas exchange within the culture media and stabilizing formation of the bicarbonate ion(142,160).

Perfusion introduction returned the pH level to normal as according to the indicator within the first 12 hours of circulation.

Outgrowth of Yamato cells in the 3D scaffold format appears to show considerable proliferation. Fluorescent staining revealed multiple layers of growth throughout the scaffold. Nuclear structures were observable in the forefront (blue), while large clusters of cell bodies are visible at a deeper layer of the scaffold (green) as seen in figure 31.

We believe the Perfusion Pal® system provides a viable system to increase rapid cell expansion and organoid formation. Future studies will reveal if patient immune components can be incorporated in order to present a more complete *in vitro* analysis capable of replicating the physiological matrix to a high degree.

5. Conclusions

Synovial sarcoma remains a disease with limited treatment options and bleak prognoses. Typical treatment regimens of synovial sarcoma, which have not been updated or improved over the last 30 years, consist of tumor resection, radiation therapy, and adjuvant follow-up with doxorubicin hydrochloride in hopes of eliminating potential metastatic sites of synovial sarcoma formation. The harsh and limited treatment with doxorubicin leaves many patients with lasting cardiac damage and no recourse in the case of recurring synovial sarcoma outside of further surgical intervention. The low diagnosis rate of synovial sarcoma has stunted efforts into developing new treatment options over the past decades. More cancer awareness, as well as new animal models and a greater understanding of the genetic profile of synovial sarcoma, have

allowed for an increase in effective synovial sarcoma research. Yet, with the highly epigenetic nature of synovial sarcoma, determining any one single best chemotherapeutic agent or regimen remains an elusive task.

5.1. Ossification and Synovial Sarcoma

Within an already rare disease, complications such as ossification have the potential to threaten patient outcomes and prognoses based on the phenotypic profile and severity of the ossification. Painful, bony growths decrease patient quality of life beyond simple synovial sarcoma tumors and can interfere with surgical resection.

Our research of ossification events has shown that, while extremely unfortunate and incredibly painful, ossification within synovial sarcoma does not increase likelihood of metastasis. They are, in fact, independent of each other but are both dependent on time. As metastasis develops over time, ossification also has the chance to develop alongside synovial sarcoma. Early diagnosis and treatment remain the best recourse against potential ossification occurrence.

5.2. HSP90 and Synovial Sarcoma

HSP90, an omnipresent protein throughout the entire biological system, plays important roles in both mediating protein folding and stabilizing protein structure during high stress events within cells, such as high temperatures or oxidative stress. In many cancers, the HSP90 system is hijacked, leading to increased expression of HSP90. This increased expression acts to

downregulate apoptotic cell signaling and stabilizes oncoproteins, further increasing cancer proliferation.

Upregulation of HSP90 also leads to localization outside of the cytosol and into the cellular membrane. While anchored to the outside of the cell membrane, HSP90 can act to stabilize extracellular migration agents, such as MMP-9, breaking down surrounding tissue and allowing tumor expansion. HSP90 can also act to import signaling molecules and growth factors from neighboring cancer cells through active uptake.

This unique expression at the cell surface formed the basis of our research in this project; selective uptake should be possible through the unique ATP binding site of HSP90, using an inhibitor incapable of passive diffusion through the cell membrane. HSP90 inhibition is believed to disrupt the cancer cell dependence on this oncogene stabilizer, potentially leading to greater vulnerability of cancer cells to traditional chemotherapy. Previous passive diffusion HSP90 inhibitors have led to unintended off-target effects in distant tissues, specifically ocular tissue.

5.3. HSP90 Profiling within Synovial Sarcoma

Our work detailed the differences in HSP90 expression between metastatic, non-metastatic, and normal, non-cancerous tissue. RNA sequencing revealed an upregulation of HSP90 present in both types of cancer cells, with a lower amount of HSP90 being present in normal tissue. With this upregulation of HSP90 confirmed, Western immunoblotting was performed on sequential cell fractionation to qualitatively measure the presence of HSP90 within the cytoplasm and cell membrane. HSP90 was observed in both portions of the cell extract, with

approximately twice as much present within the cytoplasm as compared to the cell membrane; this proportion is reasonable considering the much higher volume of cytoplasm as compared to available cell surface.

Having confirmed the presence of membrane-bound, extracellular HSP90, we then worked to profile the metastatic potential of our *PTEN* deletion mouse models as compared to non-deletion and non-diseased mice. Using an ELISA immunosorbent assay specific to HSP90, circulating plasma samples were collected from multiple of each of the three types of mice and analyzed. Results from the assay showed a significant amount of HSP90 present in circulation in *PTEN*-deletion mice as compared to both the non-deletion and non-diseased models of mice, helping to further confirm both the metastatic potential of *PTEN* deletion and the necessity of cell-membrane expression of HSP90 to drive a metastatic profile.

5.4. Drug Treatment Analysis of HSP90 Inhibitor Against Synovial Sarcoma

With the profile and verification of HSP90 completed within Synovial Sarcoma, analysis of the novel inhibitors HS-10, HS-131, and HS-198 was ready to be performed. Using human SS and osteosarcoma cell lines, the inhibitors were tested separately along a scale of increasing concentration to establish baseline cellular response to each individual drug. Decrease in cell viability was observed only in the HS-10 treated cells, with the exception of Yamato cells, which indicated response to all three inhibitors. It is apparent that the free traversal of the cell membrane allows more accessible uptake of the HSP90 inhibitor.

When the inhibitors were utilized in combination with doxorubicin hydrochloride, results showed similar outcomes when compared to inhibitor-only treatment. The greatest decreases in cell viability were seen exclusively in Yamato treated with HS-10. Surprisingly, HSSY-II showed no response below 50% decrease, and both osteosarcoma lines indicated only minor effects at higher concentrations of HS-10. The minimum baseline to begin observation of HS-10 working alongside doxorubicin appears to be 500nM, at which every concentration of doxorubicin along the increasing scale showed at least a 50% reduction in cell viability. Inhibitors HS-131 and HS-198 indicated practically no response of any cell line below 50% cell viability, which is logical for the dummy inhibitor HS-198, but is unexpected from what should be pharmacologically active HS-131.

With this drastic difference in cellular response between drug, we desired to confirm cellular uptake of HS-131 in order to verify the proposed cellular uptake does in fact occur. Using fluorescent timelapse microscopy, Yamato cells were treated with HS-131, where accumulation within the cell could in fact be observed. However, upon repeat analysis among other cell lines and Yamato again, uptake could not be observed as readily.

5.5. Drug Treatment Analysis of HSP90 within Synovial Sarcoma Model Mice

Before beginning full-scale *in vivo* dosing, efforts were made to confirm specific targeting of HS-131 to synovial sarcoma in the biological setting. 24 hours after dosing with HS-131, mice were euthanized and organs collected and imaged using fluorescence to determine the presence of HS-131 accumulation, if any. Accumulation was decidedly visible within SS tumors, as well as

the lungs, liver, and spleen, but no accumulation was evident within the heart nor kidneys. As metastasis frequent occurs first in the lungs, and the liver and spleen are used to filter circulating blood, it is logical to see accumulation there, as there is likely metastasis within these organs as well. Also notable, when comparing our *PTEN*-deletion metastatic model to a non-deletion non-metastatic model, there is no visible accumulation of HS-131 within the non-metastatic tumor. Thus, we concluded that HS-131 is able to not only traverse the cell membrane *in vivo*, but also to target specific tissue where HSP90-membrane expression is present, particularly in a metastatic disease model.

Finally, we looked to confirm the proposed model within the biological setting. Establishing cohorts of SS18-SSX, metastatic mouse models, treatment was performed using HS-10, HS-131, and HS-198 individually and in combination with doxorubicin, with doxorubicin alone, and with a saline positive control; results from the *in vivo* trials showed considerably different outcomes than the *in vitro* experiments, with a significant response observed in the HS-131/doxorubicin cohort. Response was also observed in HS-10 and doxorubicin cohorts, but with considerable toxicity occurring among those mice. A Kaplan-Meier survival analysis also determined a significant increase in survival probability among the HS-131/doxorubicin cohort as compared to all other cohorts.

5.6. 3D Culturing and Treatment Implications

It was unclear as to why there was such variation and lack of reproducibility among our *in vitro* testing results especially as compared to our *in vivo* treatment trials, specifically with

regards to HS-131/doxorubicin outcomes between the two models. We propose that this disparity arises from cellular stress levels between the two models; *in vitro* 2D cultured cells have ready access to oxygen and supplemented media, whereas *in vivo* SS cells undergo nutrient and oxygen competition, with the inner cells not having equal access as compared to outer layers of tumors. Our 2D cultured cell lines thus did not consistently have the necessary stressors in order to promote and localize HSP90 to the cellular membrane.

A relevant, reproducible 3D culture model should help to overcome and verify this barrier. We have developed a protocol for the culture of synovial and other soft tissue sarcomas, with varying degrees of success among different primary tumor types. More stromal or connective primary tissues such as breast or intestinal cancer require more rigorous digestion and establishment protocols, but once *in vitro* culture is established appear to follow a consistent culture regimen and propagation as other soft tissues. Embedding within Matrigel allows cells to divide and remain clustered like an *in vivo* system, developing inner and outer layers and competition for oxygen and media; as such, these organoids should more relevantly represent the biological system. With primary human tissue samples, it should be possible to create patient-specific organoids available for functional precision testing.

However, Matrigel-embedded culture still holds the potential to drift away from original phenotypical expression. Through epigenetic differential expression, over time the population may skew towards cells that have more favorable mutations for *in vitro* culture. This is particularly true in the case of oxygen limitations within *in vitro* culture as compared to *in vivo* systems; without active oxygen perfusion into the media, transcriptional drift holds a high

likelihood to occur. Likewise, co-culture alongside other immune-system components proves difficult with limited oxygen delivery. We have sought to develop an improved oxygen delivery system using the Perfusion Pal® culture system, using a fiberglass scaffold and oscillating media flow to provide more surface area for propagation and oxygen delivery, respectively. Limited exposure to an air-liquid oxygen interface as well as improved liquid-liquid oxygen transfer through use of a hemoglobin-like blood substitute indicates an improved rate of cellular proliferation and organoid formation. Further analysis is still required to determine if immune components such as t-cells and macrophages can be co-cultured and continued to proliferate alongside patient cancer cultures.

5.7. Future Directions and Continued Outlook

Overall, this paper has strived to determine if HSP90 inhibition can effectively be used alongside established adjuvant therapies in order to more effectively combat synovial sarcoma formation and metastasis. With effective HSP90 inhibition, it should be possible also to reduce the effective dose for chemotherapies such as doxorubicin hydrochloride and other harsh treatments that are limited in overall patient exposure while improving patient survivability rates. Our preliminary *in vivo* results with a metastatic synovial sarcoma mouse model hold merit, as we were able to effectively double survival within the HS-131/doxorubicin cohort after only an initial treatment regimen of 28 days. Further long-term studies would help to confirm if repeated treatment periods could be endured with continued improved outcomes within the study cohorts. Likewise, functional precision testing using patient-derived organoids, an

unachieved goal and anticipated follow-up of this research, would help to confirm the viability and relevance of a three-dimensional, *ex vivo* method of cancer response.

We once again emphasize the need to develop a more accurate and reproducible *in vitro* model for culture and treatment of synovial sarcoma and other types of cancers. This would allow the reduction of animal model use as well as yielding direct, patient-relevant results when using primary patient material as the culture source. This point is directly relevant when comparing our *in vitro* treatment results to our *in vivo* treatment results; *in vitro* yielded unanticipated and irreproducible uptake (or lack thereof) and viability reduction, while anticipated outcomes such as tissue-specific uptake and tumor reductions were observable within our *in vivo* studies.

With continued research into patient-based, three-dimensional ex vivo cell cultures, and further studies with HSP90 inhibitors in conjunction with other established chemotherapeutic agents, we hope to find continued success in advancing clinically accepted treatment options in the field of synovial sarcoma and further.

6. Citations

1. Simon G. Exstirpation einer sehr grossen, mit dicken stiele angerwachsenen kneigelenkmaus mit gIucklichem Erfolge. Langenbecks Arch Klin Chir Ver Dtsch Z Chir. 1865;(6):573–6.

2. Lejars M, Rubens-Duval M. Les sarcomes primitifs des synoviales articulaires. Rev Chir. 1910;(41):751–83.

3. Deshmukh R, Mankin HJ, Singer S. Synovial sarcoma: the importance of size and location for survival. Clin Orthop Relat Res. 2004 Feb;(419):155–61.

4. Barrott JJ, Illum BE, Jin H, Hedberg ML, Wang Y, Grossmann A, et al. Paracrine osteoprotegerin and β-catenin stabilization support synovial sarcomagenesis in periosteal cells. J Clin Invest. 2018 Jan 2;128(1):207–18.

5. Hara S, Hatori M, Hosaka M, Komatsu T, Tsuchiya T, Kimura N. Synovial sarcoma with massive ossification--a case report. Ups J Med Sci. 2003;108(2):151–8.

6. Hisaoka M, Matsuyama A, Shimajiri S, Akiba J, Kusano H, Hiraoka K, et al. Ossifying synovial sarcoma. Pathol Res Pract. 2009;205(3):195–8.

7. Milchgrub S, Ghandur-Mnaymneh L, Dorfman HD, Albores-Saavedra J. Synovial sarcoma with extensive osteoid and bone formation. Am J Surg Pathol. 1993 Apr;17(4):357–63.

8. Ud Din N, Hopkins A, Memon A, Ahmad Z, Ahmed R. Calcifying/ossifying synovial sarcoma: a clinicopathologic and molecular study of 5 cases. Indian J Pathol Microbiol. 2015 Jan;58(1):55–8.

9. Winnepenninckx V, De Vos R, Debiec-Rychter M, Samson I, Brys P, Hagemeijer A, et al. Calcifying/ossifying synovial sarcoma shows t(X;18) with SSX2 involvement and mitochondrial calcifications. Histopathology. 2001 Feb;38(2):141–5.

10. Shipley JM, Clark J, Crew AJ, Birdsall S, Rocques PJ, Gill S, et al. The t(X;18)(p11.2;q11.2) translocation found in human synovial sarcomas involves two distinct loci on the X chromosome. Oncogene. 1994 May;9(5):1447–53.

11. Leeuw B de, Balemans M, Olde Weghuis D, Geurts van Kessel AHM. Identification of two alternative fusion genes, SYT-SSX1 and SYT-SSX2, in t (X; 18)(p11. 2; q11. 2)-positive synovial sarcomas. 1995; Available from: https://repository.ubn.ru.nl/bitstream/handle/2066/22251/22251___.PDF

12. Limon J, Mrozek K, Mandahl N, Nedoszytko B, Verhest A, Rys J, et al. Cytogenetics of synovial sarcoma: presentation of ten new cases and review of the literature. Genes Chromosomes Cancer. 1991 Sep;3(5):338–45.

13. Sandberg AA. Cytogenetics and molecular genetics of bone and soft-tissue tumors. Am J Med Genet. 2002 Oct 30;115(3):189–93.

14. Jones KB, Barrott JJ, Xie M, Haldar M, Jin H, Zhu J-F, et al. The impact of chromosomal translocation locus and fusion oncogene coding sequence in synovial sarcomagenesis. Oncogene. 2016 Sep 22;35(38):5021–32.

15. Svejstrup JQ. Synovial sarcoma mechanisms: a series of unfortunate events. Cell. 2013 Mar 28;153(1):11–2.

16. Aytekin MN, Öztürk R, Amer K, Yapar A. Epidemiology, incidence, and survival of synovial sarcoma subtypes: SEER database analysis. J Orthop Surg . 2020 Jan;28(2):2309499020936009.

17. Synovial Sarcoma [Internet]. National Cancer Institute. 2019 [cited 2022 Feb 1]. Available from:https://www.cancer.gov/pediatric-adult-rare-tumor/rare-tumors/rare-soft-tissue-tumors/synovial-sarcoma

18. Ladanyi M, Antonescu CR, Leung DH, Woodruff JM, Kawai A, Healey JH, et al. Impact of SYT-SSX fusion type on the clinical behavior of synovial sarcoma: a multi-institutional retrospective study of 243 patients. Cancer Res. 2002 Jan 1;62(1):135–40.

19. Masliah-Planchon J, Bièche I, Guinebretière J-M, Bourdeaut F, Delattre O. SWI/SNF chromatin remodeling and human malignancies. Annu Rev Pathol. 2015;10:145–71.

20. Peterson CL, Herskowitz I. Characterization of the yeast SWI1, SWI2, and SWI3 genes, which encode a global activator of transcription. Cell. 1992 Feb 7;68(3):573–83.

21. Li J, Mulvihill TS, Li L, Barrott JJ, Nelson ML, Wagner L, et al. A Role for SMARCB1 in Synovial Sarcomagenesis Reveals That SS18–SSX Induces Canonical BAF Destruction. Cancer Discov. 2021 Oct 1;11(10):2620–37.

22. McBride MJ, Pulice JL, Beird HC, Ingram DR, D'Avino AR, Shern JF, et al. The SS18-SSX Fusion Oncoprotein Hijacks BAF Complex Targeting and Function to Drive Synovial Sarcoma. Cancer Cell. 2018 Jun 11;33(6):1128-1141.e7.

23. Barus CE, Monsey RD, Kalof AN. Poorly differentiated synovial sarcoma of the lumbar spine in a fourteen-year-old girl. A case report. J Bone Joint Surg Am. 2009 Jun;91(6):1471–6.

24. Mullah-Ali A, Ramsay JA, Bourgeois JM, Hodson I, Macdonald P, Midia M, et al. Paraspinal synovial sarcoma as an unusual postradiation complication in pediatric abdominal neuroblastoma. J Pediatr Hematol Oncol. 2008 Jul;30(7):553–7.

25. El Beaino M, Araujo DM, Gopalakrishnan V, Lazar AJ, Lin PP. Prognosis of T1 synovial sarcoma depends upon surgery by oncologic surgeons. J Surg Oncol. 2016 Sep;114(4):490–4.

26. Drugs Approved for Soft Tissue Sarcoma [Internet]. National Cancer Institute. 2013 [cited 2022 Feb 1]. Available from: https://www.cancer.gov/about-cancer/treatment/drugs/soft-tissue-sarcoma

27. Baldi GG, Orbach D, Bertulli R, Magni C, Sironi G, Casanova M, et al. Standard treatment and emerging drugs for managing synovial sarcoma: adult's and pediatric oncologist perspective. Expert Opin Emerg Drugs. 2019 Mar;24(1):43–53.

28. Demicco EG, Maki RG, Lev DC, Lazar AJ. New therapeutic targets in soft tissue sarcoma. Adv Anat Pathol. 2012 May;19(3):170–80.

29. Swain SM, Whaley FS, Ewer MS. Congestive heart failure in patients treated with doxorubicin: a retrospective analysis of three trials. Cancer. 2003 Jun 1;97(11):2869–79.

30. Krieg AH, Hefti F, Speth BM, Jundt G, Guillou L, Exner UG, et al. Synovial sarcomas usually metastasize after >5 years: a multicenter retrospective analysis with minimum follow-up of 10 years for survivors. Ann Oncol. 2011 Feb;22(2):458–67.

31. He M, Abro B, Kaushal M, Chen L, Chen T, Gondim M, et al. Tumor mutation burden and checkpoint immunotherapy markers in primary and metastatic synovial sarcoma. Hum Pathol. 2020 Jun;100:15–23.

32. Nan X, Ng HH, Johnson CA, Laherty CD, Turner BM, Eisenman RN, et al. Transcriptional repression by the methyl-CpG-binding protein MeCP2 involves a histone deacetylase complex. Nature. 1998 May 28;393(6683):386–9.

33. Lubieniecka JM, de Bruijn DRH, Su L, van Dijk AHA, Subramanian S, van de Rijn M, et al. Histone Deacetylase Inhibitors Reverse SS18-SSX–Mediated Polycomb Silencing of the Tumor Suppressor Early Growth Response 1 in Synovial Sarcoma. Cancer Res. 2008 Jun 2;68(11):4303–10.

34. Trautmann M, Sievers E, Aretz S, Kindler D, Michels S, Friedrichs N, et al. SS18-SSX fusion protein-induced Wnt/β-catenin signaling is a therapeutic target in synovial sarcoma. Oncogene. 2014 Oct 16;33(42):5006–16.

35. Isfort I, Cyra M, Elges S, Kailayangiri S, Altvater B, Rossig C, et al. SS18-SSX–Dependent YAP/TAZ Signaling in Synovial Sarcoma. Clin Cancer Res. 2019 Jun 14;25(12):3718–31.

36. Brien GL, Remillard D, Shi J, Hemming ML, Chabon J, Wynne K, et al. Targeted degradation of BRD9 reverses oncogenic gene expression in synovial sarcoma. Elife. 2018 Nov 15;7:e41305.

37. Laporte AN, Barrott JJ, Yao RJ, Poulin NM, Brodin BA, Jones KB, et al. HDAC and Proteasome Inhibitors Synergize to Activate Pro-Apoptotic Factors in Synovial Sarcoma. PLoS One. 2017 Jan 5;12(1):e0169407.

38. Herzog CE. Overview of sarcomas in the adolescent and young adult population. J Pediatr Hematol Oncol. 2005 Apr;27(4):215–8.

39. Varela-Duran J, Enzinger FM. Calcifying synovial sarcoma. Cancer. 1982 Jul 15;50(2):345–52.

40. Haldar M, Hancock JD, Coffin CM, Lessnick SL, Capecchi MR. A conditional mouse model of synovial sarcoma: insights into a myogenic origin. Cancer Cell. 2007 Apr;11(4):375–88.

41. Barrott JJ, Kafchinski LA, Jin H, Potter JW, Kannan SD, Kennedy R, et al. Modeling synovial sarcoma metastasis in the mouse: PI3'-lipid signaling and inflammation. J Exp Med. 2016;213(13):2989–3005.

42. Jin H, Barrott JJ, Cable MG, Monument MJ, Lerman DM, Smith-Fry K, et al. The Impact of Microenvironment on the Synovial Sarcoma Transcriptome. Cancer Microenviron. 2017 Dec;10(1–3):1–7.

43. Barrott JJ, Illum BE, Jin H, Zhu J-F, Mosbruger T, Monument MJ, et al. β-catenin stabilization enhances SS18-SSX2-driven synovial sarcomagenesis and blocks the mesenchymal to epithelial transition. Oncotarget. 2015 Sep 8;6(26):22758–66.

44. Malyshev I. Immunity, tumors and aging: the role of Hsp70. Springer Science & Business Media; 2013.

45. Lindquist S. The heat-shock response. Annu Rev Biochem. 1986;55:1151–91.

46. Whitesell L, Lindquist SL. HSP90 and the chaperoning of cancer. Nat Rev Cancer. 2005 Oct;5(10):761–72.

47. Kampinga HH, Hageman J, Vos MJ, Kubota H, Tanguay RM, Bruford EA, et al. Guidelines for the nomenclature of the human heat shock proteins. Cell Stress Chaperones. 2009 Jan;14(1):105–11.

48. Haase M, Fitze G. HSP90AB1: Helping the good and the bad. Gene. 2016 Jan 10;575(2 Pt 1):171–86.

49. Chen B, Piel WH, Gui L, Bruford E, Monteiro A. The HSP90 family of genes in the human genome: Insights into their divergence and evolution. Genomics. 2005 Dec 1;86(6):627–37.

50. Lees-Miller SP, Anderson CW. Two human 90-kDa heat shock proteins are phosphorylated in vivo at conserved serines that are phosphorylated in vitro by casein kinase II. J Biol Chem. 1989 Feb 15;264(5):2431–7.

51. Ullrich SJ, Moore SK, Appella E. Transcriptional and translational analysis of the murine 84- and 86-kDa heat shock proteins. J Biol Chem. 1989 Apr 25;264(12):6810–6.

52. Coskunpinar E, Akkaya N, Yildiz P, Oltulu YM, Aynaci E, Isbir T, et al. The significance of HSP90AA1, HSP90AB1 and HSP90B1 gene polymorphisms in a Turkish population with non-small cell lung cancer. Anticancer Res. 2014 Feb;34(2):753–7.

53. Wang H, Deng G, Ai M, Xu Z, Mou T, Yu J, et al. Hsp90ab1 stabilizes LRP5 to promote epithelial-mesenchymal transition via activating of AKT and Wnt/β-catenin signaling pathways in gastric cancer progression. Oncogene. 2019 Feb;38(9):1489–507.

54. Csermely P, Schnaider T, Soti C, Prohászka Z, Nardai G. The 90-kDa molecular chaperone family: structure, function, and clinical applications. A comprehensive review. Pharmacol Ther. 1998 Aug;79(2):129–68.

55. Meng J, Liu Y, Han J, Tan Q, Chen S, Qiao K, et al. Hsp90β promoted endothelial cell-dependent tumor angiogenesis in hepatocellular carcinoma. Mol Cancer. 2017 Mar 31;16(1):72.

56. Biaoxue R, Xiling J, Shuanying Y, Wei Z, Xiguang C, Jinsui W, et al. Upregulation of Hsp90-beta and annexin A1 correlates with poor survival and lymphatic metastasis in lung cancer patients. J Exp Clin Cancer Res. 2012 Aug 28;31:70.

57. Yufu Y, Nishimura J, Nawata H. High constitutive expression of heat shock protein 90α in human acute leukemia cells. Leuk Res. 1992 Jun 1;16(6):597–605.

58. Shamovsky I, Nudler E. New insights into the mechanism of heat shock response activation. Cell Mol Life Sci. 2008 Mar;65(6):855–61.

59. Bardwell JC, Craig EA. Eukaryotic Mr 83,000 heat shock protein has a homologue in Escherichia coli. Proc Natl Acad Sci U S A. 1987 Aug;84(15):5177–81.

60. Pratt WB, Morishima Y, Peng H-M, Osawa Y. Proposal for a role of the Hsp90/Hsp70-based chaperone machinery in making triage decisions when proteins undergo oxidative and toxic damage. Exp Biol Med . 2010 Mar;235(3):278–89.

61. Picard D, Khursheed B, Garabedian MJ, Fortin MG, Lindquist S, Yamamoto KR. Reduced levels of hsp90 compromise steroid receptor action in vivo. Nature. 1990 Nov;348(6297):166–8.

62. Pratt WB, Dalman FC, Meshinchi S, Scherrer LC. The relationship between glucocorticoid receptor binding to Hsp90 and receptor function. Nihon Naibunpi Gakkai Zasshi. 1990 Dec 20;66(12):1185–97.

63. Young JC, Hoogenraad NJ, Hartl FU. Molecular chaperones Hsp90 and Hsp70 deliver preproteins to the mitochondrial import receptor Tom70. Cell. 2003 Jan 10;112(1):41–50.

64. Whittier JE, Xiong Y, Rechsteiner MC, Squier TC. Hsp90 Enhances Degradation of Oxidized Calmodulin by the 20 S Proteasome*. J Biol Chem. 2004 Oct 29;279(44):46135–42.

65. Chen S, Sullivan WP, Toft DO, Smith DF. Differential interactions of p23 and the TPR-containing proteins Hop, Cyp40, FKBP52 and FKBP51 with Hsp90 mutants. Cell Stress Chaperones. 1998 Jun;3(2):118–29.

66. Smith DF, Baggenstoss BA, Marion TN, Rimerman RA. Two FKBP-related proteins are associated with progesterone receptor complexes. J Biol Chem. 1993 Aug 25;268(24):18365–71.

67. Panaretou B, Siligardi G, Meyer P, Maloney A, Sullivan JK, Singh S, et al. Activation of the ATPase activity of hsp90 by the stress-regulated cochaperone aha1. Mol Cell. 2002 Dec;10(6):1307–18.

68. Lotz GP, Lin H, Harst A, Obermann WMJ. Aha1 binds to the middle domain of Hsp90, contributes to client protein activation, and stimulates the ATPase activity of the molecular chaperone. J Biol Chem. 2003 May 9;278(19):17228–35.

69. Müller P, Ceskova P, Vojtesek B. Hsp90 Is Essential for Restoring Cellular Functions of Temperature-sensitive p53 Mutant Protein but Not for Stabilization and Activation of Wild-type p53: IMPLICATIONS FOR CANCER THERAPY*. J Biol Chem. 2005 Feb 25;280(8):6682–91.

70. Walerych D, Gutkowska M, Klejman MP, Wawrzynow B, Tracz Z, Wiech M, et al. ATP binding to Hsp90 is sufficient for effective chaperoning of p53 protein. J Biol Chem. 2010 Oct 15;285(42):32020–8.

71. Whitesell L, Sutphin PD, Pulcini EJ, Martinez JD, Cook PH. The physical association of multiple molecular chaperone proteins with mutant p53 is altered by geldanamycin, an hsp90-binding agent. Mol Cell Biol. 1998 Mar;18(3):1517–24.

72. Deb D, Chakraborti AS, Lányi A, Troyer DA, Deb S. Disruption of functions of wild-type p53 by hetero-oligomerization. Int J Oncol. 1999 Sep;15(3):413–22.

73. Pick E, Kluger Y, Giltnane JM, Moeder C, Camp RL, Rimm DL, et al. High HSP90 expression is associated with decreased survival in breast cancer. Cancer Res. 2007 Apr 1;67(7):2932–7.

74. Becker B, Multhoff G, Farkas B, Wild P-J, Landthaler M, Stolz W, et al. Induction of Hsp90 protein expression in malignant melanomas and melanoma metastases. Exp Dermatol. 2004 Jan;13(1):27–32.

75. Flandrin P, Guyotat D, Duval A, Cornillon J, Tavernier E, Nadal N, et al. Significance of heat-shock protein (HSP) 90 expression in acute myeloid leukemia cells. Cell Stress Chaperones. 2008 Sep;13(3):357–64.

76. Kubota H, Yamamoto S, Itoh E, Abe Y, Nakamura A, Izumi Y, et al. Increased expression of co-chaperone HOP with HSP90 and HSC70 and complex formation in human colonic carcinoma. Cell Stress Chaperones. 2010 Nov;15(6):1003–11.

77. Sidera K, Patsavoudi E. Extracellular HSP90: Conquering the cell surface. Cell Cycle. 2008 Jun 1;7(11):1564–8.

78. Gress TM, Müller-Pillasch F, Weber C, Lerch MM, Friess H, Büchler M, et al. Differential expression of heat shock proteins in pancreatic carcinoma. Cancer Res. 1994 Jan 15;54(2):547–51.

79. Crouch B, Murphy H, Belonwu S, Martinez A, Gallagher J, Hall A, et al. Leveraging ectopic Hsp90 expression to assay the presence of tumor cells and aggressive tumor phenotypes in breast specimens. Sci Rep. 2017 Dec 13;7(1):17487.

80. Snigireva AV, Vrublevskaya VV, Skarga YY, Morenkov OS. [The Role of Membrane-Bound Heat Shock Proteins Hsp90 in Migration of Tumor Cells in vitro and Involvement of Cell Surface Heparan Sulfate Proteoglycans in Protein Binding to Plasma Membrane]. Biofizika. 2016 Mar;61(2):328–36.

81. Eustace BK, Sakurai T, Stewart JK, Yimlamai D, Unger C, Zehetmeier C, et al. Functional proteomic screens reveal an essential extracellular role for hsp90 alpha in cancer cell invasiveness. Nat Cell Biol. 2004 Jun;6(6):507–14.

82. Sahu D, Zhao Z, Tsen F, Cheng C-F, Park R, Situ AJ, et al. A potentially common peptide target in secreted heat shock protein-90α for hypoxia-inducible factor-1α-positive tumors. Mol Biol Cell. 2012 Feb;23(4):602–13.

83. Li W, Sahu D, Tsen F. Secreted heat shock protein-90 (Hsp90) in wound healing and cancer. Biochim Biophys Acta. 2012 Mar;1823(3):730–41.

84. Picard D. HSP90 Interactors [Internet]. picardLab. 02/2022 [cited 2022 Apr 1]. Available from: https://www.picard.ch/downloads/Hsp90interactors.pdf

85. Taipale M, Krykbaeva I, Koeva M, Kayatekin C, Westover KD, Karras GI, et al. Quantitative analysis of HSP90-client interactions reveals principles of substrate recognition. Cell. 2012 Aug 31;150(5):987–1001.

86. Samant RS, Clarke PA, Workman P. The expanding proteome of the molecular chaperone HSP90. Cell Cycle. 2012 Apr 1;11(7):1301–8.

87. Kamal A, Thao L, Sensintaffar J, Zhang L, Boehm MF, Fritz LC, et al. A high-affinity conformation of Hsp90 confers tumour selectivity on Hsp90 inhibitors. Nature. 2003 Sep;425(6956):407–10.

88. Barrott JJ, Haystead TAJ. Hsp90, an unlikely ally in the war on cancer. FEBS J. 2013 Mar;280(6):1381–96.

89. Sidera K, Samiotaki M, Yfanti E, Panayotou G, Patsavoudi E. Involvement of Cell Surface HSP90 in Cell Migration Reveals a Novel Role in the Developing Nervous System*. J Biol Chem. 2004 Oct 29;279(44):45379–88.

90. Saito K, Dai Y, Ohtsuka K. Enhanced expression of heat shock proteins in gradually dying cells and their release from necrotically dead cells. Exp Cell Res. 2005 Oct 15;310(1):229–36.

91. Zhang G, Liu Z, Ding H, Zhou Y, Doan HA, Sin KWT, et al. Tumor induces muscle wasting in mice through releasing extracellular Hsp70 and Hsp90. Nat Commun. 2017 Sep 19;8(1):1–16.

92. Hanahan D, Weinberg RA. Hallmarks of Cancer: The Next Generation. Cell. 2011 Mar 4;144(5):646–74.

93. Pearl LH, Prodromou C, Workman P. The Hsp90 molecular chaperone: an open and shut case for treatment. Biochem J. 2008 Mar 15;410(3):439–53.

94. Calderwood SK, Khaleque MA, Sawyer DB, Ciocca DR. Heat shock proteins in cancer: chaperones of tumorigenesis. Trends Biochem Sci. 2006 Mar;31(3):164–72.

95. Isaacs JS, Xu W, Neckers L. Heat shock protein 90 as a molecular target for cancer therapeutics. Cancer Cell. 2003 Mar;3(3):213–7.

96. Harris SF, Shiau AK, Agard DA. The crystal structure of the carboxy-terminal dimerization domain of htpG, the Escherichia coli Hsp90, reveals a potential substrate binding site. Structure. 2004 Jun;12(6):1087–97.

97. Buchner J. Hsp90 & Co. - a holding for folding. Trends Biochem Sci. 1999 Apr;24(4):136–41.

98. Stebbins CE, Russo AA, Schneider C, Rosen N, Hartl FU, Pavletich NP. Crystal Structure of an Hsp90–Geldanamycin Complex: Targeting of a Protein Chaperone by an Antitumor Agent. Cell. 1997 Apr 18;89(2):239–50.

99. Meyer P, Prodromou C, Hu B, Vaughan C, Roe SM, Panaretou B, et al. Structural and functional analysis of the middle segment of hsp90: implications for ATP hydrolysis and client protein and cochaperone interactions. Mol Cell. 2003 Mar;11(3):647–58.

100. Johnson BD, Chadli A, Felts SJ, Bouhouche I, Catelli MG, Toft DO. Hsp90 chaperone activity requires the full-length protein and interaction among its multiple domains. J Biol Chem. 2000 Oct 20;275(42):32499–507.

101. Gupta RS. Phylogenetic analysis of the 90 kD heat shock family of protein sequences and an examination of the relationship among animals, plants, and fungi species. Mol Biol Evol. 1995 Nov;12(6):1063–73.

102. Lee C-T, Graf C, Mayer FJ, Richter SM, Mayer MP. Dynamics of the regulation of Hsp90 by the co-chaperone Sti1. EMBO J. 2012 Mar 21;31(6):1518–28.

103. Prodromou C, Roe SM, O'Brien R, Ladbury JE, Piper PW, Pearl LH. Identification and structural characterization of the ATP/ADP-binding site in the Hsp90 molecular chaperone. Cell. 1997 Jul 11;90(1):65–75.

104. DeBoer C, Meulman PA, Wnuk RJ, Peterson DH. Geldanamycin, a new antibiotic. J Antibiot . 1970 Sep;23(9):442–7.

105. Whitesell, Mimnaugh. Inhibition of heat shock protein HSP90-pp60v-src heteroprotein complex formation by benzoquinone ansamycins: essential role for stress proteins in oncogenic

…. Proc Estonian Acad Sci Biol Ecol [Internet]. 1994; Available from: https://sci-hub.ren/https://www.pnas.org/content/91/18/8324.short

106. Nozawa K, Nakajima S. Isolation of Radicicol from Penicillium luteo-aurantium, and Meleagrin, A New Metabolite from Penicillium meleagrinum. J Nat Prod. 1979 Jul 1;42(4):374–7.

107. Neckers L, Schulte TW, Mimnaugh E. Geldanamycin as a potential anti-cancer agent: its molecular target and biochemical activity. Invest New Drugs. 1999;17(4):361–73.

108. Workman P, Burrows F, Neckers L, Rosen N. Drugging the cancer chaperone HSP90: combinatorial therapeutic exploitation of oncogene addiction and tumor stress. Ann N Y Acad Sci. 2007 Oct;1113:202–16.

109. Banerji, Walton, Raynaud, Grimshaw. Pharmacokinetic-pharmacodynamic relationships for the heat shock protein 90 molecular chaperone inhibitor 17-allylamino, 17-demethoxygeldanamycin in human …. Clin Cancer Drugs [Internet]. 2005; Available from: https://sci-hub.ren/https://clincancerres.aacrjournals.org/content/11/19/7023.short

110. Banerji U, O'Donnell A, Scurr M, Pacey S, Stapleton S, Asad Y, et al. Phase I pharmacokinetic and pharmacodynamic study of 17-allylamino, 17-demethoxygeldanamycin in patients with advanced malignancies. J Clin Oncol. 2005 Jun 20;23(18):4152–61.

111. Ronnen EA, Kondagunta GV, Ishill N, Sweeney SM, Deluca JK, Schwartz L, et al. A phase II trial of 17-(Allylamino)-17-demethoxygeldanamycin in patients with papillary and clear cell renal cell carcinoma. Invest New Drugs. 2006 Nov;24(6):543–6.

112. Hollingshead M, Alley M, Burger AM, Borgel S, Pacula-Cox C, Fiebig H-H, et al. In vivo antitumor efficacy of 17-DMAG (17-dimethylaminoethylamino-17-demethoxygeldanamycin

hydrochloride), a water-soluble geldanamycin derivative. Cancer Chemother Pharmacol. 2005 Aug;56(2):115–25.

113. Adams J, Gao Y, Georges Evangelinos AT, Grenier L, Pak RH, Porter JR, et al. Analogs of benzoquinone-containing ansamycins for the treatment of cancer. Infinity Pharmaceuticals. INC; 2005.

114. Sydor JR, Normant E, Pien CS, Porter JR, Ge J, Grenier L, et al. Development of 17-allylamino-17-demethoxygeldanamycin hydroquinone hydrochloride (IPI-504), an anti-cancer agent directed against Hsp90. Proc Natl Acad Sci U S A. 2006 Nov 14;103(46):17408–13.

115. Lee K, Ryu JS, Jin Y, Kim W, Kaur N, Chung SJ, et al. Synthesis and anticancer activity of geldanamycin derivatives derived from biosynthetically generated metabolites. Org Biomol Chem. 2008 Jan 21;6(2):340–8.

116. Menzella HG, Tran T-T, Carney JR, Lau-Wee J, Galazzo J, Reeves CD, et al. Potent non-benzoquinone ansamycin heat shock protein 90 inhibitors from genetic engineering of Streptomyces hygroscopicus. J Med Chem. 2009 Mar 26;52(6):1518–21.

117. Janin YL. ATPase inhibitors of heat-shock protein 90, second season. Drug Discov Today. 2010 May;15(9–10):342–53.

118. Zhou D, Liu Y, Ye J, Ying W, Ogawa LS, Inoue T, et al. A rat retinal damage model predicts for potential clinical visual disturbances induced by Hsp90 inhibitors. Toxicol Appl Pharmacol. 2013 Dec 1;273(2):401–9.

119. Zhou D, Teofilovici F, Liu Y, Ye J, Ying W, Shin Ogawa L, et al. Associating retinal drug exposure and retention with the ocular toxicity profiles of Hsp90 inhibitors. J Clin Orthod. 2012 May 20;30(15_suppl):3086–3086.

120. Kanamaru C, Yamada Y, Hayashi S, Matsushita T, Suda A, Nagayasu M, et al. Retinal toxicity induced by small-molecule Hsp90 inhibitors in beagle dogs. J Toxicol Sci. 2014 Feb;39(1):59–69.

121. Crowe LB, Hughes PF, Alcorta DA, Osada T, Smith AP, Totzke J, et al. A Fluorescent Hsp90 Probe Demonstrates the Unique Association between Extracellular Hsp90 and Malignancy in Vivo. ACS Chem Biol. 2017 Apr 21;12(4):1047–55.

122. Harrison. The outgrowth of the nerve fiber as a mode of protoplasmic movement. J Exp Zool [Internet]. 1910; Available from: https://www.moscalab.org/s/Harrison-1910.pdf

123. Breslin S, O'Driscoll L. Three-dimensional cell culture: the missing link in drug discovery. Drug Discov Today. 2013 Mar;18(5–6):240–9.

124. Sanyal S. Culture and assay systems used for 3D cell culture. Corning. 2014;

125. Jacoby W, Pasten I. Methods in Enzymology: Cell Culture. Vol. 58. 1979;

126. Hutchinson L, Kirk R. High drug attrition rates—where are we going wrong? Nat Rev Clin Oncol. 2011 Mar 30;8(4):189–90.

127. Rangaraju S, Solis GM, Thompson RC, Gomez-Amaro RL, Kurian L, Encalada SE, et al. Suppression of transcriptional drift extends C. elegans lifespan by postponing the onset of mortality. Elife. 2015 Dec 1;4:e08833.

128. McCandlish DM, Plotkin JB. Transcriptional errors and the drift barrier. Proceedings of the National Academy of Sciences. 2016;113(12):3136–8.

129. Wilkening S, Stahl F, Bader A. Comparison of primary human hepatocytes and hepatoma cell line Hepg2 with regard to their biotransformation properties. Drug Metab Dispos. 2003 Aug;31(8):1035–42.

130. Larson B, Cameron G, Hunt S, Long D, Moeller T. The Effect of Cell Culture Method on Long-Term Primary Hepatocyte Cell Health [Internet]. Biotek.com. 2014 [cited 2021 Nov 15]. Available from: https://www.biotek.com/resources/application-notes/the-effect-of-cell-culture-method-on-long-term-primary-hepatocyte-cell-health/

131. Nelson CM, Bissell MJ. Of extracellular matrix, scaffolds, and signaling: tissue architecture regulates development, homeostasis, and cancer. Annu Rev Cell Dev Biol. 2006;22:287–309.

132. von der Mark K, Gauss V, von der Mark H, Müller P. Relationship between cell shape and type of collagen synthesised as chondrocytes lose their cartilage phenotype in culture. Nature. 1977 Jun 9;267(5611):531–2.

133. Mseka T, Bamburg JR, Cramer LP. ADF/cofilin family proteins control formation of oriented actin-filament bundles in the cell body to trigger fibroblast polarization. J Cell Sci. 2007 Dec 15;120(Pt 24):4332–44.

134. Pampaloni F, Reynaud EG, Stelzer EHK. The third dimension bridges the gap between cell culture and live tissue. Nat Rev Mol Cell Biol. 2007 Oct;8(10):839–45.

135. Breslin S, O'Driscoll L. The relevance of using 3D cell cultures, in addition to 2D monolayer cultures, when evaluating breast cancer drug sensitivity and resistance. Oncotarget. 2016 Jul 19;7(29):45745–56.

136. Driehuis E, Kretzschmar K, Clevers H. Establishment of patient-derived cancer organoids for drug-screening applications. Nat Protoc. 2020 Sep 14;15(10):3380–409.

137. Nguyen HTL, Soragni A. Patient-Derived Tumor Organoid Rings for Histologic Characterization and High-Throughput Screening. STAR Protoc [Internet]. 2020 Sep 18;1(2). Available from: http://dx.doi.org/10.1016/j.xpro.2020.100056

138. Dekkers JF, Alieva M, Wellens LM, Ariese HCR, Jamieson PR, Vonk AM, et al. High-resolution 3D imaging of fixed and cleared organoids. Nat Protoc. 2019 Jun;14(6):1756–71.

139. Broutier L, Andersson-Rolf A, Hindley CJ, Boj SF, Clevers H, Koo B-K, et al. Culture and establishment of self-renewing human and mouse adult liver and pancreas 3D organoids and their genetic manipulation. Nat Protoc. 2016 Sep;11(9):1724–43.

140. Lin R-Z, Chang H-Y. Recent advances in three-dimensional multicellular spheroid culture for biomedical research. Biotechnol J. 2008 Oct;3(9–10):1172–84.

141. Neal JT, Li X, Zhu J, Giangarra V, Grzeskowiak CL, Ju J, et al. Organoid Modeling of the Tumor Immune Microenvironment. Cell. 2018 Dec 13;175(7):1972-1988.e16.

142. Shoemaker JT, Zhang W, Atlas SI, Bryan RA, Inman SW, Vukasinovic J. A 3D Cell Culture Organ-on-a-Chip Platform With a Breathable Hemoglobin Analogue Augments and Extends Primary Human Hepatocyte Functions in vitro. Front Mol Biosci. 2020 Oct 19;7:568777.

143. Marquart J, Chen EY, Prasad V. Estimation of the Percentage of US Patients With Cancer Who Benefit From Genome-Driven Oncology. JAMA Oncol. 2018 Aug 1;4(8):1093–8.

144. Dempster JM, Krill-Burger J, Warren A, McFarland JM, Golub TR, Tsherniak A. Gene expression has more power for predicting in vitro cancer cell vulnerabilities than genomics [Internet]. bioRxiv. 2020 [cited 2022 Jun 27]. p. 2020.02.21.959627. Available from: https://www.biorxiv.org/content/10.1101/2020.02.21.959627v1

145. Flaherty KT, Gray RJ, Chen AP, Li S, McShane LM, Patton D, et al. Molecular Landscape and Actionable Alterations in a Genomically Guided Cancer Clinical Trial: National Cancer Institute Molecular Analysis for Therapy Choice (NCI-MATCH). J Clin Oncol. 2020 Nov 20;38(33):3883–94.

146. Letai A. Functional precision cancer medicine—moving beyond pure genomics. Nat Med. 2017 Sep 1;23(9):1028–35.

147. Jones PA, Baylin SB. The fundamental role of epigenetic events in cancer. Nat Rev Genet. 2002 Jun;3(6):415–28.

148. Egger G, Liang G, Aparicio A, Jones PA. Epigenetics in human disease and prospects for epigenetic therapy. Nature. 2004 May;429(6990):457–63.

149. Robertson KD. DNA methylation and chromatin - unraveling the tangled web. Oncogene. 2002 Aug 12;21(35):5361–79.

150. Guo Y, Collaco CR, Bruera E. Heterotopic ossification in critical illness and cancer: A report of 2 cases. Arch Phys Med Rehabil. 2002 Jun 1;83(6):855–9.

151. Chang W-M, Lin Y-F, Su C-Y, Peng H-Y, Chang Y-C, Hsiao J-R, et al. Parathyroid Hormone-Like Hormone is a Poor Prognosis Marker of Head and Neck Cancer and Promotes Cell Growth via RUNX2 Regulation. Sci Rep. 2017 Jan 25;7:41131.

152. Park SI, Lee C, Sadler WD, Koh AJ, Jones J, Seo JW, et al. Parathyroid Hormone–Related Protein Drives a CD11b+Gr1+ Cell–Mediated Positive Feedback Loop to Support Prostate Cancer Growth. Cancer Res. 2013 Nov 14;73(22):6574–83.

153. Diaz-Montero CM, Salem ML, Nishimura MI, Garrett-Mayer E, Cole DJ, Montero AJ. Increased circulating myeloid-derived suppressor cells correlate with clinical cancer stage, metastatic tumor burden, and doxorubicin-cyclophosphamide chemotherapy. Cancer Immunol Immunother. 2009 Jan;58(1):49–59.

154. Soragna D, Papi L, Ratti MT, Sestini R, Tupler R, Montalbetti L. An Italian family affected by Nasu-Hakola disease with a novel genetic mutation in the TREM2 gene. J Neurol Neurosurg Psychiatry. 2003 Jun;74(6):825–6.

155. GeneCards Human Gene Database. GAPDH Gene [Internet]. [cited 2022 Aug 15]. Available from: https://www.genecards.org/cgi-bin/carddisp.pl?gene=GAPDH#localization

156. Yang J, Li Y-H, He M-T, Qiao J-F, Sang Y, Cheang LH, et al. HSP90 regulates osteosarcoma cell apoptosis by targeting the p53/TCF-1-mediated transcriptional network. J Cell Physiol. 2020 Apr;235(4):3894–904.

157. Mori M, Hitora T, Nakamura O, Yamagami Y, Horie R, Nishimura H, et al. Hsp90 inhibitor induces autophagy and apoptosis in osteosarcoma cells. Int J Oncol. 2015 Jan;46(1):47–54.

158. Ory B, Baud'huin M, Verrecchia F, Royer BB-L, Quillard T, Amiaud J, et al. Blocking HSP90 Addiction Inhibits Tumor Cell Proliferation, Metastasis Development, and Synergistically Acts with Zoledronic Acid to Delay Osteosarcoma ProgressionBlocking HSP90 Addiction Delays Osteosarcoma Progression. Clin Cancer Res. 2016 May 12;22(10):2520–33.

159. DeRose YS, Gligorich KM, Wang G, Georgelas A, Bowman P, Courdy SJ, et al. Patient-derived models of human breast cancer: protocols for in vitro and in vivo applications in tumor biology and translational medicine. Curr Protoc Pharmacol. 2013 Mar;Chapter 14:Unit14.23.

160. Mitaka T, Sattler GL, Pitot HC. The bicarbonate ion is essential for efficient DNA synthesis by primary cultured rat hepatocytes. In Vitro Cell Dev Biol. 1991 Jul;27A(7):549–56.

Figure 6 Reprint Authorization